UNIVERSITY OF ZAGREB
Faculty of Mechanical Engineering and Naval Architecture

MASTER'S THESIS

Luka Ćulić

Zagreb, 2018

UNIVERSITY OF ZAGREB
Faculty of Mechanical Engineering and Naval Architecture

VALIDATION OF THE HARMONIC BALANCE SOLVER FOR TURBOMACHINERY START-UP AND SHUT-DOWN SIMULATIONS

Supervisor:
Prof. Hrvoje Jasak, PhD

Student:
Luka Ćulić

Zagreb, 2018

I hereby declare that this thesis is entirely the result of my own work except where otherwise indicated. I have fully cited all used sources and I have only used the ones given in the list of references.

I would like to express my sincere gratitude to Professor Hrvoje Jasak for giving me the opportunity to work under the guidance of such a fascinating and inspiring teacher.

I am truly thankful to Gregor Cvijetić for his time and patience who was always willing to help me with all sorts of problems that I have encountered while writing this thesis and without his knowledge and experience this thesis would not be possible.

I would also like to thank my friends and colleagues for all the support and encouragement during the work on this thesis. Special thanks goes to my four colleagues Dino, Ivica, Filip S. and Filip V. with whom I had numerous discussions and plenty of fun times during the study.

Finally I would like to thank to my family for all the support they have provided me over the years. Thank you for your patience and for being of such great support.

Thank you all,
Luka Ćulić

SVEUČILIŠTE U ZAGREBU
FAKULTET STROJARSTVA I BRODOGRADNJE
Središnje povjerenstvo za završne i diplomske ispite
Povjerenstvo za diplomske ispite studija strojarstva za smjerove:
procesno-energetski, konstrukcijski, brodostrojarski i inženjersko modeliranje i računalne simulacije

Sveučilište u Zagrebu	
Fakultet strojarstva i brodogradnje	
Datum	Prilog
Klasa:	
Ur. broj:	

DIPLOMSKI ZADATAK

Student: **Luka Ćulić** Mat. br.: 0035191701

Naslov rada na hrvatskom jeziku: **Validacija rješavača metodom harmonijske ravnoteže za simulacije pokretanja i zaustavljanja turbostrojeva**

Naslov rada na engleskom jeziku: **Validation of the Harmonic Balance solver for turbomachinery start-up and shut-down simulations**

Opis zadatka:

The Harmonic Balance (HB) method in Computational Fluid Dynamics (CFD) tackles the problem of transient quasi-periodic flows via a spectral decomposition of the time signal using the Finite Volume Method (FVM). HB is usually applied to turbulent flows in turbomachinery to investigate transient instabilities which occur at specific operating points. On the other hand, machine start-up and shut-down have been investigated only using the transient approach so far, which is extremely computationally demanding because it is necessary to simulate a large number of periods during which start-up/shut-down take place. Although HB is widely used to simulate a single operating point and flow regime and, thus providing an insight into the rotor-stator interaction, the behavior during start-up and shut-down is currently not in the spotlight of the HB method.

In this study, the candidate shall investigate and validate the HB method as a tool for simulating turbomachinery start-up and shut-down.

The candidate shall perform the following tasks within this project:

- Perform a literature survey on spectral methods in CFD, including HB and other variants, as well as investigate the most common turbomachinery start-up and shut-down simulation methods;
- Perform a detailed investigation of the turbomachinery start-up and shut-down effects;
- Suggest possible improvements of the existing implementation of HB method, better suited to capture the flow regime during start-up/shut-down;
- Perform a two-dimensional HB simulation of a turbomachine with one cycle including both start-up and shut-down with regards to chosen operating point;
- Perform a validation of the HB start-up/shut-down method by comparing the results to the transient method, taking into account that a sufficient number of periods has to be simulated;
- Compare the results and computational time for the HB and transient solution.

The Thesis shall list the bibliography and any assistance received during this study.

Zadatak zadan:	Datum predaje rada:	Predviđeni datum obrane:
18. siječnja 2018.	22. ožujka 2018.	28., 29. i 30. ožujka 2018.

Zadatak zadao: Predsjednica Povjerenstva:

Prof. dr. sc. Hrvoje Jasak

Prof. dr. sc. Tanja Jurčević Lulić

Table of Contents

List of Figures

List of Tables

Nomenclature

Greek letters

ε	Turbulence dissipation rate	m^2/s^3
γ	Diffusivity	m^2/s
ν	Kinematic viscosity	m^2/s
ω	Angular frequency	$1/s$
ϕ	Transported scalar variable	-
ρ	Density	kg/m^3
σ	Cauchy Stress Tensor	Pa
τ	Viscous stress tensor	Pa

Latin letters

$\mathbf{g}$	Gravitational acceleration	m/s^2
$\mathbf{u}$	Velocity vector	m/s
Q_0	Scalar field, zeroth harmonic of Fourier series	-
Q_{C_n}	Scalar field, Fourier coefficient of *n*th harmonic multiplying the cosine term	-
Q_{S_n}	Scalar field, Fourier coefficient of *n*th harmonic multiplying the sine term	-
R_0	Convection and diffusion term, zeroth harmonic of Fourier series	-
R_{C_n}	Convection and diffusion term, Fourier coefficient of *n*th harmonic multiplying the cosine term	-
R_{S_n}	Convection and diffusion term, Fourier coefficient of *n*th harmonic multiplying the sine term	-
$\mathscr{Q}$	Scalar field in time domain	-
$\mathscr{R}$	Scalar transport equation convection and diffusion term	-
$\underline{\underline{A}}$	Coefficient matrix	-
$\underline{\underline{E}}$	Fourier Transformation matrix from frequency to time domain	-
$\underline{\underline{E}}^{-1}$	Fourier Transformation matrix from time to frequency domain	-

$\underline{\underline{E}}_{sr}$	Fourier Transformation matrix from frequency to time domain with rotor time instants and stator dominant frequency	-
$\underline{\underline{E}}_{sr}^{-1}$	Fourier Transformation matrix from frequency to time domain with rotor time instants and stator dominant frequency	-
$\underline{\underline{Q}}$	Fourier coefficient matrix	-
$\underline{\underline{R}}$	Fourier coefficient matrix	-
ν	Kinematic viscosity	m^2/s
a_0	First term of Fourier series, mean value	-
a_n	Fourier coefficient of nth harmonic multiplying cosine term	-
A_n^2	Energy of the nth harmonic	-
b_n	Fourier coefficient of nth harmonic multiplying sine term	-
f	Frequency of the period	Hz
I	Turbulence intensity	-
i	Summation index	-
k	Turbulent kinetic energy	m^2/s^2
N	Number of harmonics	-
n	Number of harmonics in Fourier series	-
n	number of harmonics of outer simulation	-
p	Kinematic pressure	m^2/s^2
P_i	Coefficient substituting the summation term	-
q_v	Volumetric sources and sinks of the scalar field	-
T	Period in Fourier series	s
t	Time	s
t_n	nth time step within a period	s
x	Argument of the function decomposed in Fourier series	-
x_0	Initial point of the period	-

Abbreviations

CFD Computational Fluid Dynamics

PDE Partial Differential Equation

GGI General Grid Interface

HB Harmonic balance

DFT Discrete Fourier Transform

FV Finite Volume

PL Part load

BEP Best efficiency point

HL High load

Abstract

Luka Ćulić

VALIDATION OF THE HARMONIC BALANCE SOLVER FOR TURBOMACHINERY START-UP AND SHUT-DOWN SIMULATIONS

This thesis investigates different turbomachinery flow regimes and transient behavior during regime change. One of the main reasons why turbomachinery is working in the different flow regimes are changes in the global electricity market. Global incitation for alternative, renewable and sustainable energy, such as wind and solar energy, has increased grid disruption because solar panel, wind turbines, etc., do not produce electricity according to demand. The volatility of the electric grid needs to be reduced and it is most often regulated by changing the flow regime in the hydro-power plant. This has resulted in frequent load variations in turbines and as a consequence shorter operating life. In order to adjust turbines to this new regime of work, fluid flow during whole transient period needs to be calculated and predicted. Simulating the complete transient period with available methods, is too expensive for industrial applications and therefore the Harmonic Balance method for transient flows is developed.

In this thesis mathematical model and Harmonic Balance method will be presented. Furthermore, a novel approach to calculate changing flow regimes is presented. At the end, experimental results obtained as a part of the Francis 99 workshop will be compared with obtained numerical results in order to evaluate the method for turbine start-up and shut-down application.

Keywords: *CFD*, `foam-extend`, *Harmonic Balance Method*, *Francis turbine, Transient flow*, *Start-up*, *Shut-down*

Sažetak

(ABSTRACT IN CROATIAN)

Luka Ćulić

VALIDACIJA RJEŠAVAČA METODOM HARMONIJSKE RAVNOTEŽE ZA SIMULACIJE POKRETANJA I ZAUSTAVLJANJA TURBOSTROJEVA

Tema ovoga rada je istraživanje rada turbostrojeva u različitim režimima strujanja. Glavni uzroci promjenjivih režima rada su novosti u području proizvodnje električne energije. Vlade vodećih država svijeta potiču proizvodnju energije iz obnovljivih i održivih izvora energije, poput vjetra i solarne energije. Posljedica toga su oscilacije u električnoj mreži jer se električna energija ne proizvodi prema potrebi već ovisno o prirodnim uvjetima. U svrhu smanjivanja oscilacija električne mreže, najčešće se regulira snaga hidroelektrana. To je rezultiralo čestim promjenama opterećenja u turbinama, a za posljedicu ima kraći radni vijek. Da bi turbine prilagodili promjenama u režimu rada, potrebno je izračunati strujanje fluida tijekom cijelog perioda u kojem se mijenja režim strujanja. Simuliranje tako promjenjivih režima rada je skupo i neefikasno te je zbog toga je razvijen novi pristup metodom harmonijske ravnoteže za izračun tranzijentnih strujanja.

U ovom radu prikazan je matematički model i metoda harmonijske ravnoteže koja će se koristiti za izračun tranzijentnih strujanja. Na kraju, eksperimentalni rezultati dostupni sa radionice Francis 99, bit će uspoređeni s dobivenim numeričkim rezultatima, kako bi se validirala metoda za izračun strujanja pri pokretanju i zatvaranju turbine.

Ključne riječi: *Računalna dinamika fluida*, `foam-extend`, *metoda harmonijske ravnoteže*, *Francisova turbina*, *tranzijentno strujanje*, *pokretanje turbine*, *zaustavljanje turbine*

Prošireni Sažetak (Extended Abstract in Croatian)

Uvod

Tema ovoga rada je istraživanje rada turbostrojeva u različitim režimima strujanja. Glavni uzroci promjenjivih režima rada su novosti u području proizvodnje električne energije. Vlade vodećih država svijeta potiču proizvodnju energije iz obnovljivih i održivih izvora energije, poput vjetra i solarne energije. Posljedica toga su oscilacije u električnoj mreži jer se električna energija ne proizvodi prema potrebi već ovisno o prirodnim uvjetima. U svrhu smanjivanja oscilacija električne mreže, najčešće se regulira snaga hidroelektrana. To je rezultiralo čestim promjenama opterećenja u turbinama, a za posljedicu ima kraći radni vijek. Da bi turbine prilagodili promjenama u režimu rada, potrebno je izračunati strujanje fluida tijekom cijelog perioda u kojem se mijenja režim strujanja. Simuliranje tako promjenjivih režima rada je skupo i neefikasno te je zbog toga razvijena metoda harmonijske ravnoteže za izračun tranzijentnih strujanja.

Računalna dinamika fluida važan je alat u analizi i projektiranju turbostrojeva već desetljećima, tako i u rješavanju ovdje navedenih izazova zauzima važno mjesto. Na tragu toga pokrenuta je međunarodna konferencija "Francis 99", organizirana od strane Norveškog sveučilišta znanosti i tehnologije (NTNU) i LuelåSveučilišta u Švedskoj. Za potrebe konferencije otvoren je pristup tehničkoj dokumentaciji, CAD modelima i rezultatima eksperimenata modela turbine instalirane u hidroelektrani Tokke u Norveškoj [1].

U sklopu ovog rada analizirat će se rješavač metodom harmonijske ravnoteže za simulacije pokretanja i zaustavljanja turbostrojeva. Pristup će prvo biti testiran na jednom jednostavnom slučaju u kojem će se usporediti s postojećim tranzijentnim rješavačima dostupnima u `foam-extend` open source programu [2]. Nakon toga simulirat će se pokretanje i zaustavljanje Francis turbine, te će rezultati biti validiran usporedbom s eksperimentalnim rezultatima.

Matematički model

Matematički model korišten za modeliranje nestlačivog, turbulentnog, viskoznog i jednofaznog strujanja opisan je jednadžbom očuvanja mase te Navier-Stokesovim jednadžbama, koje predstavljaju zakon očuvanja količine gibanja [3]:

$$\nabla \cdot \mathbf{u} = 0, \tag{1}$$

$$\frac{\partial \rho \mathbf{u}}{\partial t} + \nabla \cdot (\rho \mathbf{u} \otimes \mathbf{u}) = \rho \mathbf{g} + \nabla \cdot \sigma, \tag{2}$$

gdje je $\mathbf{u}$ brzina, ρ je gustoća fluida, ν predstavlja koeficijent kinematičke viskoznosti, g je gravitacijska konstanta dok je σ tenzor naprezanja.

Jednadžba (2) sastoji se od:

- vremenskog člana $\frac{\partial \rho \mathbf{u}}{\partial t}$,
- konvektivnog člana $\nabla \cdot (\rho \mathbf{u} \otimes \mathbf{u})$,
- izvorskog člana $\rho \mathbf{g} + \nabla \cdot \sigma$.

Metoda Harmonijske Ravnoteže

Matematički model metode harmonijske ravnoteže dan je u nastavku, te primijenjen na skalarnu transportnu jednadžbu.

Pod pretpostavkom da je problem periodičan, konvekcijsko-difuzijska jednadžba glasi:

$$\frac{\partial \mathscr{Q}}{\partial t} + \mathscr{R} = 0, \tag{3}$$

gdje je $\mathscr{R}$ pojednostavljen zapis konvekcijskog, difuzijsog i izvorskog člana:

$$\mathscr{R} = \nabla \cdot (\mathbf{u}\mathscr{Q}) - \nabla \cdot (\gamma \nabla \mathscr{Q}) - S_{\mathscr{Q}}, \tag{4}$$

gdje je $\mathbf{u}$ brzina, a γ koeficijent difuzije. Osnovne varijable $\mathscr{Q}$ i $\mathscr{R}$ mogu se zapisati pomoću Fourieova razvoja s n harmonika na sljedeći način:

$$\mathscr{Q} = Q_0 + \sum_{i=1}^{n} Q_{S_i} sin(i\omega t) + Q_{C_i} cos(i\omega t), \tag{5}$$

$$\mathscr{R} = R_0 + \sum_{i=1}^{n} R_{S_i} sin(i\omega t) + R_{C_i} cos(i\omega t), \tag{6}$$

U jednadžbama (5) i (6) za zapis u vremenskoj domeni se koristi notacija $\mathscr{Q}$ i $\mathscr{R}$, dok se za zapis u frekvencijskoj domeni koristi Q i R. Ako se jednadžbe (5) i (6) ubace u jednadžbu (1) te se grupiraju članovi uz sinus i kosinus dobivamo sljedeći sustav jednadžbi.
n jednadžbi uz sinus:

$$-i\omega Q_{C_i} + R_{S_i} = 0, \quad \text{for} \quad i = 1 \ldots n, \tag{7}$$

jednu jednadžbu za srednju vrijednost

$$R_0 = 0, \tag{8}$$

i n jednadžbi uz kosinus:

$$i\omega Q_{S_i} + R_{C_i} = 0, \quad \text{for} \quad i = 1 \dots n. \tag{9}$$

Ako jednadžbe (7), (8) i (9) zapišemo u kompaktnom obliku dobivamo sljedeće:

$$\omega \underline{\underline{A}}\,\underline{Q} + \underline{R} = \underline{0}, \tag{10}$$

gdje je:

$$\underline{\underline{A}} = \begin{bmatrix} & & & & & 0 & -1 & & & & & \\ & & & & & 0 & & -2 & & & & \\ & & 0 & & & . & & & -3 & & & \\ & & & & & . & & & & \ddots & & \\ & & & & & . & & & & & & -n \\ 0 & 0 & 0 & \dots & 0 & 0 & 0 & \dots & 0 & 0 & 0 & \\ 1 & & & & & . & & & & & & \\ & 2 & & & & . & & & & & & \\ & & 3 & & & . & & & 0 & & & \\ & & & \ddots & & 0 & & & & & & \\ & & & & n & 0 & & & & & & \end{bmatrix}, \underline{Q} = \begin{bmatrix} Q_{C_1} \\ Q_{C_2} \\ Q_{C_3} \\ \vdots \\ Q_{C_n} \\ Q_0 \\ Q_{S_1} \\ Q_{S_2} \\ Q_{S_3} \\ \vdots \\ Q_{S_n} \end{bmatrix}, \underline{R} = \begin{bmatrix} R_{C_1} \\ R_{C_2} \\ R_{C_3} \\ \vdots \\ R_{C_n} \\ R_0 \\ R_{S_1} \\ R_{S_2} \\ R_{S_3} \\ \vdots \\ R_{S_n} \end{bmatrix}. \tag{11}$$

Ako želimo riješiti jednadžbu (10), diferencijalni operater R treba biti transformiran iz vremenske u frekvencijsku domenu, a to nije poželjno. Kako bi se to riješilo na jednostavniji način, jednadžbu (10) ćemo prebaciti iz frekvencijske u vremensku domenu pomoću matrice transformacije. Prvo ćemo definirati diskretni vektor varijable $\mathscr{Q}$ u vremenskoj domeni, kako bi se postiglo jednostavno mapiranje jedan-na-jedan:

$$\underline{\mathscr{Q}}^T = [\mathscr{Q}_{t_1} \quad \mathscr{Q}_{t_2} \quad \mathscr{Q}_{t_3} \quad \dots \quad \mathscr{Q}_{t_{2n+1}}], \tag{12}$$

gdje t_i predstavlja:

$$t_i = \frac{iT}{2n+1}, \quad \text{for} \quad i = 1 \dots 2n+1. \tag{13}$$

Uz pomoć transformacijske matrice $\underline{\underline{E}}$ možemo povezati vektore $\mathscr{Q}$ i Q, odnosno služi za

transformaciju iz vremenske u frekvencijsku domenu.

$$\underline{Q} = \underline{\underline{E}}\,\underline{\mathscr{Q}}, \tag{14}$$

$$\underline{\underline{E}} = \frac{2}{2n+1}\begin{bmatrix} \sin(\omega t_1) & \sin(\omega t_1) & \sin(\omega t_3) & ... & \sin(\omega t_{2n+1}) \\ \sin(2\omega t_1) & \sin(2\omega t_1) & \sin(2\omega t_3) & ... & \sin(2\omega t_{2n+1}) \\ \sin(3\omega t_1) & \sin(3\omega t_1) & \sin(3\omega t_3) & ... & \sin(3\omega t_{2n+1}) \\ \vdots & \vdots & \vdots & & \vdots \\ \sin(n\omega t_1) & \sin(n\omega t_1) & \sin(n\omega t_3) & ... & \sin(n\omega t_{2n+1}) \\ \frac{1}{2} & \frac{1}{2} & \frac{1}{2} & & \frac{1}{2} \\ \cos(\omega t_1) & \cos(\omega t_1) & \cos(\omega t_3) & ... & \cos(\omega t_{2n+1}) \\ \cos(2\omega t_1) & \cos(2\omega t_1) & \cos(2\omega t_3) & ... & \cos(2\omega t_{2n+1}) \\ \cos(3\omega t_1) & \cos(3\omega t_1) & \cos(3\omega t_3) & ... & \cos(3\omega t_{2n+1}) \\ \vdots & \vdots & \vdots & & \vdots \\ \cos(n\omega t_1) & \cos(n\omega t_1) & \cos(n\omega t_3) & ... & \cos(n\omega t_{2n+1}) \end{bmatrix}. \tag{15}$$

Množenjem jednadžbe (14) matricom $\underline{\underline{E}}^{-1}$ s lijeva, dobiva se transformacija iz frekvencijske u vremensku domenu:

$$\underline{\mathscr{Q}} = \underline{\underline{E}}^{-1}\underline{Q}, \tag{16}$$

$$\underline{\underline{E}}^{-1} = \begin{bmatrix} \sin(\omega t_1) & \sin(2\omega t_1) & ... & \sin(n\omega t_1) & 1 & \cos(\omega t_1) & \cos(2\omega t_1) & ... & \cos(n\omega t_1) \\ \sin(\omega t_2) & \sin(2\omega t_2) & ... & \sin(n\omega t_2) & 1 & \cos(\omega t_2) & \cos(2\omega t_2) & ... & \cos(n\omega t_2) \\ \sin(\omega t_3) & \sin(2\omega t_3) & ... & \sin(n\omega t_3) & 1 & \cos(\omega t_3) & \cos(2\omega t_3) & ... & \cos(n\omega t_3) \\ & & & & \vdots & & & & \\ & & & & \vdots & & & & \\ \sin(\omega t_n) & \sin(2\omega t_n) & ... & \sin(n\omega t_n) & 1 & \cos(\omega t_n) & \cos(2\omega t_n) & ... & \cos(n\omega t_n) \end{bmatrix}, \tag{17}$$

Dalje, jednadžba (10) će biti formulirana u frekvencijskoj domeni, ali s varijablama vremenske domene $\mathscr{Q}$ i $\mathscr{R}$, uz korištenje jednadžbe (14) i analogne jednadžbe za varijablu $\mathscr{R}$:

$$\omega\underline{\underline{A}}\,\underline{\underline{E}}\,\underline{\mathscr{Q}} + \underline{\underline{E}}\,\underline{\mathscr{R}} = \underline{0}. \tag{18}$$

Sustav jednadžbi iz jednadžbe (18) moguće je riješiti, ali računanje izvora i protoka u

frekvencijskoj domeni je skupo i mukotrpno. Da bismo izbjegli to, prvo ćemo pretvoriti jednadžbu natrag u vremensku domenu a to će radimo množenjem jednadžbe (18) s lijeve strane s $\underline{\underline{E}}^{-1}$:

$$\omega \underline{\underline{E}}^{-1} \underline{\underline{A}} \underline{\underline{E}} \underline{\mathscr{Q}} + \underline{\mathscr{R}} = \underline{0}. \tag{19}$$

Dobivena jednadžba predstavlja spregnuti sustav $2n+1$ stacionarnih problema. Uspoređujući jednadžbu (18) s originalnom skalarnom transportnom jednadžbom (3), mogu se uočiti dvije bitne karakteristike:

- $\mathscr{R}$ je zamijenjen diskretnom varijablom $\underline{\mathscr{R}}$, pri čemu upućuje da su rješenja dobivena u određenom broju diskretnih vremenskih trenutaka. Broj vremenskih trenutaka određen je korištenim brojem harmonika n, prema izrazu (11).,
- Vremenski član zamijenjen je spregnutim izvornim članovima koji međusobno povezuju različite vremenske trenutke. Takav pristup istovjetan je računanju derivacije harmonijskog signala po vremenu u $2n+1$ ekvidistantnih vremenskih trenutaka, uključujući i rješenje srednje vrijednosti.

Matrica $\underline{\underline{E}}^{-1} \underline{\underline{A}} \underline{\underline{E}}$ u jednadžbi (19) ima sljedeći oblik:

$$\underline{\underline{E}}^{-1} \underline{\underline{A}} \underline{\underline{E}} = \frac{2}{2n+1} \begin{bmatrix} 0 & P_1 & P_2 & P_3 & \dots & \dots & P_{2n} \\ -P_1 & 0 & P_1 & P_2 & P_3 & & \vdots \\ -P_2 & -P_1 & 0 & P_1 & P_2 & & \vdots \\ -P_3 & -P_2 & -P_3 & 0 & P_1 & & \vdots \\ \vdots & & & & \ddots & & P_2 \\ \vdots & & & & & \ddots & P_1 \\ -P_{2n} & \dots & \dots & -P_3 & -P_2 & -P_1 & 0 \end{bmatrix}. \tag{20}$$

gdje je P_n definiran kao:

$$P_n = \sum_{k=1}^{n} k \sin(k\omega i t_1) = \sum_{k=1}^{n} k \sin(\frac{2i\pi k}{2n+1}), \qquad \text{for} \quad i = \{1, 2n\} \tag{21}$$

Budući da koeficijenti P_n ovise samo o broju harmonika, koji su unaprijed određeni, možemo ih izračunati prije simulacije i spremiti ih. Tako smanjujemo vrijeme potrebno za izračun. Matrica $\underline{\underline{E}}^{-1} \underline{\underline{A}} \underline{\underline{E}}$ napisana u jednadžbi (19) uračunava vremensku udaljenost, što

znači da trenutak bliži trenutku računanja ima veći utjecaj na rješenje u odnosu na trenutak daleko od trenutka za koji se rješenje računa.

Koristeći jednadžbu (19) zajedno s jednadžbom (20), prošireni oblik spregnutih jednadžbi za skalarni transport u formi metode harmonijske ravnoteže moguće je zapisati:

$$\nabla \cdot (\mathbf{u}\mathscr{Q}_{t_j}) - \nabla \cdot (\gamma \mathscr{Q}_{t_j}) = -\frac{2\omega}{2n+1}\left(\sum_{i=1}^{2n} P_{i-j}\mathscr{Q}_{t_j}\right), \quad \text{for} \quad j = 1\ldots 2n+1. \tag{22}$$

S obzirom na to da u ovom radu koristimo Navier-Stokesove jednadžbe za nestlačiva strujanja, zapisat ćemo ih u oblik harmonijske ravnoteže koristeći postupak opisan iznad:

$$\nabla \cdot \mathbf{u}_{t_j} = 0, \tag{23}$$

$$\begin{gathered}\nabla \cdot (\mathbf{u}_{t_j}\mathbf{u}_{t_j}) - \nabla \cdot (\nu \mathbf{u}_{t_j}) = -\nabla p_{t_j} - \frac{2\omega}{2n+1}\left(\sum_{i=1}^{2n} P_{i-j}\mathbf{u}_{t_j}\right), \\ \text{for} \quad j = 1\ldots 2n+1.\end{gathered} \tag{24}$$

Implementacija za procese pokretanja i zaustavljanja turbostrojeva

Do sada je metoda harmonijske ravnoteže korištena samo za slučajeve s periodičnim strujanjima konstantnim u vremenu. U sklopu ovoga rada proširena je upotreba metode harmonijske ravnoteže i na slučajeve kada se strujanja mijenjaju tijekom vremena, poput pokretanja i zaustavljanja turbostrojeva.

Novi pristup se sastoji od $2n+1$ unutarnjih i jedne vanjske simulacije. Unutarnje simulacije koriste samo jedan harmonik budući datakav pristup daje rezultate zadovoljavajuće točnosti. Razlog tomu je što samo posljednji vremenski trenutak iz svake unutarnje simulacije se prenosi u vanjsku simulaciju. Velika simulacija ima n_B harmonika i taj broj se određuje sa svaki slučaj posebno. Pri određivanju broja harmonika dvije stvari treba uzeti u obzir, vrijeme potrebno za izračun i aproksimaciju početne funkcije.

Prvi korak pri rješavanju simulacija pokretanja i zaustavljanja je određivanje funkcije promjene određene varijable tijekom pokretanja i zaustavljanja, koja će biti implementirana kao rubni uvjet. Nakon toga se odredi $2n_B+1$ jednako razmaknutih vremenskih trenutaka u kojima ćemo računati unutarnje simulacije. Jedan primjer takve funkcije i vremenskih trenutaka je dan na Slici 1. U ovom primjeri vanjska simulacija koristi 6 harmonika što znači da treba izračunati 13 unutarnjih simulacija, a samim time i 13 različitih rubnih uvjeta postavljenih za 13 jednako razmaknutih vremenskih trenutaka.

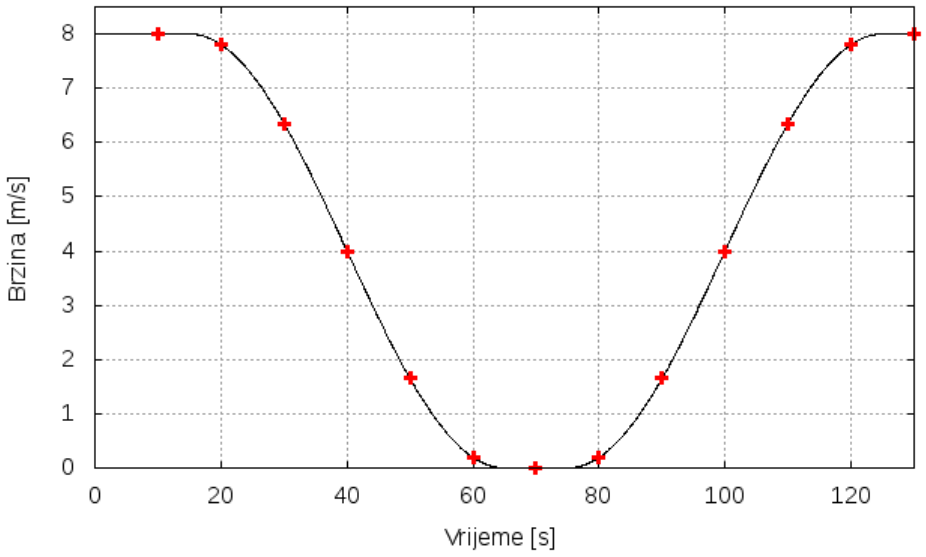

Slika 1: Vremenski trenutci u kojima se računaju "male" simulacije.

Nakon što su sve unutarnje simulacije izračunate, rezultati tih simulacija se postavljaju kao početni uvjeti vanjske simulacije. Tijekom vanjske simulacije rezultati su rekonstruirani, što znači da su dostupni u bilo kojem vremenskom trenutku a ne samo u $2n+1$ početno izračunatih trenutaka.

U svrhu smanjenja vremena potrebnog za izračun rezultata, moguće je uvesti dodatno pojednostavljenje. Ako se funkcija napravi tako da su vremenski trenutci u kojima se izračunavaju unutarnje simulacije simetrični, onda je potrebno izračunati $n+1$ a ne početnih $2n+1$ unutarnjih simulacija. Ostalih n simulacija se dobije kopiranjem rezultata iz prvih n simulacija za preostale trenutke. Uvođenjem tog pojednostavljenja proces se ubrza za faktor do 2.

Testni rezultati

U ovom odlomku prikazat će se usporedba metode harmonijske ravnoteže s postojećom metodom za simuliranje tokova promjenjivih u vremenu. Geometrija korištena u ovim simulacijama je vrlo jednostavna, s malim brojem ćelija kako potrebno vrijeme izračuna ne bi bilo predugo. Na Slici 2 se može vidjeti cijela geometrija koja se sastoji od tri statorske i četiri rotorske lopatice. Također je prikazana i mreža kontrolnih volumena.

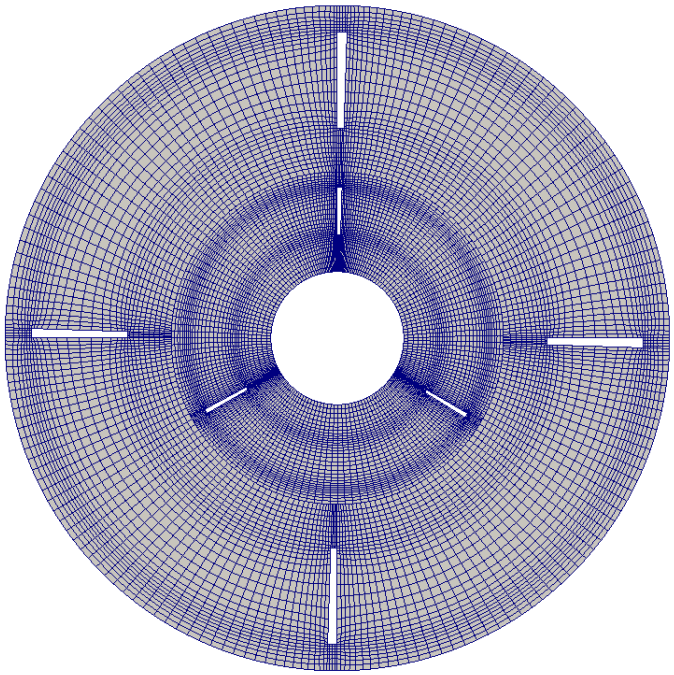

Slika 2: Geometrija i mreža kontrolni volumena.

Simuliranje procesa pokretanja i zaustavljanja turbina u ovom slučaju postići će se smanjivanjem odnosno povećavanjem vrijednosti brzine na ulazu u domenu, a samim time je smanjen ili povećan protok. Promjena brzine na ulazu prati sinusnu funkciju:

$$y = y_0 + a * \sin(bx + c) = 4 + 4 * \sin(\frac{2\pi}{\mathrm{T}}x + \frac{\pi}{2}), \tag{25}$$

gdje je T period sinusne funkcije i iznosi 100 s. Period trajanja cijelog procesa zaustavljanja i pokretanja je 130 s. Cijeli proces je prikazan na Slici 1. Prvih 15 s, brzina je održavana na 8 m/s i to se smatra točkom u kojoj će početi proces zaustavljanja. Zaustavljanje traje 50 s sve dok ne dođe do točke kada je brzina 0 m/s. Zatim se 10 s brzina održava na toj razini. Nakon toga započinje proces pokretanja, koji traje jednako kao i proces zaustavljanja, 50 s.

U tablici 1 može se vidjeti usporedba vremena potrebnih za izračun procesa zaustavljanja i pokretanja. Korištenjem stare metode bilo je potrebno 18.7 h dok je korištenjem metode harmonijske ravoteže vrijeme smanjeno 96.48% i iznosi 2366 min.

Tablica 1: Vrijeme računanja.

	Jedna unutarnja sim.	Sedam unutarnjih sim.	Stara metoda	Smanjenje[%]
Vrijeme [s]	338	2366	67300	96.48%
Vrijeme [h]	0.094	0.66	18.7	96.48%

U tablici 2 mogu se vidjeti koordinate točaka u kojima su mjereni tlak i vrijeme kroz vrijeme. Rezultati tih mjerenja predstavljeni su na Slici 3, gdje se može vidjeti da metoda

harmonijske ravnoteže dobro simulira proces zaustavljanja i pokretanja u ovom konkretnom slučaju. Na Slici 4 su uspoređena polja brzina tijekom pet vremenskih trenutaka za dvije korištene metode.

Tablica 2: Koordinate točaka za mjerenje tlaka i brzine.

	x	y
Point 1	0.048	0.2885
Point 2	0.0509	0.5879
Point 3	-0.1548	0.8416

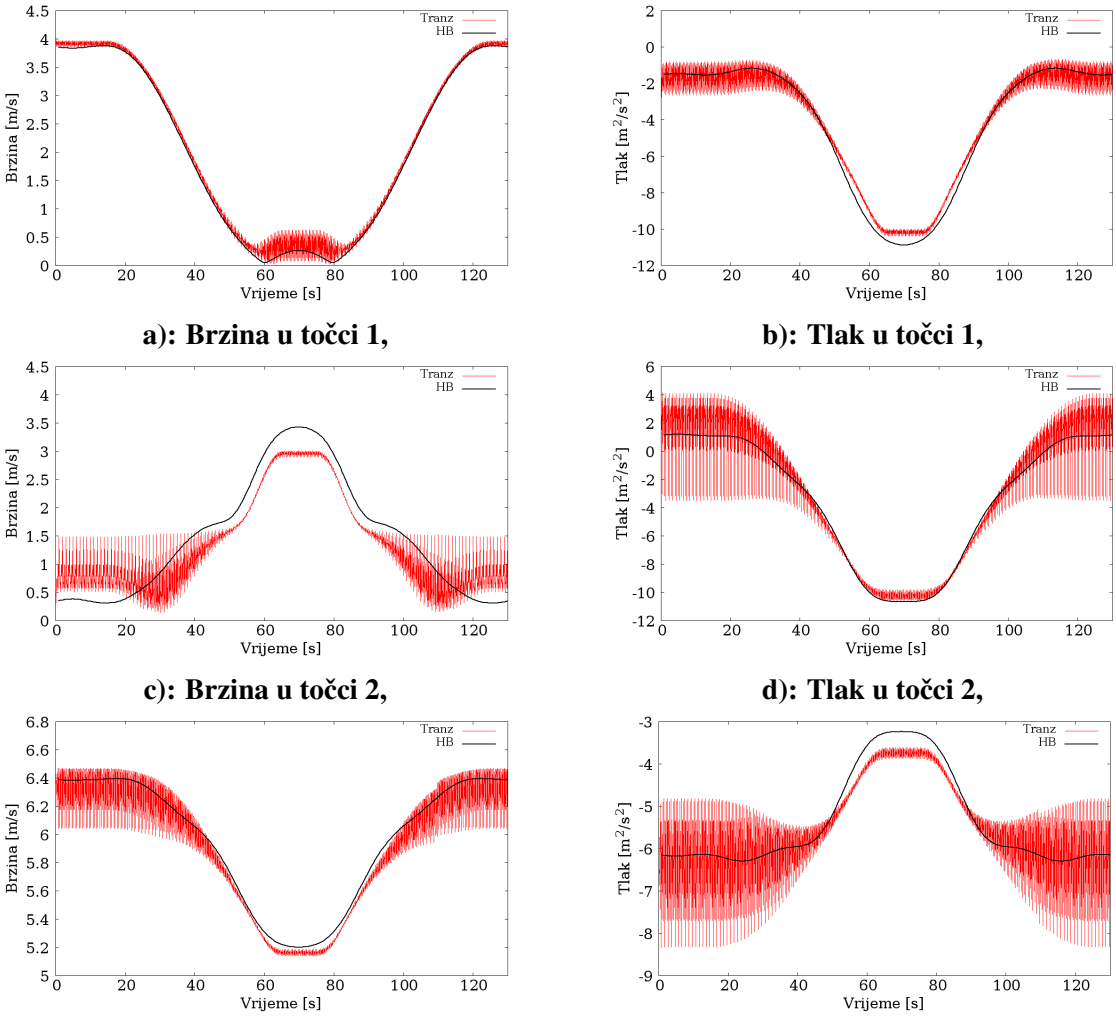

a): Brzina u točci 1, **b): Tlak u točci 1,**

c): Brzina u točci 2, **d): Tlak u točci 2,**

e): Brzina u točci 3, **f): Tlak u točci 3,**

Slika 3: Brzina i tlak u različitim točkama tijekom vremena.

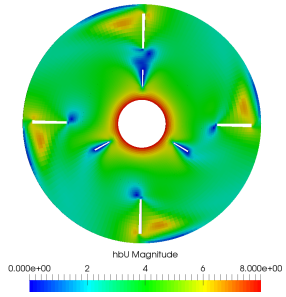

a): HB, $U_{ul} = 8\text{m/s}$**,** $t = 13\text{s}$

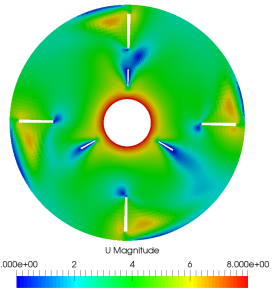

b): Tranz, $U_{ul} = 8\text{m/s}$**,** $t = 13\text{s}$

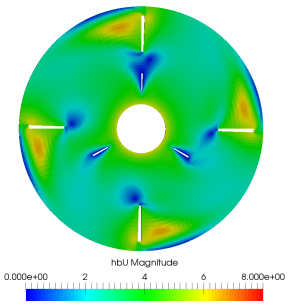

c): HB, $U_{ul} = 6\text{m/s}$**,** $t = 32\text{s}$

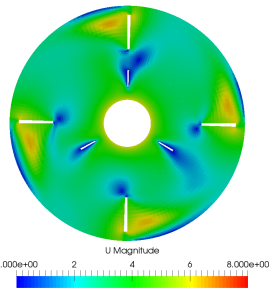

d): Tranz, $U_{ul} = 6\text{m/s}$**,** $t = 32\text{s}$

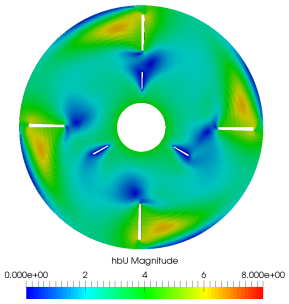

e): HB, $U_{ul} = 4\text{m/s}$**,** $t = 40\text{s}$

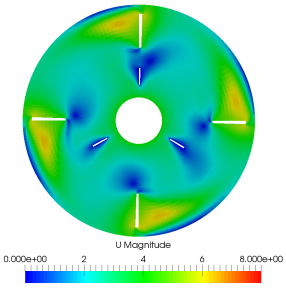

f): Tranz, $U_{ul} = 4\text{m/s}$**,** $t = 40\text{s}$

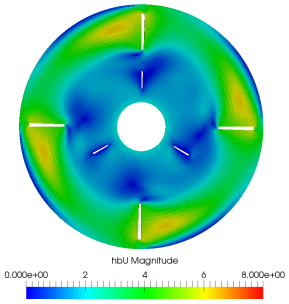

g): HB, $U_{ul} = 2\text{m/s}$**,** $t = 48\text{s}$

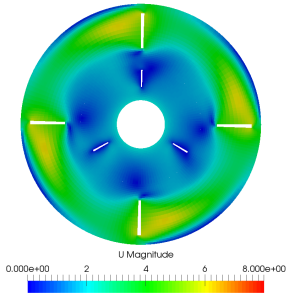

h): Tranz, $U_{ul} = 2\text{m/s}$**,** $t = 48\text{s}$

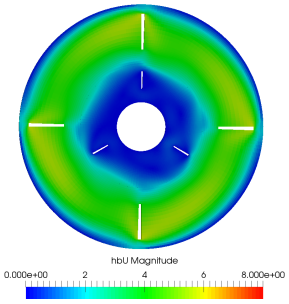

i): HB, $U_{ul} = 0\text{m/s}$**,** $t = 70\text{s}$

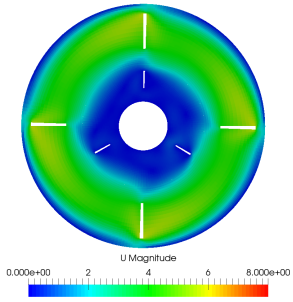

j): Tranz, $U_{ul} = 0\text{m/s}$**,** $t = 70\text{s}$

Slika 4: Polja brzine tijekom vremena.

Francis Turbina

U nastavku će biti prikazani rezultati simulacije pokretanja i zaustavljanja Francis turbine. Geometrija i eksperimentalni rezultati su dostupni u sklopu radionice Francis 99. Model turbine iz hidroelektrane Tokke korišten je za Francis 99 studiju. Model je izrađen u mjerilu 1:5.1. Rotor se sastoji od 15 lopatica pune duljine i 15 skraćenih lopatica; stator se sastoji od jednog stupnja nepomičnih lopatica, dok regulacijske lopatice čine drugi stupanj. Parametre modela prikazuje tablica 3. Slika 5 prikazuje reducirani model koji je korišten u simulacijama.

Tablica 3: Parametri modela i prototipa Francis 99 tubine.

	$H[m]$	$d_{ulaz}[m]$	$d_{izlaz}[m]$	$n[min^{-1}]$	$Q[m^3/s]$	$P[kW]$	$Re[-]$
Model	12	0.63	0.349	335	0.2	22	$1.8x10^6$
Prototip	377	3.216	1.779	375	31	110000	$4.1x10^7$

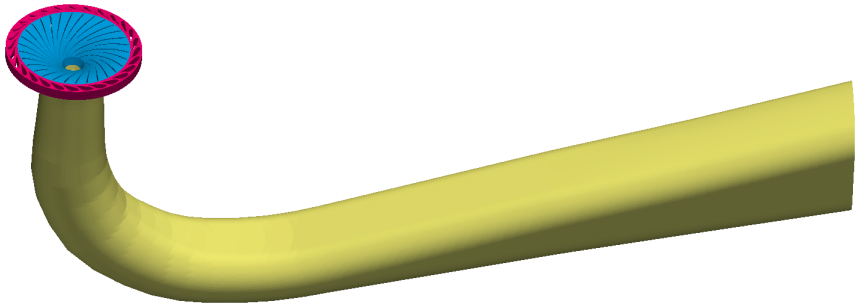

Slika 5: Reducirani model.

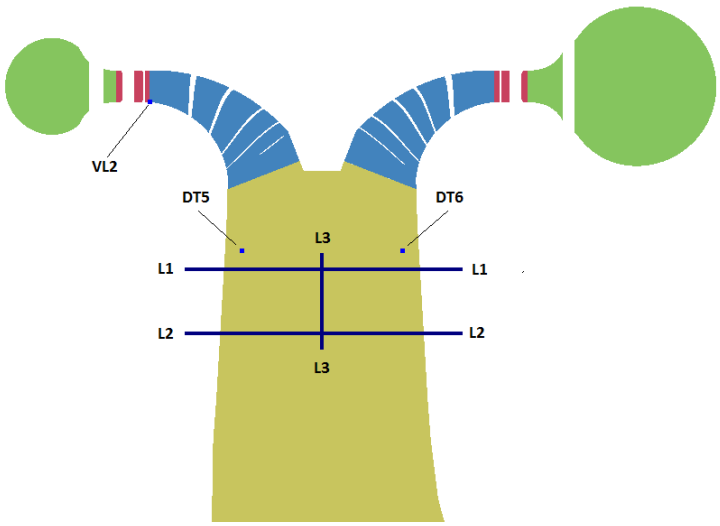

Slika 6: Pozicije mjernih mjesta tlaka i brzina.

Na slici 6 se mogu vidjeti lokacije na kojima su mjereni tlak i brzina tijekom eksperimenta.

Lokacije VL2, DT5 i DT6 označavaju mjesta na kojima je mjeren tlak dok linije L1, L2 i L3 označavaju linije na kojima je mjeren brzina.

Mreža kontrolnih volumena rađena je u programu Pointwise [4]. Mreža se sastoji od tri regije: regulacijske lopatice, rotor i izlazni kanal. Broj ćelija u svakoj regiji i ukupan broj ćelija dani su u tablici 4. Na Slici 7 prikazana je mreža kontrolnih volumena za određene dijelove geometrije.

Tablica 4: Veličina mreže konačnih volumena.

Zone	Number of cells
Regulacijske lopatice	1 764 980
Rotor	4 047 225
Izlazni kanal	430 474
Ukupno	6 242 679

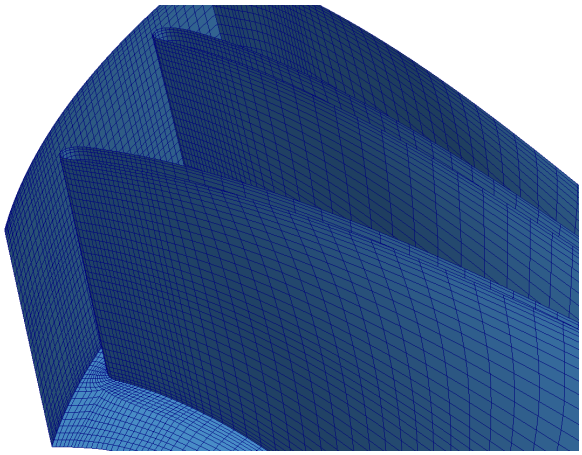

a): Lopatice rotora,

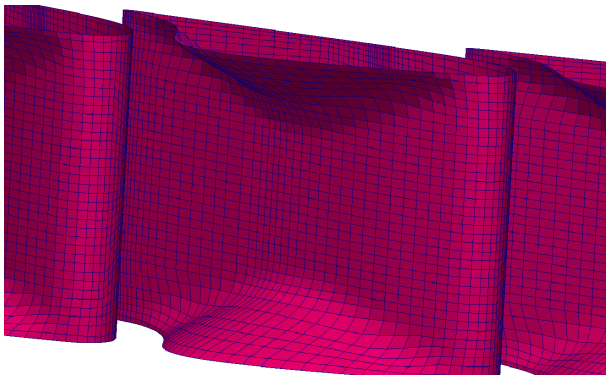

b): Regulacijske lopatice,

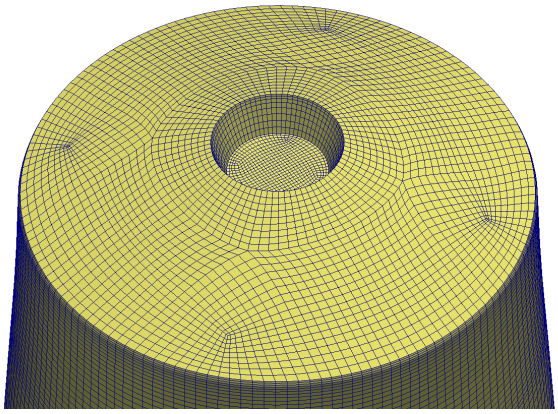

c): Granica između rotora i izlaznog kanala,

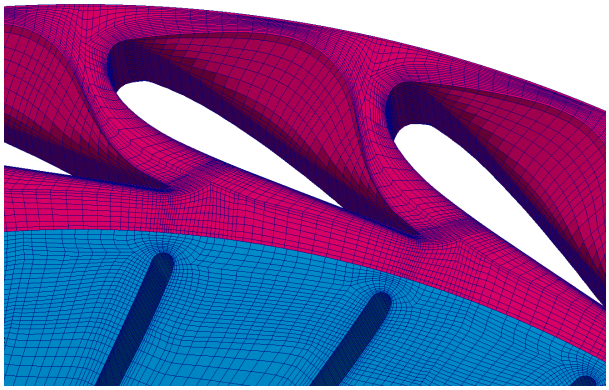

d): Granica između rotora i regulacijskih lopatica.

Slika 7: Prikaz mreže kontrolnih volumena.

Prvo su napravljene simulacije nazivne radne točke budući da je u tom režimu rada dostupno najviše eksperimentalnih rezultata, a i objavljeno najviše članaka. Kod simulacija nazivne

radne točke na ulazu u domenu zadana je brzina strujanja, dok je za tlak zadan nulti gradijent. Na izlaznoj površini zadana je vrijednost tlaka od 0 $[m^2/s^2]$. Na ulazu su zadane vrijednosti turbulentnih veličina k i ε. Izračunate su kao funkcija poznate brzine na ulazu i uz pretpostavku intenziteta turbulencije od I = 7,24%. Broj okretaja rotora je konstantan, 333 min^{-1} . Rezultati integralnih vrijednosti prikazani su u tablici 5. Visina tlaka H, snaga turbine P i efikasnost η definirane su prema sljedećim izrazima:

$$H = \frac{\Delta p_0}{\rho g} = \frac{\Delta p}{\rho g} + \frac{v_i^2 - v_o^2}{2g} + \Delta z; \quad P = \omega \tau; \quad \eta = \frac{\omega \tau}{\Delta p_0 Q}; \tag{26}$$

Tablica 5: Usporedba integralnih vrijednosti.

	P [W]	H [m]	η [%]
Eksperiment	21 617	11.94	92.39
Simulacija	22 457	11.53	94.40
Odstupanje	3.74%	3.43%	2.13%

Tablica 6: Usporedba vrijednosti tlaka u mjernim točkama.

Mjerne točke	VL2	DT5	DT6
Eksperimentalni tlak, [kPa]	173.60	105.01	104.80
Izračunati tlak, [kPa]	170.43	109.53	109.15
Odstupanje	1.80%	4.12%	3.98%

Također je napravljena usporedba vrijednosti tlaka u mjernim točkama. Vrijednosti izmjerenih tlakova te odstupanja prikazani su u tablici 6. Iz tablica 5 i 6 može se vidjeti da su rezultati dobiveni metodom harmonijske ravnoteže vrlo slični eksperimentalnim rezultatima. Polje brzine na mjestu interakcije rotora i statora prikazano je na Slici 8.

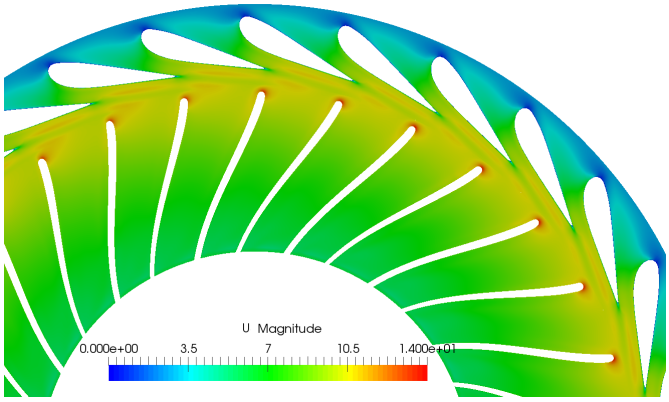

Slika 8: Polje brzine u rotoru.

Nakon što su prikazani rezultati simulacija za nazivnu radnu točku, sada ćemo prikazati rezultate simulacija za proces pokretanja i zaustavljanja Francis turbine. Postavke rubnih uvjeta su jednake kao i za nazivnu radnu točku, samo se vrijednosti mijenjaju. Promjena brzine na ulazu mijenja se u skladu s promjenom protoka. Eksperimentalni podaci dostupni na radionici Francis 99 nisu točni budući da mjerni uređaj nije mogao precizno mjeriti promjenu protoka [1]. Zbog toga eksperimentalisti preporučuju da se promjena protoka računa linearno kako je prikazano na Slici 9. Uzimajući to u obzir, na Slici 10 prikazan je konačan profil promjene ulazne brzine tijekom procesa pokretanja i zaustavljanja. Kako se može vidjeti sa slike, prvih 2.1s turbina radi u nazivnoj radnoj točci. Nakon toga počinje proces zaustavljanja koji traje 7s. Kada se turbina zaustavila do točke minimalnog opterećenja prestaje proces zaustavljanja i održava se ta točka sljedećih 1.4s. Poslije toga započinje proces ponovnog pokretanja koji također traje 7s nakon čega je turbina ponovno u nazivnoj radnoj točci i održava se tu sljedećih 0.7s. Budući da za proces pokretanja i gašenja koristimo 6 harmonika sa simetričnim vremenskim trenutcima, potrebno je izračunati "male" simulacije za sedam različitih vrijednosti rubnih uvjeta popisanih u tablici 7.

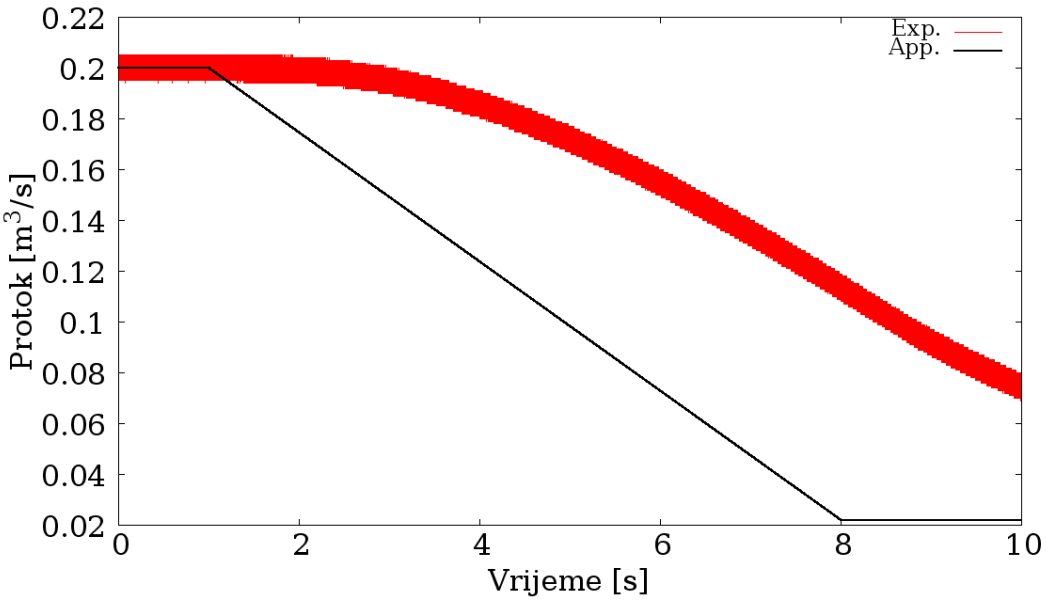

Slika 9: Promjena protoka tijekom procesa zaustavljanja.

Tablica 7: Rubni uvjeti za proces pokretanja i zaustavljanja.

Varijabla	Točka 1	Točka 2	Točka 4	Točka 3	Točka 5	Točka 6	Točka 7
U_r [m/s]	1.413	1.287	1.036	0.784	0.533	0.281	0.156
U_t [m/s]	2.118	1.930	1.553	1.176	0.799	0.422	0.233
k [m^2/s^2]	0.052	0.042	0.027	0.016	0.007	0.002	0.0006
ε [m^2/s^3]	25.535	16.938	7.101	2.321	0.495	0.038	0.004

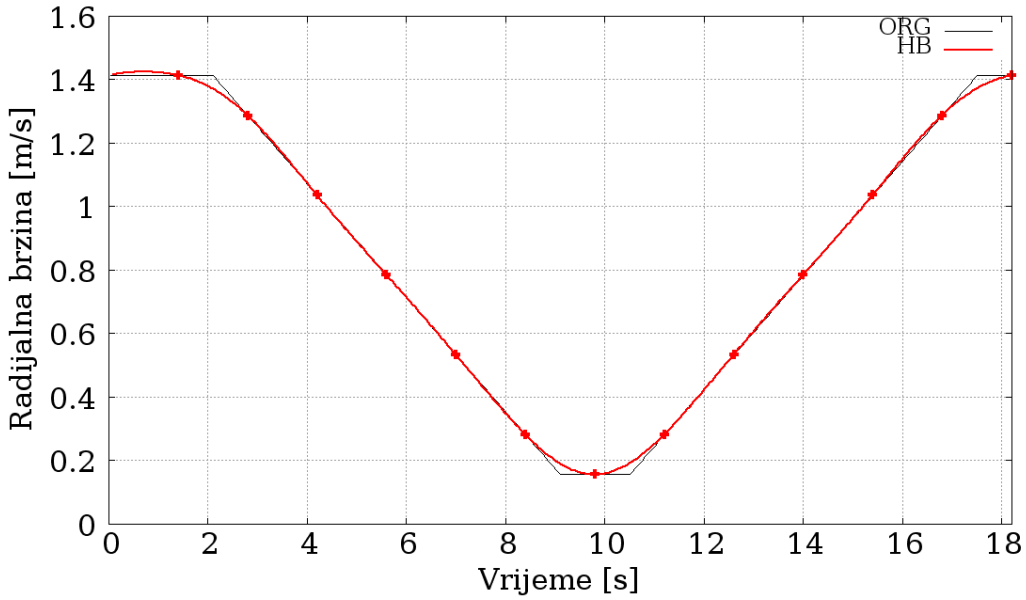

Slika 10: Promjena ulazne brzine tijekom procesa pokretanja i zaustavljanja.

Na slici 11 uspoređeni su tlakovi dobiveni eksperimentalno i u simulacijama. Vidi se da u oba slučaja tlak prati isti trend te da rezultati simulacija odstupaju oko 4% od eksperimentalnih rezultata što je slično kao i odstupanja dobivena za nazivnu radnu točku. Na slici 12 je prikazana pojava "vortex rope" koja je karakteristična za strujanja van nazivne radne točke. Prikazan je u četiri različita vremenska trenutka tijekom proces zaustavljanja turbine. Može se vidjeti da je pri većim protocima "vortex rope" manji, ali ima veću radijalnu brzinu dok se pri malim protocima ustabili. Ovim simulacijama provjerene su pretpostavke korištene metode te potvrđena njezina valjanost.

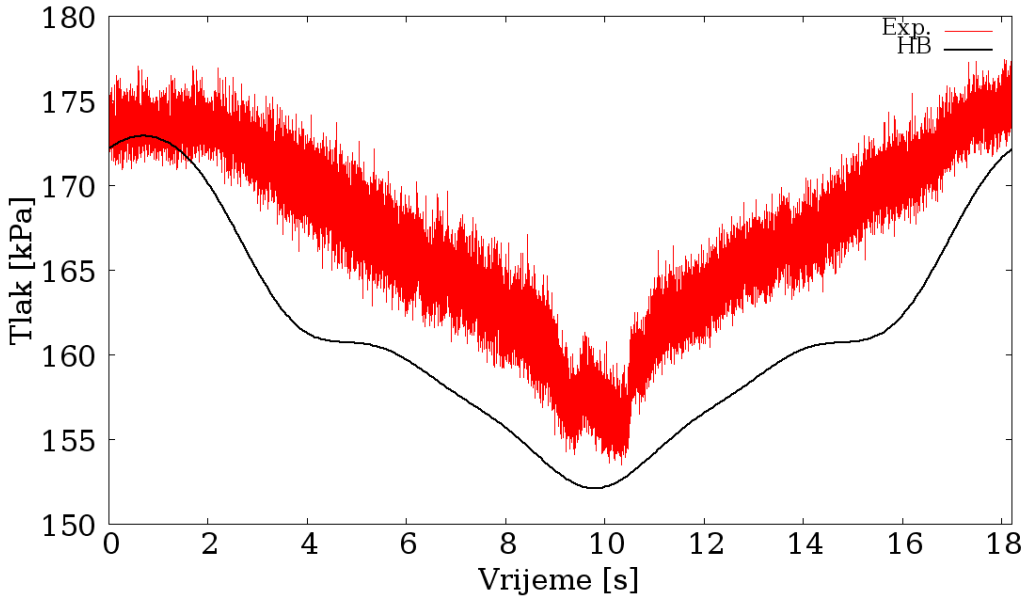

Slika 11: Tlak tijekom vremena u točci VL2.

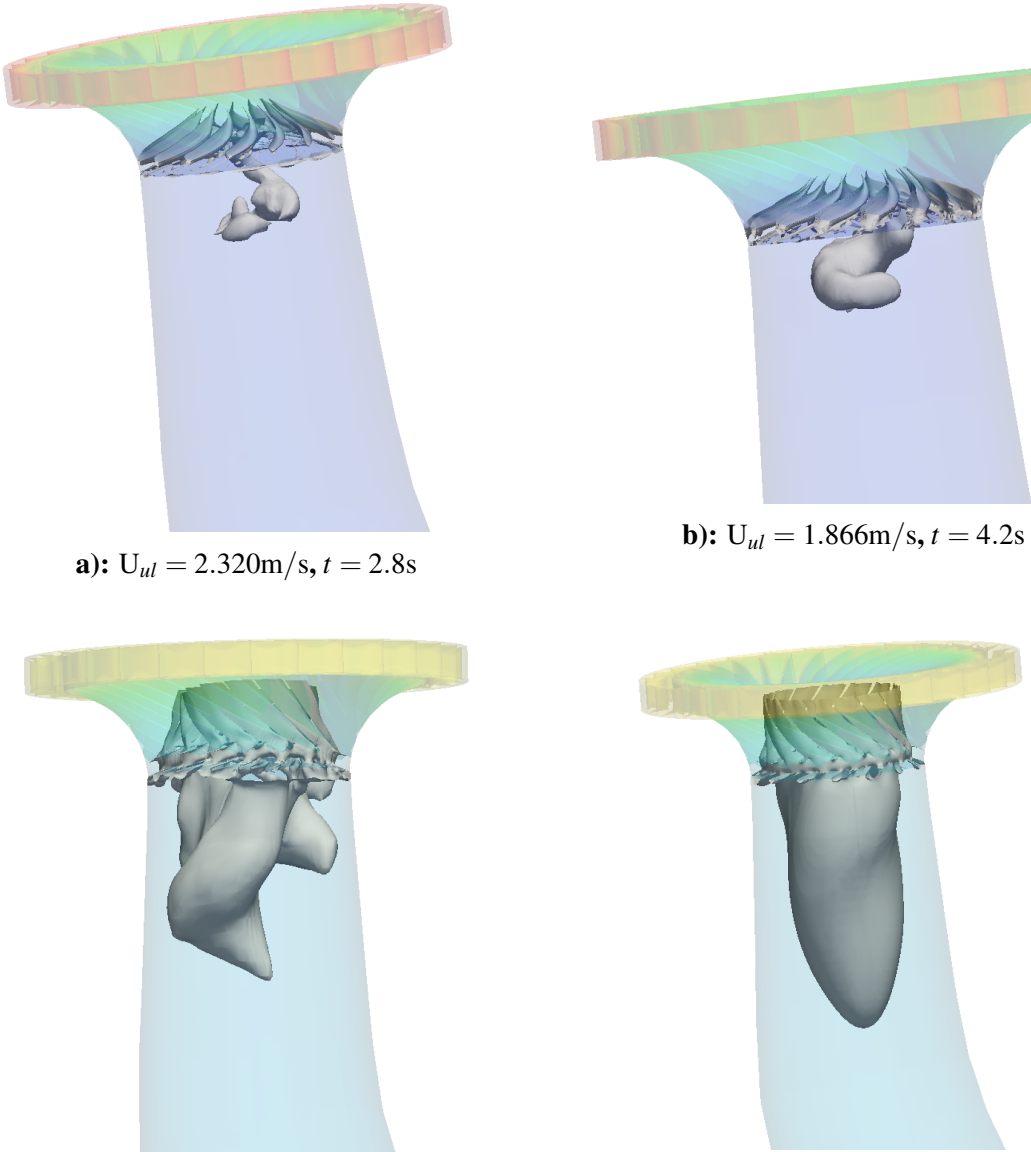

a): $U_{ul} = 2.320\text{m/s}$, $t = 2.8\text{s}$

b): $U_{ul} = 1.866\text{m/s}$, $t = 4.2\text{s}$

c): $U_{ul} = 0.507\text{m/s}$, $t = 8.4\text{s}$

d): $U_{ul} = 0.281\text{m/s}$, $t = 9.8\text{s}$

Slika 12: Formiranje "vortex rope" tijekom vremena.

Zaključak

Prikazani rezultati numeričke simulacije procesa pokretanja i zaustavljanja pokazuju zadovoljavajuću točnost u usporedbi s eksperimentalnim mjerenjima. Ne samo u globalnim vrijednostima već i u detaljima strujanja kao što je tlak u međulopatičnom prostoru. Također je prikazana i usporedba s dosadašnjim metodama, iz koje se vidi da je metodi harmonijske ravnoteže potrebno znatno kraće vrijeme za izračun procesa pokretanja i zaustavljanja.

1 Introduction

Aiming to reduce both the carbon footprint and dependency on imported fossil fuels, many countries, primarily in the European Union, implemented the feed-in tariff systems over the past decade to encourage investment in new and renewable electricity supply. These changes in European electricity markets have brought a new reality for hydro-power plants.

The global hydropower capacity reached more than 1135 GW by the end of 2013, and it increases by 4% every year [5]. The imbalance between electricity demand and generation often disrupts the power grid. Governmental incitation for alternative renewable and sustainable energy, such as wind and solar energy, has increased grid disruption because such system do not produce electricity according to demand [6].

The focus of technological development today is to increase the efficiency and flexibility. Higher efficiency is essential not only because it is economical but it is also ecological. On the other hand, flexibility ensures that machine is not efficient only in one operating point, but through a high range of operating points, which is especially important considering that wind turbines are being dominant source of renewable energy. Therefor, a new task assigned to hydro-power plants in volatile electric grid, is to regulate power. This new task has resulted in more frequent load variations, faster response time, emergency shut-downs and restarts, total load rejection events and overall off-design operation at prolonged time. Most hydroturbines, especially those of the Francis type are not designed with unsteady operation in mind, both in term of efficiency and reliability of the machines.

A turbine runner experiences unsteady pressure loading during changing operating conditions because the runner's angular speed and, simultaneously, the discharge into the runner are varying. The variation causes large pressure differences on blade surfaces. The pressure difference increases with angular movements of the guide vanes and results in asymmetric stresses on the surfaces [7]. Over time, a runner may sometimes experience a resonance condition. Surprisingly, no pressure measurement is reported in the literature for such transient conditions, specifically inside the turbine, despite the fact that the transients significantly affect the operating life of the runner [8].

1.1 Start-Up and Shut-Down

In order to increase the efficiency and flexibility of turbomachinery, not only a single operating point but rather a whole range of operating points needs to be optimized, especially at start-up and shut-down. Depending on the type of tubomachinery, different start-up and shut-down procedures are used. During startup, the gas turbine undergoes a sequence of increasing compressor spin to reach firing speed: ignition, turbine acceleration to self-sustaining speed, synchronization, and loading. There are numerous thermo-mechanical constraints during startup of the gas turbine, including limits on airflow velocity through the

compressor blades to prevent stall, vibrational limits, and combustion temperature limits to prevent turbine blade fatigue. On the other hand, if pump start-up is investigated, the pump must be filled with liquid up to the level where the impeller and casing are flooded since the pressure rise created by impeller operating in air is virtually zero due to the low density.

Since turbines cannot produce torque at zero speed, the starting mean system is used to start the gas turbine rolling, crank it to firing speed and assist the fired turbine to reach the self-sustaining speed. That is accomplished by a motor or a generator. This arrangement provides the cranking torque for turbine start-up and during shut-down this continues to rotate the turbine rotor at slow speed for cool-down purposes. Depending on the size of the turbomachine, start-up and shut-down processes can least from few seconds up to the few hours. In order to simulate the flow during these procedures and consequently increase the efficiency, a new approach is developed in this thesis.

1.2 Computational Fluid Dynamics

The fundamental basis of almost all CFD problems are the Navier–Stokes equations. Historically, methods were first developed to solve the linearized potential equations. Two-dimensional (2D) methods, using conformal transformations of the flow about a cylinder to the flow about an airfoil were developed in the 1930s [9]. Probably the first work using computers to 3D model the fluid flow, as governed by the Navier-Stokes equations, was performed at Los Alamos National Lab in 1960s [10].

One of the biggest advantages of the Computational Fluid Dynamics (CFD) analysis is that pressure and velocity fields are known in each point of modeled domain. That is very useful in order to determine forces that affect turbine during changing operating conditions. In this thesis, `foam-extend` is used, which is the fork of the open source CFD software OpenFOAM [11]. With open source software the code is available to the user, allowing him to learn how it works and write new code for his own purposes. Methods, which are used for calculation of transient phenomenon up to now, are very expensive. In other words, they require a lot of processor time. Task of this thesis is to evaluate usage of new method, called Harmonic balance (HB), in order to reduce the time of calculations, while still providing accurate results.

1.3 The Francis 99 Workshop

Francis-99 is a series of three workshops [1], which provide an open access to complete design and data of a model Francis turbine. It provides an open platform to the hydropower researchers and it gives them the possibility to explore their capabilities and enhance their skills. It is organized by the Norwegian University of Science and Technology (NTNU) and Luleå University of Technology (LTU). Organizers of these workshops provided large amount of technical documentation concerning geometry and working regime of the turbine.

Experimental data is also provided, with a lot of effort put in data assembly, so that simulations can be easily compared to it. Experiments were conducted at the Water-power Laboratory at NTNU in Trondheim, Norway on the scale model of Tokke high head Francis turbine [1].

Steady turbine operation at both the best efficiency point and off-design conditions were investigated within the first workshop. The second workshop examined effects of the transient operating conditions on the turbine, while the third workshop is planed to add further challenge by aiming at coupled fluid-structure interaction simulations.

1.4 Thesis Outline

This thesis is organised as follows. Section 2 serves as an introduction to the governing equations of incompressible fluid flow that are later modeled in terms of the Harmonic Balance method. Boundary conditions are covered at the end of Section 2 with GGI boundary condition described in more detail. Section 3 presents the Harmonic Balance method which is later used to resolve transient flows in the turbine. First, Fourier transformation is described as it is the foundation of the Harmonic Balance method. The Harmonic Balance method is derived with the Finite Volume implementation. At the end of Section 3, the novel Harmonic Balance approach for start-up and shut-down is described. In Section 4, a simple test case is presented, purpose of which is to provide comparison between existing method for transient flows and method developed in this thesis. Section 5 shows the geometry of the Francis turbine provided at Francis 99 workshop. In Section 6 the numerical simulations, for turbine start-up and shut-down, are presented and at the end of this section a comparison with experimental results is shown. Section 7 gives an overview of the thesis with a final conclusion.

2 Mathematical Model

In this chapter, the mathematical model used to describe of transient, incompressible and turbulent flow in rotating machinery will be presented. The first part is focused on the general description of the equations that are implemented in `foam-extend` [2]. In the second part, another important factor for obtaining the unique solution, boundary conditions are presented. Furthermore, the General Grid Interface (GGI) method for connecting multiple domain regions is described as well.

2.1 Governing Equations of Fluid Flow

The cornerstone of CFD are the fundamental governing equations of fluid dynamics - the continuity, momentum and energy equations which can be derived from the basic scalar transport equation. Although each fluid has different properties and behavior, these equations are general and can be applied to any fluid and any flow situation, therefore standard form can be expressed as [3]:

$$\underbrace{\frac{\partial \phi}{\partial t}}_{\text{Transient term}} + \underbrace{\nabla \cdot (\phi \mathbf{u})}_{\text{Convection term}} - \underbrace{\nabla \cdot (\gamma \nabla \phi)}_{\text{Diffusion term}} = \underbrace{q_v}_{\text{Source term}} , \tag{2.1}$$

where ϕ is concentration of a transported scalar variable, $\mathbf{u}$ is the convective velocity, γ is the diffusion coefficient and q_v is an arbitrary local volume source or the sink of a transported scalar ϕ.

In Eqn. 2.1 all four terms represent different physical phenomena:

- the transient term accounts for the accumulation of ϕ in the concerned control volume,
- the convection term accounts for the transport of ϕ due to the existence of the velocity field,
- the diffusion term accounts for the transport of ϕ due to its gradients,
- the source term accounts for any sources or sinks that cause either creation or destruction of ϕ.

Diffusion term has an elliptic nature of the Partial Differential Equation (PDE), which means that every cell in the domain feels the influence of every other cell instantaneously. On the other hand, convection term has a hyperbolic nature of the PDE meaning that cell information is defined by the direction of the convective velocity [12].

The fundamental governing equations of fluid dynamics can be derived simply by substituting the transported scalar variable ϕ in Eqn. 2.1 with the relevant property. Considering that the energy equation can be decoupled from the flow equation in incompressible turbulent flows, it is neglected.

2.1.1 Conservation of Mass

The conservation of mass is one of the basic principles of continuum mechanics and it states that for any system without any kind of transfer, the mass of that system must remain constant over time, hence the quantity of mass is conserved over time. So if we substitute transported scalar variable ϕ in Eqn. 2.1 with the density ρ and set the source term to zero we obtain the following equation:

$$\frac{\partial \rho}{\partial t} + \nabla \cdot (\rho \mathbf{u}) = 0, \tag{2.2}$$

considering that for the incompressible flow we can neglect change of the density ρ, the final equation is obtained:

$$\nabla \cdot \mathbf{u} = 0. \tag{2.3}$$

2.1.2 Conservation of Linear Momentum

Equation for the conservation of linear momentum can be derived similarly as described for conservation of mass, but now we replace transported scalar variable ϕ with the product of density and velocity $\rho\mathbf{u}$:

$$\frac{\partial \rho \mathbf{u}}{\partial t} + \nabla \cdot (\rho \mathbf{u} \otimes \mathbf{u}) = \rho \mathbf{g} + \nabla \cdot \sigma, \tag{2.4}$$

where $\mathbf{u}$ is the velocity field, ρ is the density of the fluid, $\mathbf{g}$ is gravitational acceleration, and σ is the Cauchy stress tensor.

On the right hand side of Eqn. 2.4 is a source term which represents the sum of body forces ($\nabla \cdot \sigma$) and mass forces ($\rho\mathbf{g}$). Cauchy stress tensor σ, which is included in body forces, consists of pressure p and a viscous tensor τ:

$$\sigma = -p\mathbf{I} + \tau, \tag{2.5}$$

again if we consider only incompressible flow, than Eqn. 2.4 can be rewritten as:

$$\frac{\partial \mathbf{u}}{\partial t} + \nabla \cdot (\rho \mathbf{u} \otimes \mathbf{u}) - \nabla \cdot (\nu \nabla \mathbf{u}) = \mathbf{g} - \nabla p, \tag{2.6}$$

where $\mathbf{u}$ is velocity field, ρ is density of the fluid, ν represents kinematic molecular viscosity, $\mathbf{g}$ is gravitational acceleration, and p is the kinematic pressure.

2.2 Boundary Conditions

Boundary conditions are used to isolate the system from the external environment and they can be classified as either numerical or physical boundary conditions. Physical boundary conditions relate to the domain shape so we can isolate the area for which calculations will be carried out. On the other hand, numerical boundary conditions are considered at the equation level in order for a system of partial differential equations to have a unique solution [12]. Boundary conditions have to be prescribed for each variable on domain boundaries, and to be able to do so correctly, deep understanding of the problem is required.

There are two main types of boundary conditions: Dirichlet and von Neumman boundary condition. the difference between those two is that Dirichlet boundary condition prescribes a fixed value for the transported scalar variable ϕ on the determined boundary, while von Neumman boundary condition prescribes the gradient of the transported scalar variable ϕ normal to the boundary. Other than those two, there are many other boundary conditions, known as mixed boundary conditions, but they are linear combination of the two numerical conditions mentioned, Dirichlet and von Neumman.

Most commonly used boundaries in the CFD are inlet, outlet, wall and symmetry. In order to solve the system of PDEs mentioned earlier in this section, boundary conditions need to be prescribed to those boundaries. In most cases, Dirichlet and von Neumman numerical boundary conditions are used in pair. For example, it is usual for inlet to have Dirichlet numerical boundary condition for the velocity and von Neumman numerical boundary condition for the pressure, while it is opposite for the outlet, Dirichlet numerical boundary condition for the pressure and von Neumman numerical boundary condition for the velocity. The same applies to wall, velocity on the wall is zero (there is no flux through the wall) and because of that Dirichlet numerical boundary condition is implemented for the velocity, while von Neumman numerical boundary condition is specified for the pressure. Symmetry boundary condition is used to reduce the computational domain and thereby simplify the problem. There are also many other boundary conditions used to simplify the problem and one important for this work, the GGI boundary condition, will be described in more detail in the next subsection.

2.3 General Grid Interface

Conformal periodic conditions, with identical mesh topology on coupled patches, are very often avoided in turbomachinery cases, because in stationary turbomachinery simulations, it is usually required very large number of cells to be able to achieve identical mesh. For nonstationary turbomachinery simulations, the relative rotation of mesh parts will necessarily produce non conformal interfaces between the fixed and moving sections. These problems and the patch-o-patch interpolation are solved by using the GGI boundary condition, available in `foam-extend` package.

GGI is a coupling interface used for joining two non-conformal patches [13]. The GGI connection is done in a conservative and implicit fashion, even if the nodes on the two sides of the connection are not aligned. In comparison to other coupling methods, such as mixingPlane, flow values are transfered across the patch without being averaged, however, in order to achieve a conservative discretization, weighting factors must be determined.

In Fig. 2.1 two regions are shown, consisting of guide vanes and runner, with mismatching topology on neighboring patches, where the GGI boundary condition is used to pass the information between two regions.

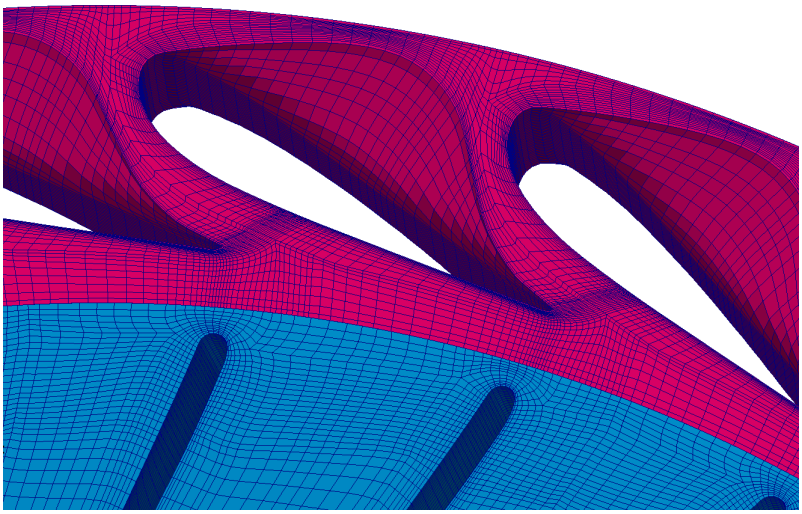

Figure 2.1: Mismatching topology between regions.

2.4 Closure

This chapter covered fundamental mathematical model used for modeling transient, incompressible and turbulent flow in the rotating machinery. Boundary conditions are briefly described with emphasis on the GGI boundary condition. In the next section, the mathematical model used for the description of the Harmonic Balance Method is described, with notes on implementation of the Harmonic Balance Method for start-up and/or shut-down of the rotating turbomachinery.

3 Harmonic Balance Method

In this section a review of the most common HB formulation will be made, after which its application to unsteady nonlinear turbulent periodic flows will be presented. First, Fourier series expansion is introduced. It is the mathematical background which whole HB method is based on. Subsequently, the HB method is described in detail. After the description of the HB method, scalar transport equation and governing equations of fluid flow will be presented in the HB form. Finally, implementation of the HB method for the start-up and/or shut-down of the rotating turbomachinery is described.

3.1 Introduction

Initially, HB was developed by He [14] as a boundary condition with clear task: to capture accurate transient flow features while still maintaining a reasonable computational cost. In comparison to conventional steady state methods, HB is able to capture transient behavior. Furthermore, it is less time consuming in comparison to transient simulations, which needs to calculate a large number of time steps in order to obtain periodic steady state. Periodic steady state means that the difference between two successive periods is small, within a required tolerance, and in some cases a large number of periods are required to obtain that tolerance [15].

The HB method, instead of using original transient mathematical model, solves a number of temporally-coupled steady state problems, and each of these problems represents one time instant within a period. This transformation from transient to temporally-coupled steady state is achieved by Fourier series expansion, suggesting that the frequency of the motion should be know in advance, while the number of harmonics is arbitrary. Before choosing the number of harmonics, two things must be taken into the consideration. First, the number of harmonics dictates the accuracy, as higher order effects get neglected, and second thing, larger number of harmonics means more equations to solve, thus resulting in higher CPU time. As mentioned before, HB solutions are obtained just for the predefined number of time instants within a representative period, but any time instant can be reconstructed as a post processing step. This is a useful tool in order to compare HB solution to transient solution.

Applications of HB are widely used in turbomachinery, where rotor and stator interactions can be resolved without long transient simulations [16] and also for wave simulations in marine engineering [17] and various other problems such as edge tone and vortex shedding [18], oscillating wings [19], opening and closing valves, etc. In theory, any behavior that shows signs of temporal periodicity can be simulated using the HB method.

3.2 Fourier Series

A Fourier series is an expansion of a periodic function $f(x)$ in terms of an infinite sum of sines and cosines and it makes use of the orthogonality relationship of the sine and cosine functions. It is extremely useful as a way to break up an arbitrary periodic function into a set of simple terms that can be solved individually and then recombined to obtain the solution of the original problem or an approximation to a desired accuraccy [20].

If $f(x)$ is a function of the real variable x and it is integrable on an interval $[x_0, x_0+T]$, where T is a repeating period of $f(x)$, then Fourier expansion reads:

$$f(x) = a_0 + \sum_{n=1}^{\infty} \left(a_n cos\left(\frac{2\pi nx}{T}\right) + b_n sin\left(\frac{2\pi nx}{T}\right)\right), \quad x \in [x_0, X_0+T]. \tag{3.1}$$

Considering that function $f(x)$ repeats with period T, the expansion is invariant of the interval chosen. In Fig. 3.1, it can be seen how different parts in Eqn. 6.1, mean value, sine and cosine terms, affect the final solution for one harmonic case.

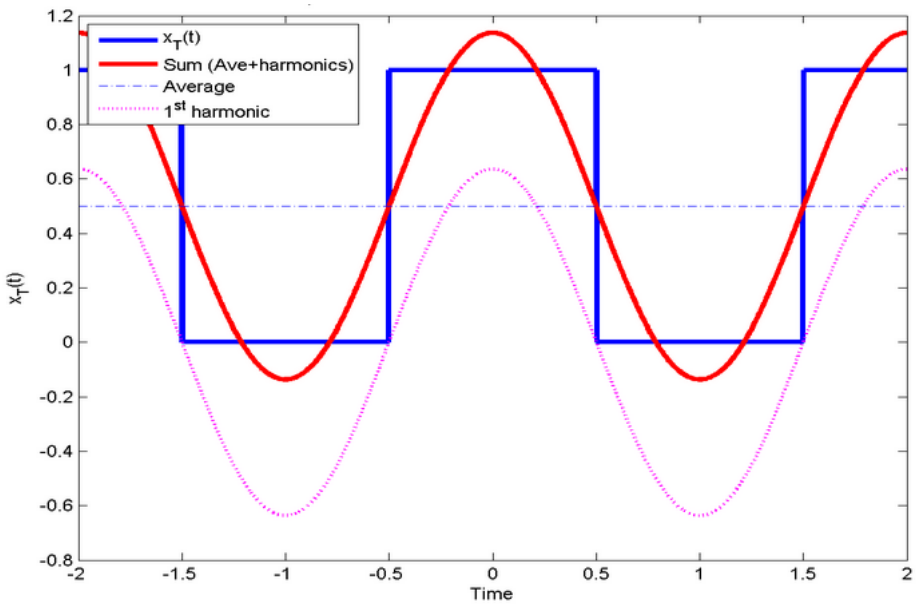

Figure 3.1: Effect of different parts of Eqn. 6.1 on the solution [21].

Coefficients a_n and b_n are called Fourier coefficients, and can be calculated using the following equations:

$$a_n = \frac{2}{T}\int_{x_0}^{x_0+T} f(x) cos\left(\frac{2\pi nx}{T}\right) dx, \tag{3.2}$$

$$b_n = \frac{2}{T}\int_{x_0}^{x_0+T} f(x)sin\left(\frac{2\pi nx}{T}\right)dx. \tag{3.3}$$

The sum in from Eqn. 6.1 is infinite, but this is not usable in CFD. We therefore need to restrict the integral limits in Eqn. 6.1 to a finite sum, but by doing that we are also reducing the accuracy of the solution. With a finite sine and cosine terms, time needed for calculation is shorter but results are less accurate. These two things need to be considered to find a compromise between accuracy and calculation time in order to obtain satisfactory results. The following equation represents a finite form of Eqn. 6.1:

$$f(x) \approx a_0 + \sum_{n=1}^{N}\left(a_n cos\left(\frac{2\pi nx}{T}\right) + b_n sin\left(\frac{2\pi nx}{T}\right)\right), \quad x \in [x_0, X_0+T], \tag{3.4}$$

where the upper limit N stands for number of harmonics. Expansion with N harmonics will have $2N+1$ terms: N sine terms, N cosine terms and the mean value. a_0 is the zeroth harmonic and it represents the mean value, while nth harmonic of Fourier series is:

$$f_n(x) = a_n cos\left(\frac{2\pi nx}{T}\right) + b_n sin\left(\frac{2\pi nx}{T}\right), \quad x \in [x_0, X_0+T]. \tag{3.5}$$

Amplitude of the nth harmonic is:

$$A_n = \sqrt{a_n^2 + b_n^2}, \tag{3.6}$$

and its square root A_n^2 is called the energy of the nth harmonic.

In Fig. 3.2 a square wave, triangle wave, sawtooth wave and semicircle functions are approximated with the different number of harmonics and it can be concluded that with the increase in the number of harmonic, approximation is becoming more accurate.

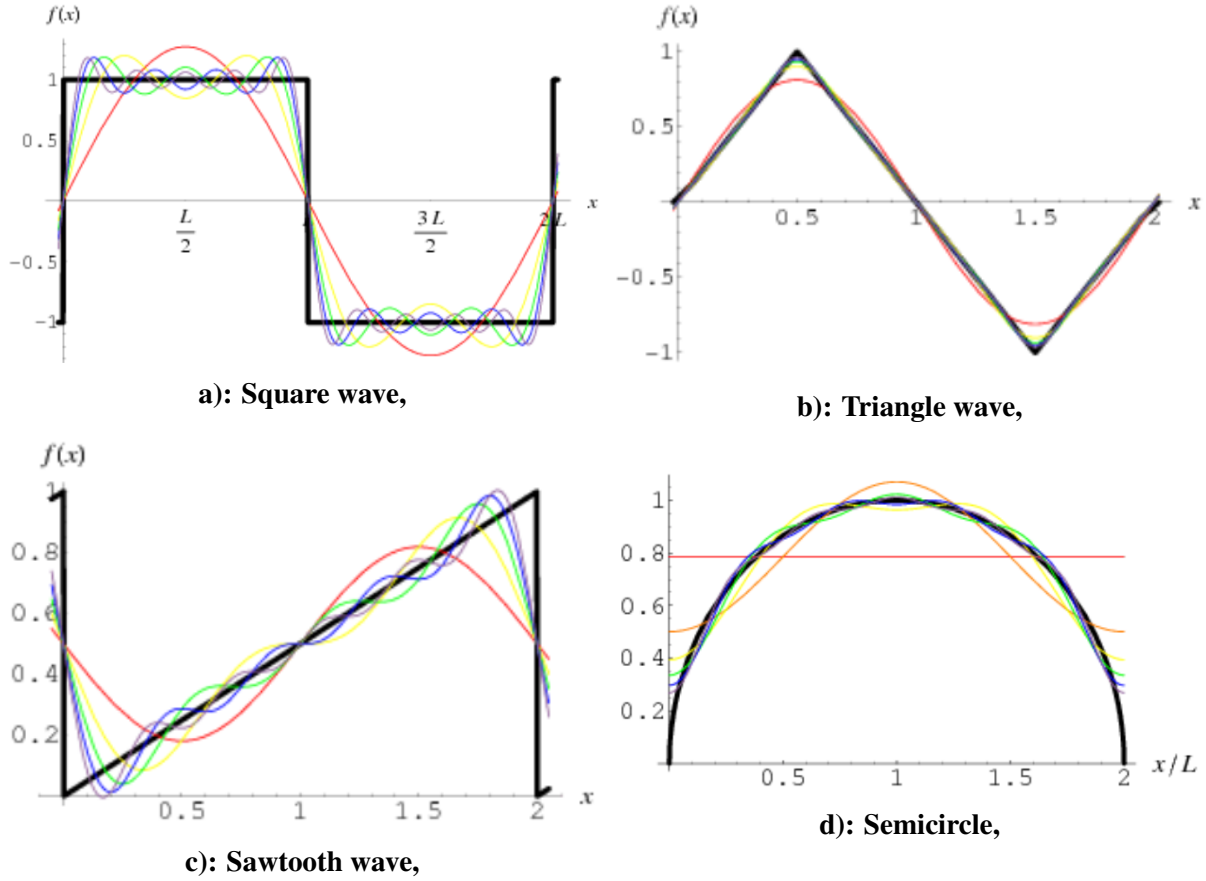

a): Square wave,

b): Triangle wave,

c): Sawtooth wave,

d): Semicircle,

Figure 3.2: Approximation of wave functions with the different number of harmonics [20].

3.3 Scalar Transport Equation in Harmonic Balance Form

In the previous subsection Fourier series was introduced and here it will be used for a detailed derivation of the HB method for a passive scalar transport equation. By assuming that each primitive variable can be accurately represented by Fourier series in time, using first n harmonics and a mean value, it will be shown that HB method needs to solve $2n+1$ steady-state problems rather than just one transient problem. Since the incompressible flow pressure equation is elliptic, only momentum equation will be transformed using HB method, while pressure equations for all time instants remain in original form. The derivation follows the work of [15].

Under assumption of periodicity, scalar transport equation is:

$$\frac{\partial \mathscr{Q}}{\partial t} + \mathscr{R} = 0, \tag{3.7}$$

where $\mathscr{R}$ is a condensed way of writing convective, diffusive and source terms:

$$\mathscr{R} = \nabla \cdot (\mathbf{u}\mathscr{Q}) - \nabla \cdot (\gamma \nabla \mathscr{Q}) - S_{\mathscr{Q}}, \tag{3.8}$$

u is the transport velocity and γ is diffusivity. The primary variables $\mathscr{Q}$ and $\mathscr{R}$ can be written as a Fourier series with n harmonics:

$$\mathscr{Q} = Q_0 + \sum_{i=1}^{n} Q_{S_i} sin(i\omega t) + Q_{C_i} cos(i\omega t), \tag{3.9}$$

$$\mathscr{R} = R_0 + \sum_{i=1}^{n} R_{S_i} sin(i\omega t) + R_{C_i} cos(i\omega t), \tag{3.10}$$

Scripture characters, e.g. $\mathscr{Q}$, denote time domain variables while Q denotes frequency domain variables. As it can be seen from Eqn. 3.9 and Eqn. 3.10, the Fourier expansions for $\mathscr{Q}$ and $\mathscr{R}$ are analogous, with Q substituted by R. Insertion of $\mathscr{Q}$ and $\mathscr{R}$ into the standard transport equation, Eqn. 3.7, yields:

$$\sum_{i=1}^{n} i\omega (Q_{S_i} cos(i\omega t) - Q_{C_i} sin(i\omega t)) + \sum_{i=1}^{n} (R_{C_i} cos(i\omega t) + R_{S_i} sin(i\omega t)) = -R_0, \tag{3.11}$$

and it represents a scalar transport equation in the frequency domain. Subscripts S and C represent sine or cosine term and index i represents for which the harmonic coefficients are calculated. If we group terms with the same harmonic part in Eqn. 3.11, the following set of $2n+1$ equations is obtained.

- n equations for sine part:

$$-i\omega Q_{C_i} + R_{S_i} = 0, \quad \text{for} \quad i = 1 \dots n, \tag{3.12}$$

- one equation for the mean part:

$$R_0 = 0, \tag{3.13}$$

- and n equations for cosine part:

$$i\omega Q_{S_i} + R_{C_i} = 0, \quad \text{for} \quad i = 1 \dots n. \tag{3.14}$$

Equations Eqn. 3.12, Eqn. 3.13 and Eqn. 3.14 written in a more compact matrix form yield:

$$\omega \underline{\underline{A}}\,\underline{Q} + \underline{R} = \underline{0}, \tag{3.15}$$

where

$$\underline{\underline{A}} = \begin{bmatrix} & & & & & 0 & -1 & & & & & \\ & & & & & 0 & & -2 & & & & \\ & & 0 & & & . & & & -3 & & & \\ & & & & & . & & & & \ddots & & \\ & & & & & . & & & & & -n & \\ 0 & 0 & 0 & \dots & 0 & 0 & 0 & \dots & 0 & 0 & 0 & \\ 1 & & & & & . & & & & & & \\ & 2 & & & & . & & & & & & \\ & & 3 & & & . & & & 0 & & & \\ & & & \ddots & & 0 & & & & & & \\ & & & & n & 0 & & & & & & \end{bmatrix}, \underline{Q} = \begin{bmatrix} Q_{C_1} \\ Q_{C_2} \\ Q_{C_3} \\ \vdots \\ Q_{C_n} \\ Q_0 \\ Q_{S_1} \\ Q_{S_2} \\ Q_{S_3} \\ \vdots \\ Q_{S_n} \end{bmatrix}, \underline{R} = \begin{bmatrix} R_{C_1} \\ R_{C_2} \\ R_{C_3} \\ \vdots \\ R_{C_n} \\ R_0 \\ R_{S_1} \\ R_{S_2} \\ R_{S_3} \\ \vdots \\ R_{S_n} \end{bmatrix}. \tag{3.16}$$

If Eqn. 3.15 wants to be solved, differential operator $\underline{R}$ would need to be transformed from time into frequency domain, and that is not desirable. In order to resolve the problem in a clearer matter, the Discrete Fourier Transform (DFT) matrix operator $\underline{\underline{E}}$ will be used to transform Eqn. 3.15 from frequency to time domain. First, the discrete time-domain vector will be defined, so we can have a unique one-to-one mapping:

$$\underline{\mathscr{Q}}^T = [\mathscr{Q}_{t_1} \quad \mathscr{Q}_{t_2} \quad \mathscr{Q}_{t_3} \quad \dots \quad \mathscr{Q}_{t_{2n+1}}], \tag{3.17}$$

where t_i stands for:

$$t_i = \frac{iT}{2n+1}, \quad \text{for} \quad i = 1 \dots 2n+1. \tag{3.18}$$

If we compute time steps from Eqn. 3.18, it can be observed that following substitution applies:

$$t_2 = 2t_1, \quad t_3 = 3t_1, \quad \dots \quad t_n = nt_1, \tag{3.19}$$

Now, components of the discrete time-domain vector $\underline{\mathscr{Q}}$ will be calculated and for the simplicity of the calculation only one harmonic will be used. For one harmonic, we will have three components calculated in three equally spaced time steps within period T, and it can be

obtained from Eqn. 3.18:

$$\begin{aligned}\mathscr{Q}_{t_1} &= Q_0 + Q_S\sin(\omega t_1) + Q_C\cos(\omega t_1),\\ \mathscr{Q}_{t_2} &= Q_0 + Q_S\sin(\omega t_2) + Q_C\cos(\omega t_2),\\ \mathscr{Q}_{t_3} &= Q_0 + Q_S\sin(\omega t_3) + Q_C\cos(\omega t_3).\end{aligned} \tag{3.20}$$

From the set of the equations given in Eqn. 3.20, coefficients Q_0, Q_C and Q_S can be calculated and then the discrete time-domain variable $\mathscr{Q}$ can be calculated for any time t . Set of the equations given in Eqn. 3.20 can be rewritten in matrix form:

$$\begin{bmatrix}\mathscr{Q}_{t_1}\\ \mathscr{Q}_{t_2}\\ \mathscr{Q}_{t_3}\end{bmatrix} = \begin{bmatrix}\sin(\omega t_1) & 1 & \cos(\omega t_1)\\ \sin(\omega t_2) & 1 & \cos(\omega t_2)\\ \sin(\omega t_3) & 1 & \cos(\omega t_3)\end{bmatrix}\begin{bmatrix}Q_S\\ Q_0\\ Q_C\end{bmatrix}, \tag{3.21}$$

or:

$$\underline{\mathscr{Q}} = \underline{\underline{E}}^{-1}\underline{Q}, \tag{3.22}$$

where $\underline{\underline{E}}^{-1}$ is the transformation matrix from the time domain to the frequency domain. If we multiply Eqn. 3.22 with $\underline{\underline{E}}$ from the left, following equation is obtained:

$$\underline{Q} = \underline{\underline{E}}\,\underline{\mathscr{Q}}, \tag{3.23}$$

where $\underline{\underline{E}}$ is the transformation matrix from the frequency domain to the time domain with the following properties:

$$\underline{\underline{E}}\,\underline{\underline{E}}^{-1} = \underline{\underline{E}}^{-1}\underline{\underline{E}} = \underline{\underline{I}}. \tag{3.24}$$

Also, it should be noted that variables $\mathscr{Q}$ and $\mathscr{R}$ have been replaced with their discrete counterparts $\underline{\mathscr{Q}}$ and $\underline{\mathscr{R}}$, meaning that solution is sought at equidistant number of $(2n+1)$ discrete time instants within period T:

$$\underline{\mathscr{Q}} = \begin{bmatrix}\mathscr{Q}_{t_1}\\ \mathscr{Q}_{t_2}\\ \mathscr{Q}_{t_3}\\ \vdots\\ \mathscr{Q}_{t_{2n+1}}\end{bmatrix}, \quad \underline{\mathscr{R}} = \begin{bmatrix}\mathscr{R}_{t_1}\\ \mathscr{R}_{t_2}\\ \mathscr{R}_{t_3}\\ \vdots\\ \mathscr{R}_{t_{2n+1}}\end{bmatrix}. \tag{3.25}$$

In Eqn. 3.21 we can see matrix $\underline{\underline{E}}^{-1}$ written for the one harmonic case, but for the arbitrary number of harmonics n, it has the following form:

$$\underline{\underline{E}}^{-1} = \begin{bmatrix} \sin(\omega t_1) & \sin(2\omega t_1) & ... & \sin(n\omega t_1) & 1 & \cos(\omega t_1) & \cos(2\omega t_1) & ... & \cos(n\omega t_1) \\ \sin(\omega t_2) & \sin(2\omega t_2) & ... & \sin(n\omega t_2) & 1 & \cos(\omega t_2) & \cos(2\omega t_2) & ... & \cos(n\omega t_2) \\ \sin(\omega t_3) & \sin(2\omega t_3) & ... & \sin(n\omega t_3) & 1 & \cos(\omega t_3) & \cos(2\omega t_3) & ... & \cos(n\omega t_3) \\ & & & & \vdots & & & & \\ & & & & \vdots & & & & \\ \sin(\omega t_n) & \sin(2\omega t_n) & ... & \sin(n\omega t_n) & 1 & \cos(\omega t_n) & \cos(2\omega t_n) & ... & \cos(n\omega t_n) \end{bmatrix}, \quad (3.26)$$

and matrix $\underline{\underline{E}}$ can analytically be expressed as:

$$\underline{\underline{E}} = \frac{2}{2n+1} \begin{bmatrix} \sin(\omega t_1) & \sin(\omega t_1) & \sin(\omega t_3) & ... & \sin(\omega t_{2n+1}) \\ \sin(2\omega t_1) & \sin(2\omega t_1) & \sin(2\omega t_3) & ... & \sin(2\omega t_{2n+1}) \\ \sin(3\omega t_1) & \sin(3\omega t_1) & \sin(3\omega t_3) & ... & \sin(3\omega t_{2n+1}) \\ \vdots & \vdots & \vdots & & \vdots \\ \sin(n\omega t_1) & \sin(n\omega t_1) & \sin(n\omega t_3) & ... & \sin(n\omega t_{2n+1}) \\ \frac{1}{2} & \frac{1}{2} & \frac{1}{2} & & \frac{1}{2} \\ \cos(\omega t_1) & \cos(\omega t_1) & \cos(\omega t_3) & ... & \cos(\omega t_{2n+1}) \\ \cos(2\omega t_1) & \cos(2\omega t_1) & \cos(2\omega t_3) & ... & \cos(2\omega t_{2n+1}) \\ \cos(3\omega t_1) & \cos(3\omega t_1) & \cos(3\omega t_3) & ... & \cos(3\omega t_{2n+1}) \\ \vdots & \vdots & \vdots & & \vdots \\ \cos(n\omega t_1) & \cos(n\omega t_1) & \cos(n\omega t_3) & ... & \cos(n\omega t_{2n+1}) \end{bmatrix}. \quad (3.27)$$

Next, Eqn. 3.15 will be formulated into the frequency domain scalar transport equation but with time domain variables $\mathscr{Q}$ and $\mathscr{R}$, with the use of Eqn. 3.23 and the equivalent equation for the variable $\underline{R}$:

$$\omega \underline{\underline{A}}\,\underline{\underline{E}}\,\underline{\mathscr{Q}} + \underline{\underline{E}}\,\underline{\mathscr{R}} = \underline{0}. \quad (3.28)$$

System of equations from Eqn. 3.28 could be solve, but evaluating sources and fluxes in the frequency domain is computationally expensive and inconvenient [22]. To avoid that, we will transform the equation back to the time domain and that will be done by multiplying the equation with $\underline{\underline{E}}^{-1}$ from the left:

$$\omega \underline{\underline{E}}^{-1}\,\underline{\underline{A}}\,\underline{\underline{E}}\,\underline{\mathscr{Q}} + \underline{\mathscr{R}} = \underline{0}. \quad (3.29)$$

This equation represents a temporally-coupled set of $2n+1$ steady state problems and if we compare it with the original scalar transport Eqn. 3.7, the following can be observed. First, variables $\mathscr{Q}$ and $\mathscr{R}$ have been replaced with $\underline{\mathscr{Q}}$ and $\underline{\mathscr{R}}$, which are shown in Eqn. 3.25, meaning that solution is sought at equidistant number of $(2n+1)$ discrete time instants within period T. Second thing, the time derivative term has been replaced by terms coupling the solution at $2n+1$ time instants. This is same as if time derivative of a harmonic signal was calculated in $2n+1$ uniformly spaced temporal snapshots, including a mean (steady) solution [15].

Next, Eqn. 3.29 will be written in the extended form:

$$\begin{aligned}
\mathscr{Q}_{t_1}: \quad & \nabla\cdot(\mathbf{u}\mathscr{Q}_{t_1}) - \nabla\cdot(\gamma\mathscr{Q}_{t_1}) = -\frac{2\omega}{2n+1}\left(\mathscr{Q}_{t_2}\sum_{k=1}^{n} k\sin(k\omega t_1) + \right.\\
& \left. \mathscr{Q}_{t_3}\sum_{k=1}^{n} k\sin(k\omega 2t_1) + \quad \ldots \quad + \mathscr{Q}_{t_{2n+1}}\sum_{k=1}^{n} k\sin(k\omega 2nt_1)\right),\\
\mathscr{Q}_{t_2}: \quad & \nabla\cdot(\mathbf{u}\mathscr{Q}_{t_2}) - \nabla\cdot(\gamma\mathscr{Q}_{t_2}) = -\frac{2\omega}{2n+1}\left(-\mathscr{Q}_{t_1}\sum_{k=1}^{n} k\sin(k\omega t_1) + \right.\\
& \left. \mathscr{Q}_{t_3}\sum_{k=1}^{n} k\sin(k\omega t_1) + \quad \ldots \quad + \mathscr{Q}_{t_{2n}}\sum_{k=1}^{n} k\sin(k\omega(2n-1)t_1)\right),\\
\mathscr{Q}_{t_3}: & \qquad\qquad \ldots\\
\vdots \quad & \qquad\qquad \vdots\\
\mathscr{Q}_{t_n}: & \qquad\qquad \ldots
\end{aligned} \tag{3.30}$$

with the following substitution used for simplification further on:

$$\begin{aligned}
P_1 &= \sum_{k=1}^{n} k\sin(k\omega t_1) = \sum_{k=1}^{n} k\sin(\frac{2\pi k}{2n+1});\\
P_2 &= \sum_{k=1}^{n} k\sin(k\omega 2t_1) = \sum_{k=1}^{n} k\sin(\frac{4\pi k}{2n+1});\\
P_3 &= \sum_{k=1}^{n} k\sin(k\omega 3t_1) = \sum_{k=1}^{n} k\sin(\frac{6\pi k}{2n+1});\\
&\vdots\\
P_n &= \sum_{k=1}^{n} k\sin(k\omega i t_1) = \sum_{k=1}^{n} k\sin(\frac{2i\pi k}{2n+1}), \qquad \text{for} \quad i=\{1,2n\},
\end{aligned} \tag{3.31}$$

where $\omega = \frac{2\pi}{T}$ and $t_1 = \frac{T}{2n+1}$. Important property of these coefficients is $P_{-i} = -P_i$. Eqn. 3.30 can then be written in the general form:

$$\nabla\cdot(\mathbf{u}\mathscr{Q}_{t_j}) - \nabla\cdot(\gamma\mathscr{Q}_{t_j}) = -\frac{2\omega}{2n+1}\left(\sum_{i=1}^{2n} P_{i-j}\mathscr{Q}_{t_j}\right), \quad \text{for} \quad j = 1\ldots 2n+1. \tag{3.32}$$

Because coefficients P_i depend only on the number of harmonics, which are predetermined, we can calculate those coefficients before the simulation and store them, thus lowering the CPU requirements. If the substitution introduced in Eqn. 3.31, is used than, matrix $\underline{\underline{E}}^{-1}\underline{\underline{A}}\,\underline{\underline{E}}$ can be written as:

$$\underline{\underline{E}}^{-1}\underline{\underline{A}}\,\underline{\underline{E}} = \frac{2}{2n+1}\begin{bmatrix} 0 & P_1 & P_2 & P_3 & \dots & \dots & P_{2n} \\ -P_1 & 0 & P_1 & P_2 & P_3 & & \vdots \\ -P_2 & -P_1 & 0 & P_1 & P_2 & & \vdots \\ -P_3 & -P_2 & -P_3 & 0 & P_1 & & \vdots \\ \vdots & & & & \ddots & & P_2 \\ \vdots & & & & & \ddots & P_1 \\ -P_{2n} & \dots & \dots & -P_3 & -P_2 & -P_1 & 0 \end{bmatrix}. \tag{3.33}$$

Matrix $\underline{\underline{E}}^{-1}\underline{\underline{A}}\,\underline{\underline{E}}$ written in Eqn. 3.33 takes into account the temporal distance between solution time instants, meaning that closer time instants have larger influence on the solution compared to the coefficients that are further away from the time instant for which the solution is being calculated. Further, in order to obtain valid solution, a set of $2n+1$ equations is the smallest required number of equations needed [15].

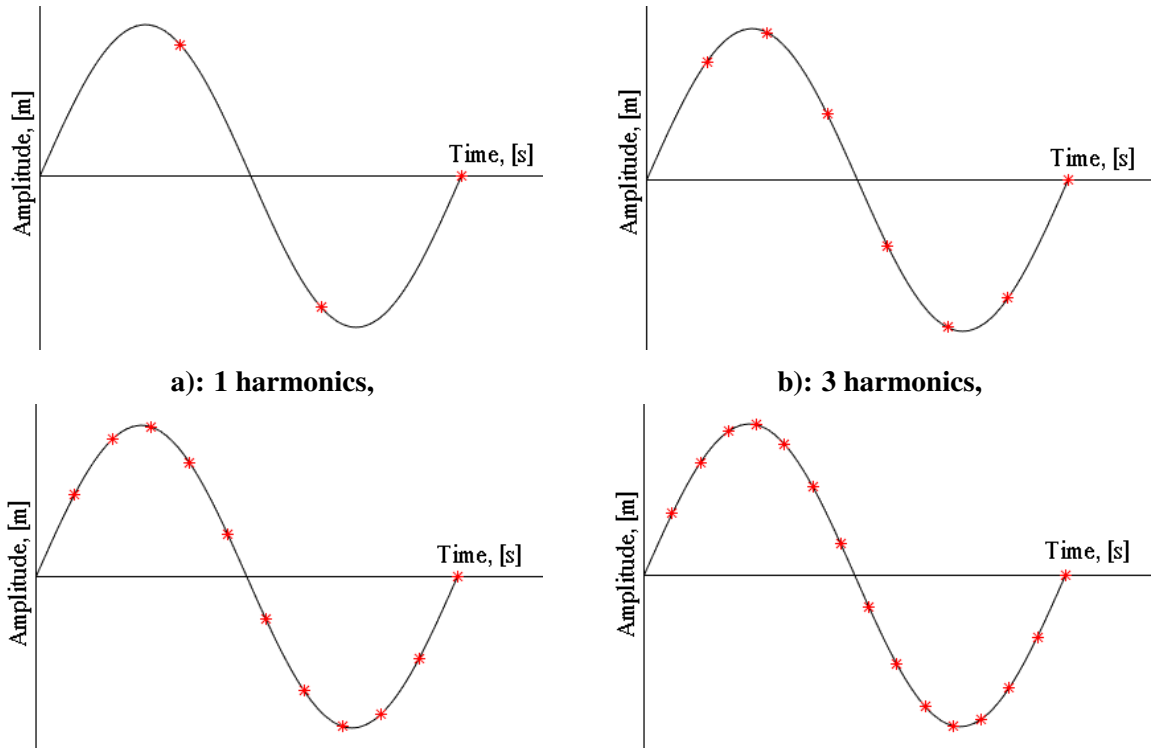

a): 1 harmonics, **b): 3 harmonics,**

c): 5 harmonics, **d): 7 harmonics,**

Figure 3.3: Temporal resolution of a single harmonic signal with 1, 3, 5 and 7 harmonics.

Fig. 3.3 shows the temporal resolution which depends on the number of harmonics. Time instants for which solution is calculated are marked with symbol * and they are always equally spaced. Their number is changed with the number of harmonics used, in accordance with relation Eqn. 3.25.

3.4 The Navier-Stokes Equations in Harmonic Balance Form

Considering that in this work Navier-Stokes equations for the incompressible flow are being solved, we will transform them into the HB form according to the procedure that has been described in the previous subsection:

$$\nabla \cdot \mathbf{u}_{t_j} = 0, \tag{3.34}$$

$$\begin{gathered}\nabla \cdot (\mathbf{u}_{t_j}\mathbf{u}_{t_j}) - \nabla \cdot (\nu \mathbf{u}_{t_j}) = -\nabla p_{t_j} - \frac{2\omega}{2n+1}\left(\sum_{i=1}^{2n} P_{i-j}\mathbf{u}_{t_j}\right), \\ \text{for} \quad j = 1 \ldots 2n+1.\end{gathered} \tag{3.35}$$

Eqn. 3.34 remains in the same form when being transformed into the HB form, as it does not have time derivative term, but only $\mathbf{u}$ is replaced with its discrete counterpart $\mathbf{u}_{t_j}$. This two equations represent $2n+1$ coupled equations with enforced periodic behavior defined by base frequency ω and number of harmonics n.

3.5 Finite Volume Implementation

In this subsection, an overview of Finite Volume (FV) method will be presented. Details of the FV discretization can be found in [23] and will not be discussed here. Notation used will be in accordance with the notation introduced by Rusche [24], where $[\cdot]$ will be used as implicit FV discretization and other terms are calculated explicitly [15]:

$$\left[\nabla \cdot \left(\mathbf{u}_{t_j}\mathbf{u}_{t_j}\right)\right] - \left[\nabla \cdot (\nu \mathbf{u}_{t_j})\right] = -\nabla p_{t_j} - \frac{2\omega}{2n+1}\left(\sum_{i=1}^{2n} P_{i-j}\mathscr{Q}_{t_j}\right), \quad \text{for} \quad j = 1 \ldots 2n+1, \tag{3.36}$$

$$\left[\nabla \cdot \left(\frac{1}{a_{Pt_j}}\nabla p_{t_j}\right)\right] = \nabla \cdot \left(\frac{\mathbf{H}(\mathbf{u}_{t_j})}{a_{Pt_j}}\right), \quad \text{for} \quad j = 1 \ldots 2n+1, \tag{3.37}$$

where a_{Pt_j} is the diagonal coefficient of the momentum equation at the time instant t_j, and

$\mathbf{H}(\mathbf{u}_{t_j})$ is the flux operator as defined by Jasak [23]. Segregated solution algorithm procedure is applied to transform continuity equation in the HB form in Eqn. 3.34 to the FV form in Eqn. 3.36. The HB method transforms one transient equation into a set of $2n+1$ coupled steady state equations. The pressure-velocity coupling will be resolved using the SIMPLE algorithm [25]. In addition to the pressure-velocity coupling at each time instant, there also exists velocity fields at different time instants. However, only one SIMPLE iteration is required for each time instant in order to resolve both pressure-velocity coupling and coupling of the velocity fields, which is solved during a forward sweep, using the latest $\mathbf{u}_{t_j}$.

3.6 Start-Up and Shut-Down Simulations

Simulations of the fluid flow during start-up and shut-down are becoming more and more important as it has been mentioned earlier in this thesis. Currently, the best way to do this type of simulations in `foam-extend` is by using transient solvers. Although transient solvers provide very good results, time required for simulations is very long. In some cases, when the computational mesh has a large number of cells, transient simulation can last for few a weeks or even months. Another approach that has been presented in [26] uses steady state solver, which is not able to capture transient behavior characteristic for these simulations.

Considering all of this, a novel approach that uses HB method has been developed. Up until now, HB method was mainly used for periodic problems, while problems which include changes in the flow regime have not been addressed. Having in mind that regime change is not a periodic process, the HB method may not be suitable for such problems in its existing form. To circumvent this, a periodic process needs to be assembled first. This is done by joining two similar processes: as change from regime A to regime B needs to happen, eventually will also the change from regime B to regime A needs to happen. Therefore, if change A-B-A is considered to be the solving period, the HB method can easily be used and furthermore, both transient occurences get solved at once. Depending on the case, start-up/shut-down process can take between several dozen periods of rotation up to several hundreds or thousands periods [27] and this is the base for choosing the HB temporal resolution.

The HB approach for start-up and shut-down simulations is divided into two parts: inner and outer simulations, where inner simulations are run using one harmonic as this has proven to be sufficiently accurate, while outer simulations depend on the regime-change profile. Inner simulations are performed in 2n+1 outer time instants and coupled over outer simulation. Small improvements that can be captured by using a higher number of harmonics are not that important considering that reconstruction of all results is performed during the outer simulation. Outer simulation has n harmonics which is determined for each case separately. Two things need to be considered while choosing n: calculation time required for the simulations and how well it fits start-up and shut-down curve. These two things needs to be balanced, as with the increase in n, calculation time is becoming longer, but it fits the curve

better.

First, the start-up and shut-down curve needs to be determined. This curve is a function that represents the change of different types of variables during the start-up and shut-down. For example, the change of mass flow rate at the inlet or change of position of the blades or any other variable which dictates the change in flow regime. In existing transient methods, that function is provided as a boundary condition, and full duration of the start-up and shut-down needs to be simulated. On the contrary, HB method needs to calculate 2n+1 inner simulations and one outer simulation, as mentioned earlier. These 2n+1 inner simulations need to be done in specific time instants, which are determined in the same manner as for HB method described in subsection 3.3. One example of the start-up and shut-down curve and corresponding time instants for the inner simulations can be seen in Fig. 3.4. In this example, outer simulation has 6 harmonics which means that it needs 13 values for boundary conditions from 13 equidistant time instants. the first step is to determine the values in these time instants and prescribe these values as boundary conditions of the inner simulations.

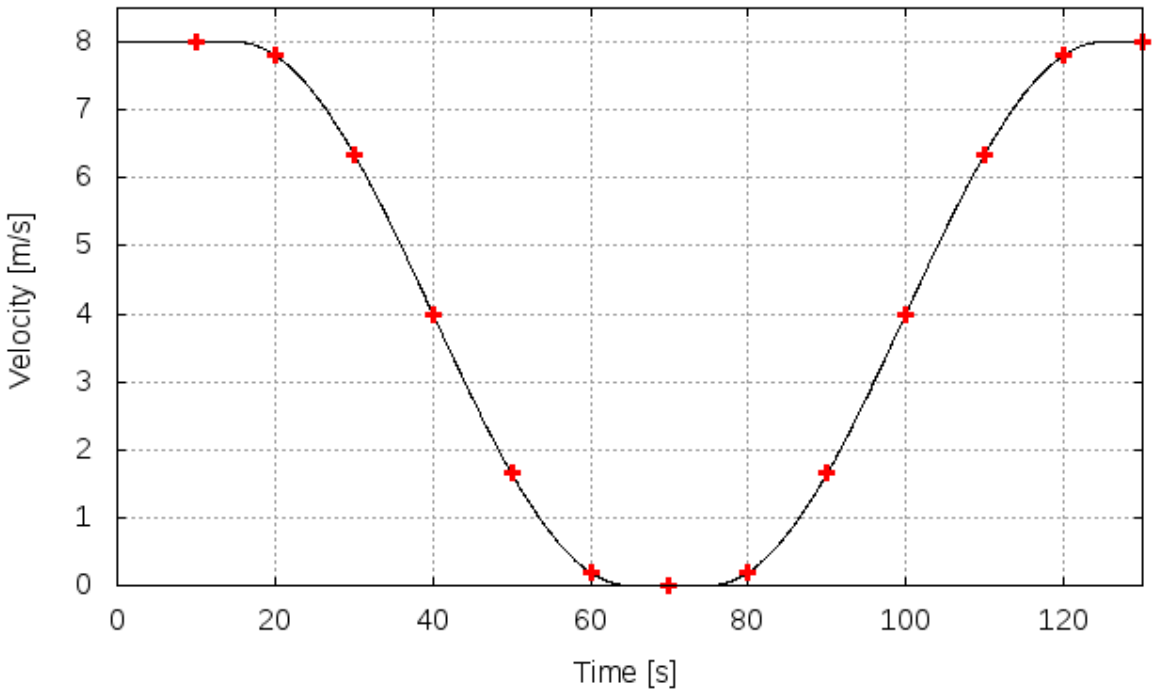

Figure 3.4: Time instants of the inner simulations.

After all 2n+1 inner simulations are calculated, their results are prescribed as starting point for the outer simulation. During the outer simulation, results are reconstructed and available in any time instant not only in 2n+1 originally calculated time instants and consequently provide

results in the same format as would a full transient start-up/shut-down simulation.

Another simplification can be made if the function is made symmetric. In that case not 2n+1 but n+1 inner simulations need to be done. In Fig. 3.4, it can be seen that six points left from the time instant t = 70*s* have the same values as six points right from the time instant t = 70*s*. In that case, inner simulations are calculated only for the first seven time instants. Results of the inner simulations for the last six time instants are obtained the first six. By doing that, time needed for calculations is reduced almost by half.

3.7 Boundary Conditions Between Regions

In subsection 2.3, the GGI boundary condition was presented as a way to connect multiple non-conformal regions without flow values being averaged. For the cases with multiple regions, dominant frequencies that are needed for the calculation of the HB coefficients are usually different and vary from the region to region. For example, rotor-stator interaction, where stator blades will be influenced by the rotor-passing frequency and rotor blades will be effected by pulsations of rotational frequency. In cases of this kind, temporal reconstruction should be preformed at the interface to account for changing interblade positions throughout the annulus. However, in special cases when blade count is equal or a multiple of each other between neighbouring rows, temporal reconstruction can be avoided and all the regions can be calculated in the same time instants. In that case Eqn. 3.29 is modified to new form, Eqn. 3.38. Full derivation of Eqn. 3.38 can be found in [28].

This new form has few important properties. First, matrices $\underline{\underline{E}}_{sr}^{-1}$ and $\underline{\underline{E}}_{sr}$ are calculated as shown in Eqn. 3.26 and Eqn. 3.27 but solution is obtained in rotor time instants and calculated using the stator dominant frequency. Second, in multistage turbomachinery cases, solution is sought only in rotor-determined time instants for all stages regardless of the number of stages or dominant frequency and no temporal interpolation is needed to match time instants at the interface. This makes simulations more efficient because there is no need to post-processing step to match solutions in rotor and stator [15].

$$\omega \underline{\underline{E}}_{sr}^{-1} \underline{\underline{A}} \underline{\underline{E}}_{sr} \underline{\mathscr{Q}}_r + \underline{\mathscr{R}}_r = \underline{0}. \tag{3.38}$$

3.8 Closure

In this section fundamentals of HB method are outlined. First, Fourier transformation is introduced after which HB is implemented for scalar transport equation. Implementation of the new method for the transient flows is described.

In the following sections, new approach will be validated on two cases. The first case is used to compare it with already existing methods for transient flows, while the second validate the method against experimental results.

4 Pump Test Case

Derivation of the HB Method was given in the previous section. In order to test the validity of the proposed method, a simple pump-like 2D test case is made. This section will present the results of the shut-down and start-up calculations made on the 2D test case.

4.1 Introduction

For the validation, the HB results need to be compared with the equivalent transient simulation. Flow simulation will start with the inlet velocity $8\,\mathrm{m/s}$ and by following the sine function it will reduce the inlet velocity, consequently reducing flow rate, until it reaches $0\,\mathrm{m/s}$. Further on, that part of the simulation is called shut-down. After which it will again accelerate to $8\,\mathrm{m/s}$ by following the same function. That part is called start-up. Whole process can be seen in Fig. 3.4 and Fig. 4.5. Geometry is made very simple so that transient simulations finish in a reasonable amount of time. First, flow fields will be shown and at the end comparison between required CPU times will be presented.

4.2 Geometry and Mesh Generation

Test case geometry, which can be seen in Fig. 4.1, consists of two regions, rotor which has 4 blades and stator which has 3 blades. All boundaries are marked in the Fig. 4.1 and listed in Table 4.1.

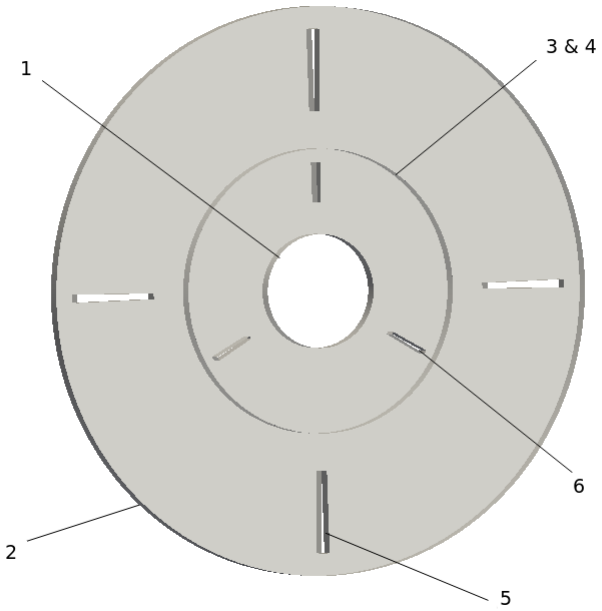

Figure 4.1: Boundary conditions of test case.

Table 4.1: Definition of patch topology of the test case.

Boundary No.	Boundary	Boundary condition
1	Inlet	inlet
2	Outlet	outlet
3	Rotor Interface	ggi
4	Stator Interface	ggi
5	Rotor Blades	wall
6	Stator Blades	wall

Mesh is made with the commercial meshing software Pointwise [4]. It consists of two zones with hexahedral cells. Mesh size and quality are assessed with `foam-extend's` utility `checkMesh`. Results of assessment presented in Table 4.2 and Table 4.3 show that quality of the mesh is very good, which can be expected for such a simple geometry.

Table 4.2: Mesh size data.

Zone	Number of cells
Rotor	6 444
Stator	6 136
Total	12 580

Table 4.3: Mesh quality data.

	Average	Maximum	Threshold
Non-orthogonality	4.069	24.7412	70.0
Skewness		0.5358	4.0
Aspect ratio		31.2963	

The mesh for the full model can be seen in Fig. 4.3, while refinements that are made around the edge of the blades are shown in Fig. 4.2.

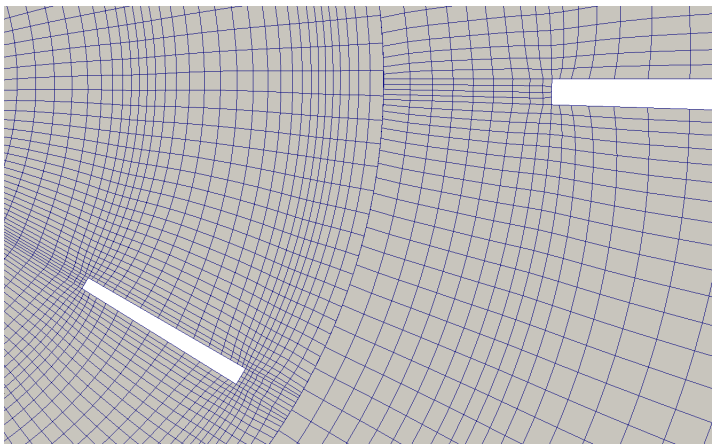

Figure 4.2: Refinements around edges of the blades.

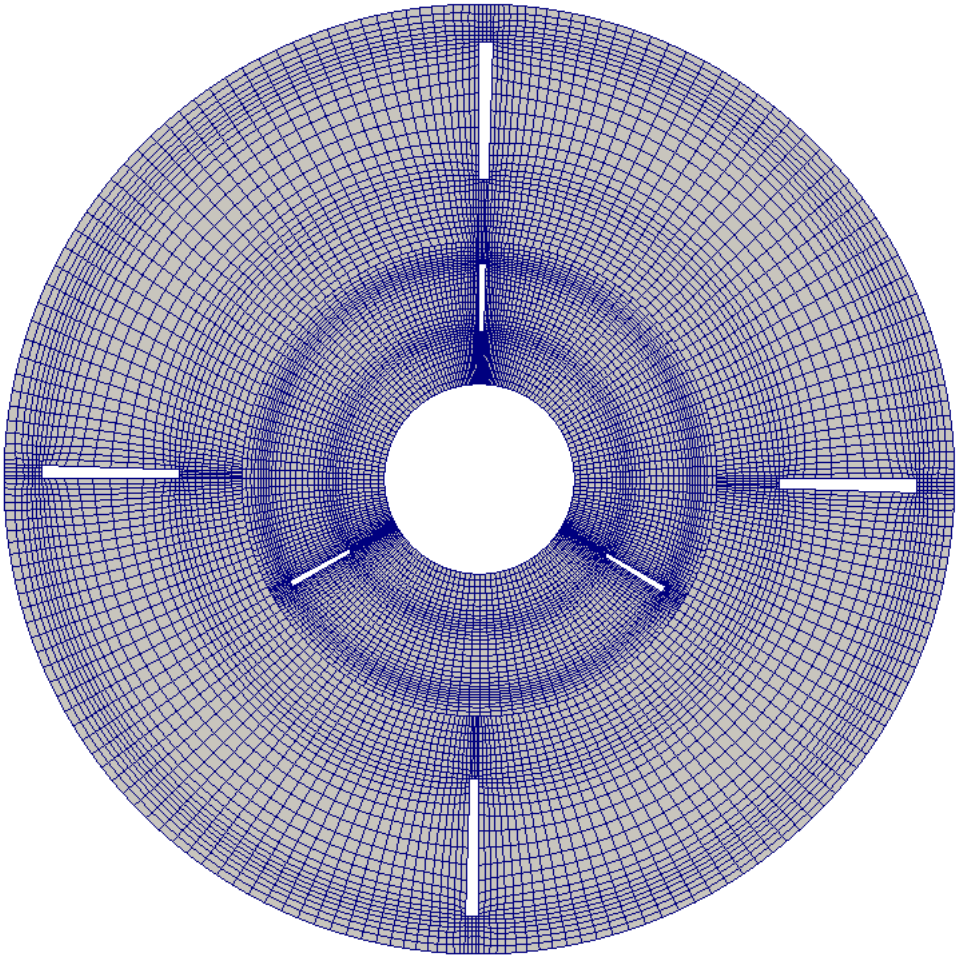

Figure 4.3: Full mesh of test case.

The inner radius of the model is 0.2m, outer is 1m while the boundary between the rotor and stator is 0.5m radius. In Table 4.4 four points are listed, in which pressure and velocity profiles will be acquired during shut-down and start-up simulation, in Fig. 4.4 their position in the model is presented.

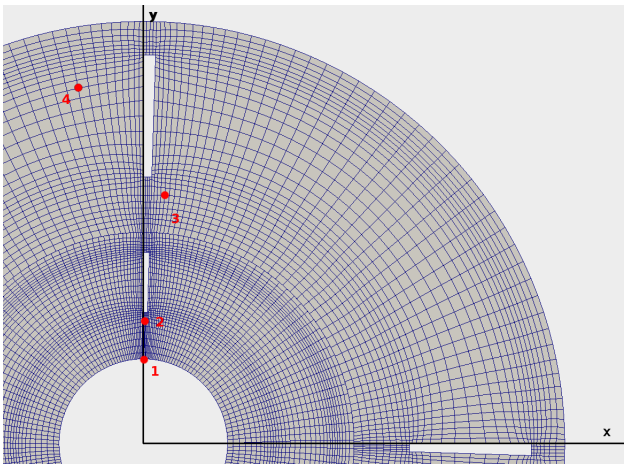

Figure 4.4: Location of points listed in Table 4.4.

Table 4.4: Coordinates of points 1-4.

	x	y
Point 1	0.0032	0.2000
Point 2	0.0480	0.2885
Point 3	0.0509	0.5879
Point 4	-0.1548	0.8416

4.3 Case setup

In this test case, start-up and shut-down process will be simulated by reducing and increasing the inlet velocity, thus reducing or increasing the flow rate. Sine function, shown in Eqn. 4.1, will be used for that purpose.

$$y = y_0 + a * \sin(bx + c) = 4 + 4 * \sin(\frac{2\pi}{\mathrm{T}}x + \frac{\pi}{2}), \tag{4.1}$$

with T being period of sine function, T= 100 s. Period of the full simulation is 130 s which is divided in 5 parts, as it can be seen in Fig. 4.5. First 15 s, marked as "a" in Fig. 4.5, inlet velocity is kept constant at 8 m/s which is considered as operating point from which the shutdown will occur. After that, in the "b" part, velocity is reduced from 8 m/s to 0 m/s, by following the sine function, Eqn. 4.1. That part lasts for half of the sine period, 50 s. In the "c" part, inlet velocity is held at 0 m/s for 10 s. In the 'd" part, acceleration to 8 m/s is again done by following sine function for the half of the sine period, 50 s. At the end, in the "e" part, inlet velocity is kept constant at 8 m/s from 125 s till 130 s, same as at the beginning. Function identical to this one, is imposed as the inlet velocity boundary condition for the transient simulation.

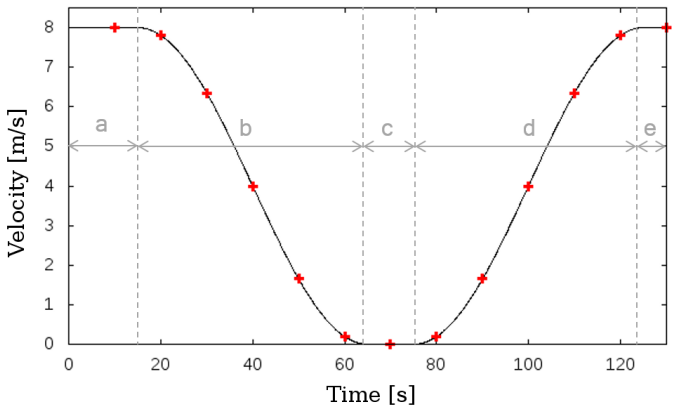

Figure 4.5: Inlet velocity profile and time instants of the inner simulations.

Previously mentioned in subsection 3.6, procedure for the HB simulation is modified in

order to capture the start-up/shut-down phenomena. In this case, the outer simulation uses 6 harmonics and consequently we need results from 13 inner simulations. For the purpose of reducing the simulation time, sine function is symmetric concerning HB time instants, as shown in Fig. 4.5. If we mirror points around y-axis through $x = 70$s, seven points on the left are coincident with seven points on right, meaning they have the same inlet velocity. After the inner simulations are completed, for the seven above mentioned points, results are imposed as starting point for the "big' simulation and inlet velocity function is obtained. In Fig. 4.7a, the reconstruction is compared to transient inlet boundary condition, showing the identical velocity profile.

In order to solve the set of partial differential equations for fluid flow, it is necessary to set boundary conditions for each physical quantity on each boundary of the numerical domain. Boundaries are listed in Table 4.1. In both simulations boundary conditions for the blades are same. For the pressure, the von Neumann boundary condition is used, while for the velocity Dirichlet boundary condition is used. On the rotor and stator interface ggi boundary condition is imposed for both pressure and velocity. `InletOutlet` is used as a velocity boundary condition on the outlet with Dirichlet boundary condition used for pressure. The only difference between these two simulations is inlet boundary condition. For transient simulation `surfaceVaryingNormalFixedValue` condition is used and for the HB `surfaceNormalFixedValue`. Purpose of these these two conditions is to impose velocity normal to the inlet surface. With difference being that `surfaceNormalFixedValue` will impose constant value through time, while `surfaceVaryingNormalFixedValue` will impose value that vary through time. Vectors of velocity imposed on the inlet can be seen in Fig. 4.6.

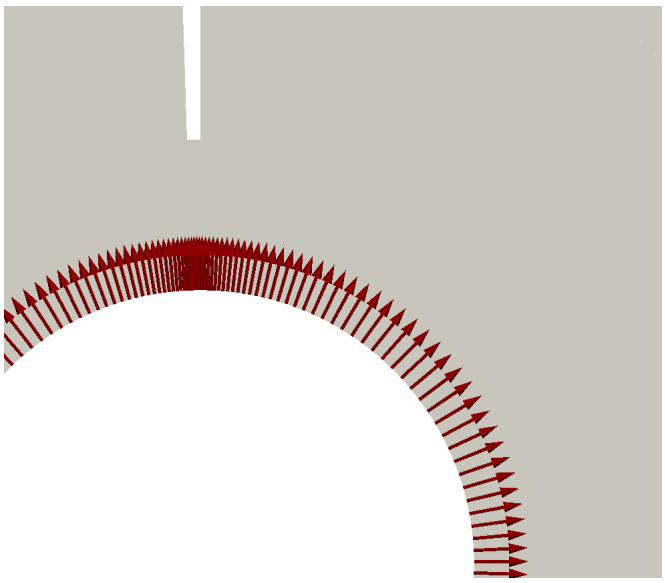

Figure 4.6: Vectors of velocity imposed on the inlet.

4.4 Results

Rotation speed in this test case is set to 60rpm. Transient simulation is done with variable time step, varying between the $4 - 8 \cdot 10^{-4}$, which was smaller than the rotor period, 1s. Because of that, relative position of the rotor compared to the stator is changing and causing oscillations which can be seen in Fig. 4.7. HB results were obtained by reconstructing results of inner simulations, as described in the previous section. Results for the "big simulations" are taken at the end of the rotor period, and consequently rotor-stator interaction is not presented in the HB results.

In Fig. 4.7 comparison between transient and HB simulation is provided. Behavior of velocity and pressure in four different points through the shut-down and start-up process is presented. It shows that the results of HB simulations are in good agreement with the results of the transient simulation.

Comparison between these two simulations is also made in terms of velocity and pressure flow fields. Fig. 4.8 shows velocity fields in five different time instants, which correspond to instants when inlet velocity is 8, 6, 4, 2 and $0\,\mathrm{m/s}$. Only the shut-down part is shown, as start-up is identical, considering the symmetry imposed. In the left column HB fields are shown, and in the right column fields obtained with transient simulation. Pressure fields are shown in Fig. 4.9. Comparing the fields, HB simulations can capture transient flow and local instabilities and results are almost the same as the results of transient simulation.

Table 4.5: Calculation time.

	One HB simulation	Full HB simulation	Transient simulation	Reduction[%]
Time [s]	338.000	2366.00	67300.0	96.48%
Time [h]	0.094	0.66	18.7	96.48%

Main purpose why HB method for transient flows is developed, is reduction in processor cost, or in other words reduction of time needed for the calculation. All simulations were calculated on the same computer on one processor. Computer has Intel processor (Intel Core i5-3570K CPU @ 3.40 GHz) and 8 GB RAM. Table 4.5 shows that time required for transient simulations is very long for such a simple case, around 18.7 h. On the contrary, time required for the full HB simulations is 40 min, which is a reduction of 96.48%.

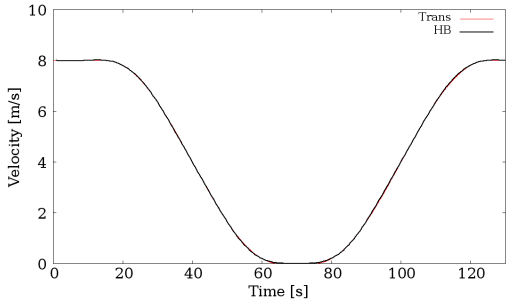

a): Velocity in point 1,

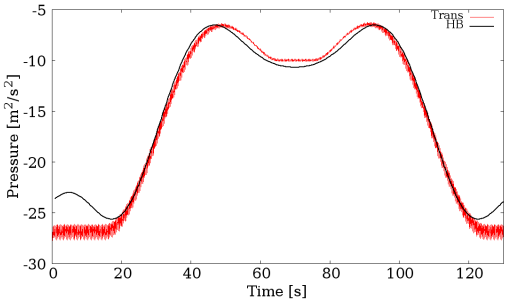

b): Pressure in point 1,

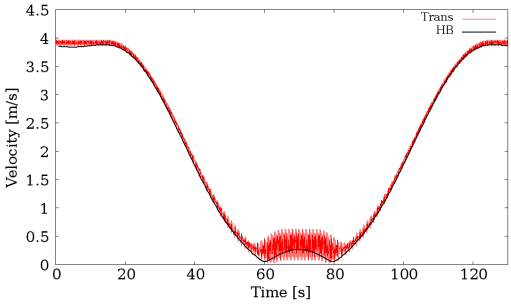

c): Velocity in point 2,

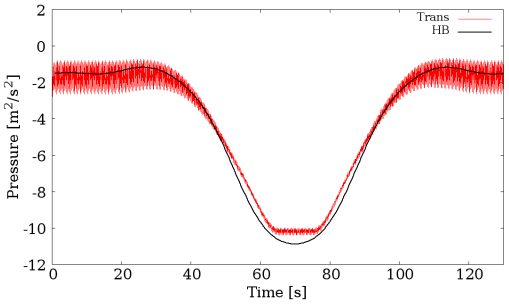

d): Pressure in point 2,

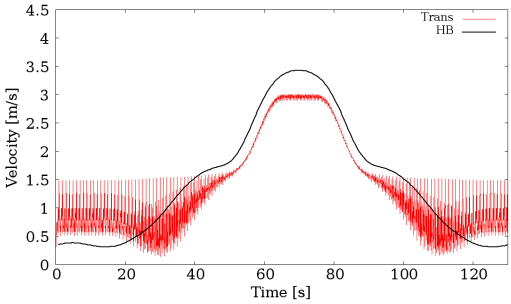

e): Velocity in point 3,

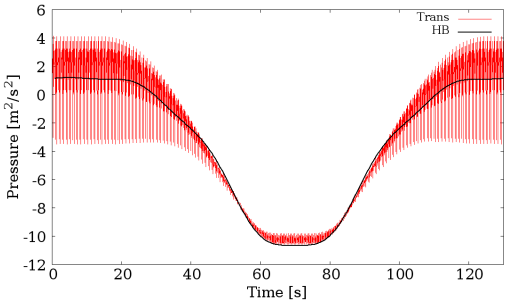

f): Pressure in point 3,

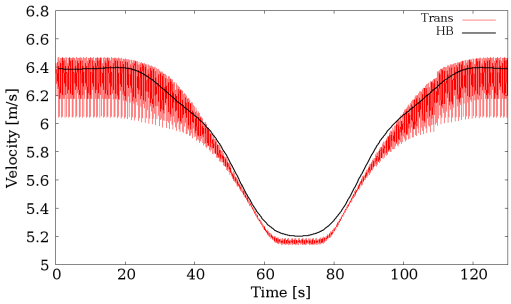

g): Velocity in point 4,

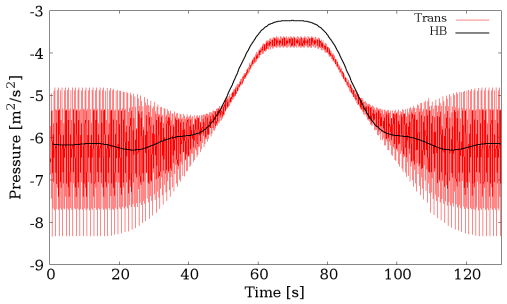

h): Pressure in point 4,

Figure 4.7: Velocity and pressure over time in different points.

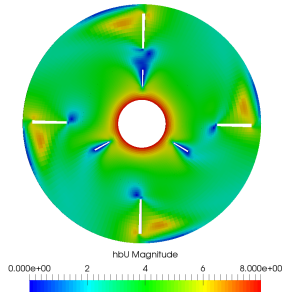

a): HB, $\mathrm{U}_{inl} = 8\mathrm{m/s}$**,** $t = 13\mathrm{s}$

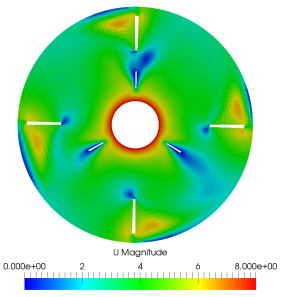

b): Transient, $\mathrm{U}_{inl} = 8\mathrm{m/s}$**,** $t = 13\mathrm{s}$

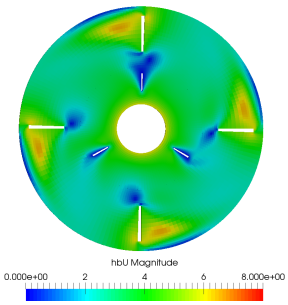

c): HB, $\mathrm{U}_{inl} = 6\mathrm{m/s}$**,** $t = 32\mathrm{s}$

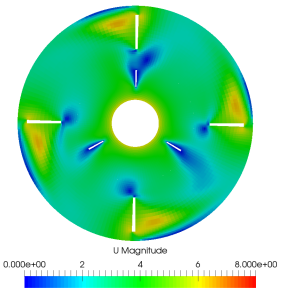

d): Transient, $\mathrm{U}_{inl} = 6\mathrm{m/s}$**,** $t = 32\mathrm{s}$

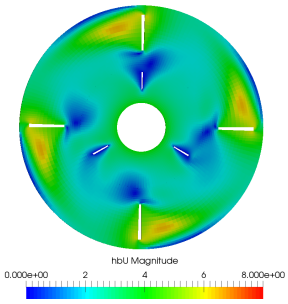

e): HB, $\mathrm{U}_{inl} = 4\mathrm{m/s}$**,** $t = 40\mathrm{s}$

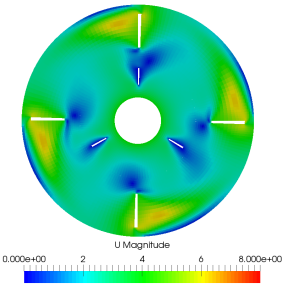

f): Transient, $\mathrm{U}_{inl} = 4\mathrm{m/s}$**,** $t = 40\mathrm{s}$

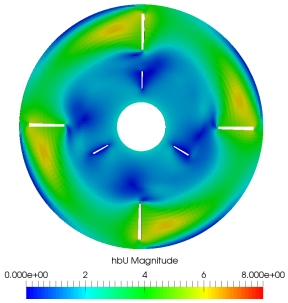

g): HB, $\mathrm{U}_{inl} = 2\mathrm{m/s}$**,** $t = 48\mathrm{s}$

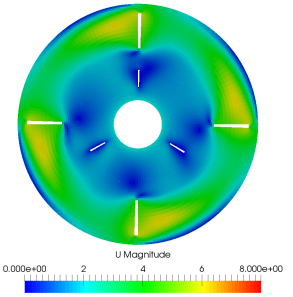

h): Transient, $\mathrm{U}_{inl} = 2\mathrm{m/s}$**,** $t = 48\mathrm{s}$

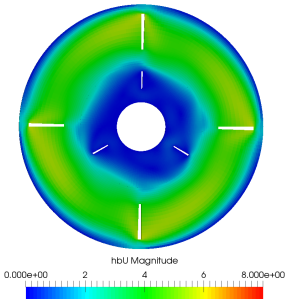

i): HB, $\mathrm{U}_{inl} = 0\mathrm{m/s}$**,** $t = 70\mathrm{s}$

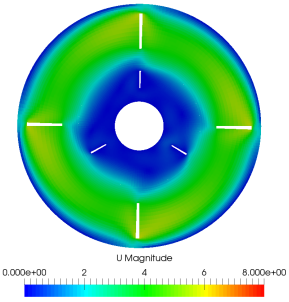

j): Transient, $\mathrm{U}_{inl} = 0\mathrm{m/s}$**,** $t = 70\mathrm{s}$

Figure 4.8: Velocity fields over time.

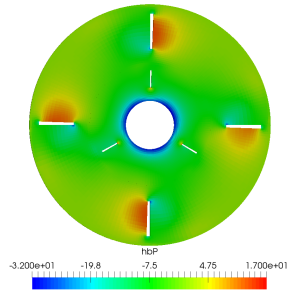

a): HB, $U_{inl} = 8\text{m/s}$**,** $t = 13\text{s}$

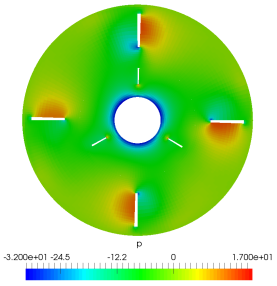

b): Transient, $U_{inl} = 8\text{m/s}$**,** $t = 13\text{s}$

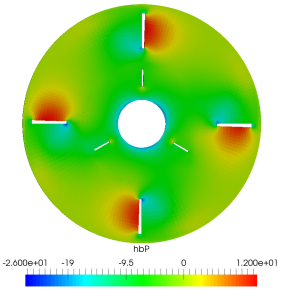

c): HB, $U_{inl} = 6\text{m/s}$**,** $t = 32\text{s}$

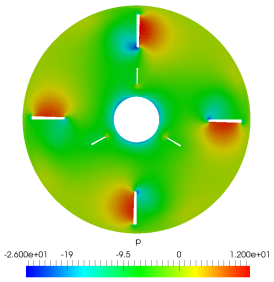

d): Transient, $U_{inl} = 6\text{m/s}$**,** $t = 32\text{s}$

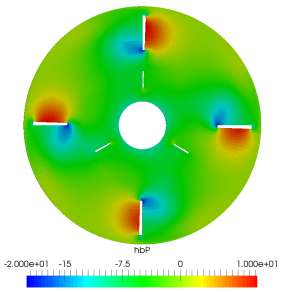

e): HB, $U_{inl} = 4\text{m/s}$**,** $t = 40\text{s}$

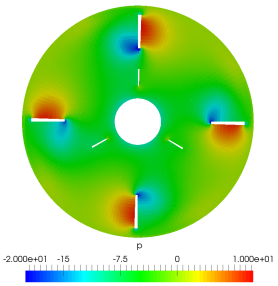

f): Transient, $U_{inl} = 4\text{m/s}$**,** $t = 40\text{s}$

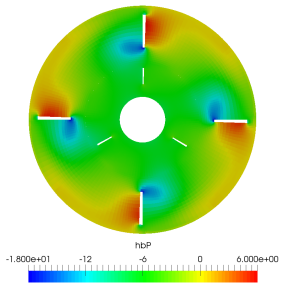

g): HB, $U_{inl} = 2\text{m/s}$**,** $t = 48\text{s}$

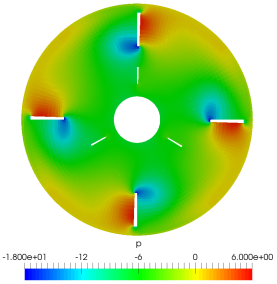

h): Transient, $U_{inl} = 2\text{m/s}$**,** $t = 48\text{s}$

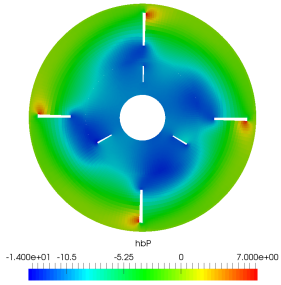

i): HB, $U_{inl} = 0\text{m/s}$**,** $t = 70\text{s}$

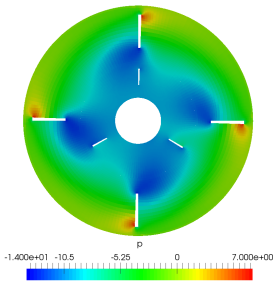

j): Transient, $U_{inl} = 0\text{m/s}$**,** $t = 70\text{s}$

Figure 4.9: Pressure fields over time.

Full HB simulation includes 7 inner and one outer simulation. For this case, all 7 inner simulations were carried out with only one harmonic. As it was shown it was sufficiently accurate. The reason for that is because only the last time frame, from all of these simulations, was taken. Small improvements that can be captured by using higher number of harmonics are not that important considering that reconstruction of all the results is in the outer simulation.

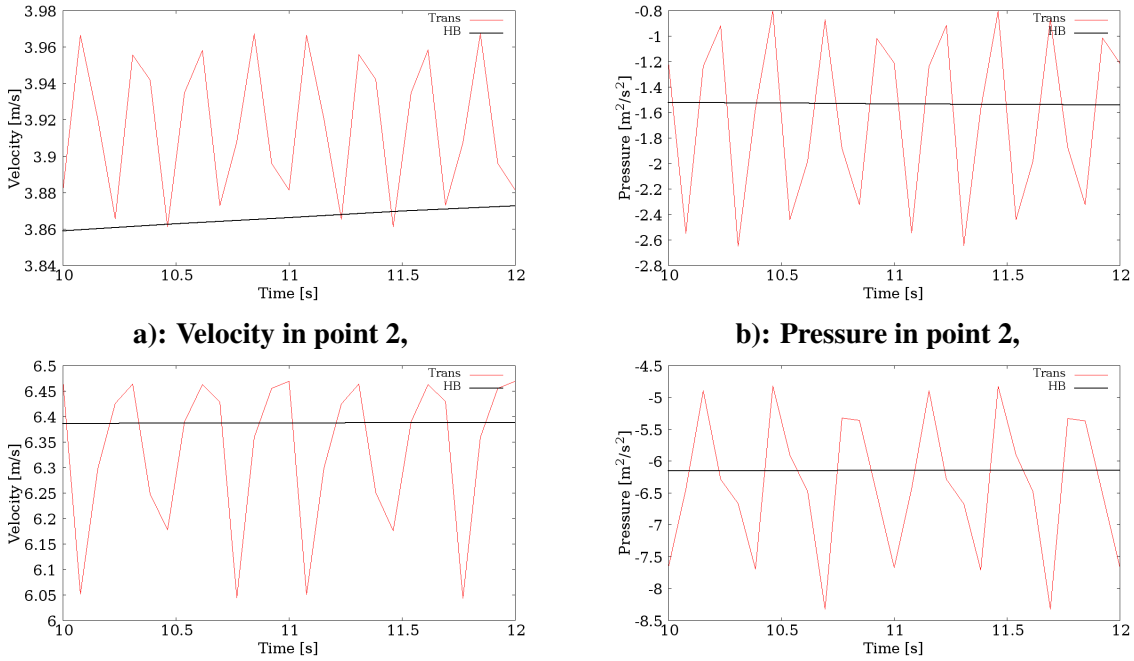

a): Velocity in point 2, **b): Pressure in point 2,**

c): Velocity in point 4, **d): Pressure in point 4,**

Figure 4.10: Oscillations of the velocity and pressure during two periods.

In Fig. 4.10 plots presented in Fig. 4.7 are zoomed to present the influence of the number of the rotor and stator blades on the dominant frequency. In the point 2, which is in the stator, frequency of the oscillations correspond to the number of the rotor blades. On the other hand in the point 4, which is in the rotor, opposite behavior can be seen.

4.5 Closure

In this section a validation of the HB method for the change of flow regime is presented. The test case is a simple pump-like 2D rotor-stator configuration, with variable inlet velocity in order to simulate turbomachinery start-up to desired operating point, followed by shut-down. Presented test case has demonstrated the accuracy of the HB method in start-up and shut-down problems, as good agreement with transient simulation is achieved. Compared features are pressure and velocity values in 4 points through time. Furthermore, pressure and velocity fields are visually compared. One of the most important findings is the time reduction achieved with the HB method: time needed for the HB simulations is 96.48% shorter compared to the transient simulation, which is the main purpose why this new approach was developed.

5 Model of Francis 99 Turbine

This section will introduce the model of the turbine which is used for obtaining experimental validation. Locations of pressure and velocity data measurements will also be highlighted. In the second part, numerical domain and grid used for the calculations will be presented.

5.1 Introduction

The Francis-99 is a series of three workshops organized by the Norwegian University of Science and Technology (NTNU) and Luleå University of Technology (LTU) [1]. Organizers of the workshops provided s large amount of technical documentation concerning the geometry and working regime of the turbine. Experimental data is also provided, with significant effort being put in order for numerical simulations to be easily comparable to it. Experiments were conducted at the Water-power Laboratory at NTNU in Trondheim, Norway on the scale model of Tokke high head Francis turbine [1].

5.2 Test Case Description

The model of a turbine used as a Francis 99 test case, located at Hydropower Laboratory the at NTNU, is a $1:5.1$ scaled model of the turbines operating at Tokke power plant in Norway. Models of the test rig and the turbine are shown in Fig. 5.1 and Fig. 5.2, respectively. The Francis turbine has a splitter blade runner, which includes 30 blades, with half of them being splitter blades (half the length) and 15 full length. The obtained maximum hydraulic efficiency of the turbine is 93.4% at the best efficiency point and the uncertainty is $\pm 0.16\%$ [29]. In the distributor there are 28 guide vanes and 14 stay vanes. The leading edge profiles of the runner main blades and splitter blades are similar. The main blades are twisted around 180° from inlet to the outlet of the runner.

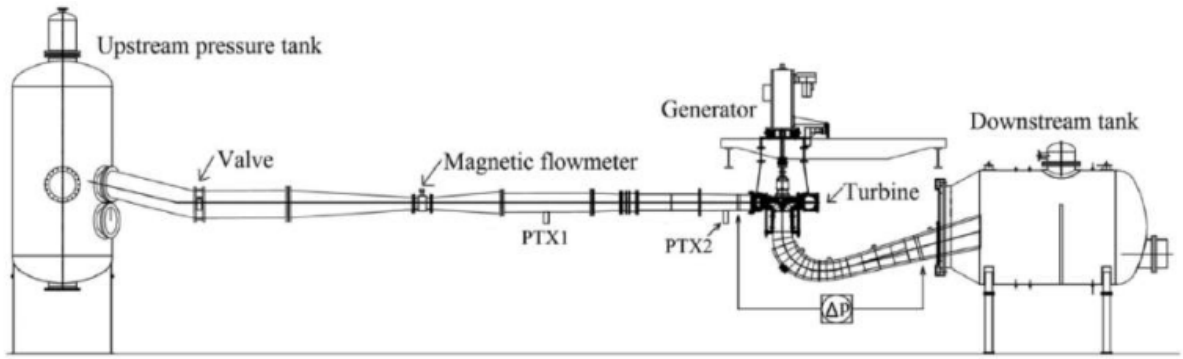

Figure 5.1: Francis 99 model test rig [30].

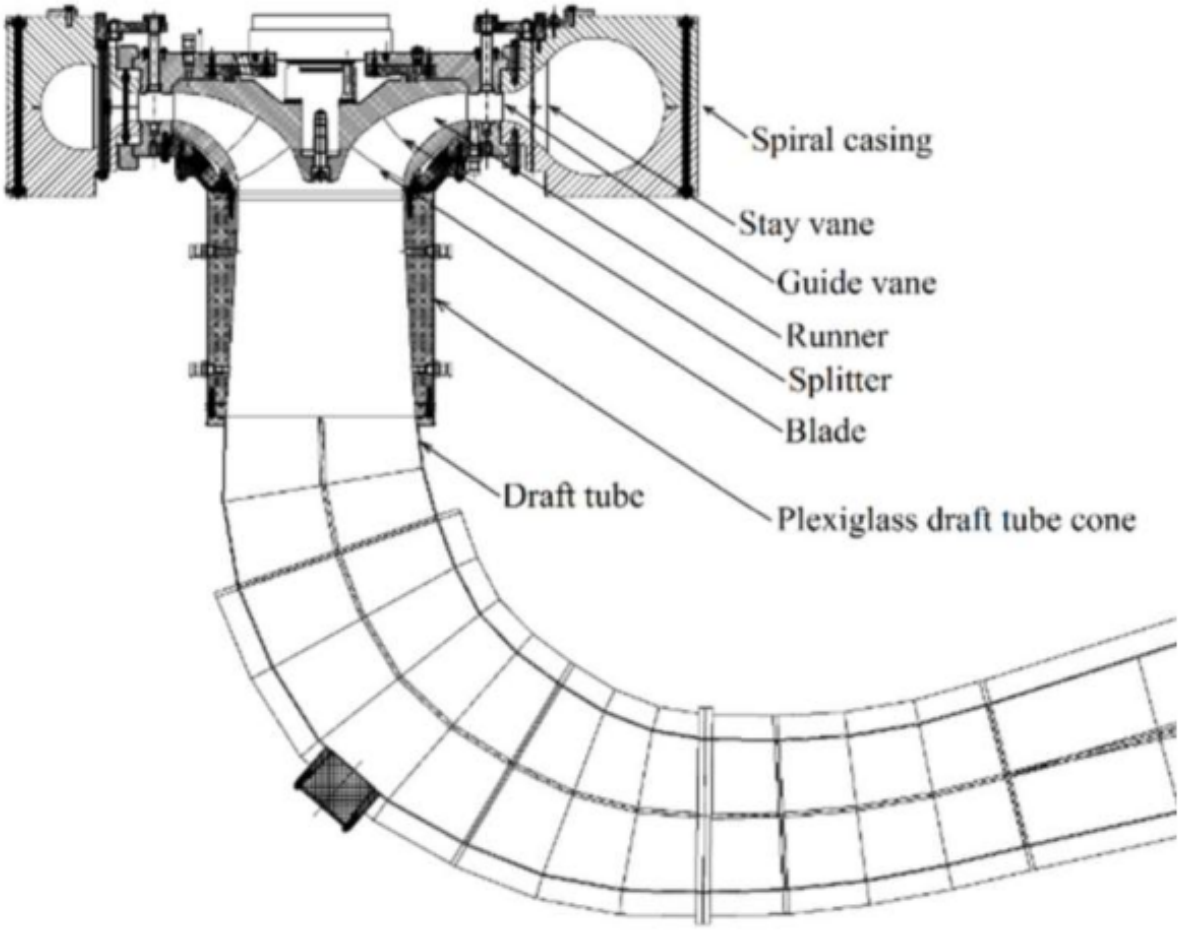

Figure 5.2: Cut view of the Francis 99 turbine model [30].

The test rig is extensively used for the model testing and for specific investigations such as rotor stator interaction, vortex rope, rotating stall with pump-turbine runner, water hammer effect, cavitation, etc. The open loop hydraulic system is used to perform transient measurements such as load variation, start-stop, and total load rejection.

The blade thickness at the trailing edge is 3 mm. Runner inlet and outlet diameters are 0.63 m and 0.349 m, respectively. The runner inlet height is 0.06 m and the specific speed is 0.27. Data mentioned above describes the geometry of the model which is compared to the prototype in Table 5.1.

Table 5.1: Francis 99 model and prototype parameters at BEP.

	$H[m]$	$d_{inlet}[m]$	$d_{outlet}[m]$	$n[min^{-1}]$	$Q[m^3/s]$	$P[kW]$	$Re[-]$
Model	12	0.630	0.349	335	0.2	22	$1.8x10^6$
Prototype	377	3.216	1.779	375	31.0	110000	$4.1x10^7$

5.3 Pressure and Velocity Measurements

Measurements were performed for both steady state (constant guide vane angle) and transient (time dependent guide vane angle) operations. Steady state measurements were performed for three different operating points: Part load (PL), BEP and High load (HL). In PL position guide vane angle is 6.72°, in BEP 9.84° and in HL 12.43°. Besides these measurements, four different transient measurements are preformed: load acceptance from PL to BEP, load reduction from BEP to PL, turbine start-up and shut-down. During the experiments, the runner rotation speed is held constant at 333 min^{-1}. For all of the mentioned situations, measurements are conducted several times in order to estimate measurements uncertainty. Locations of pressure and velocity measurements in the turbine are same for all the operating points and the global coordinate system are shown in Fig. 5.3.

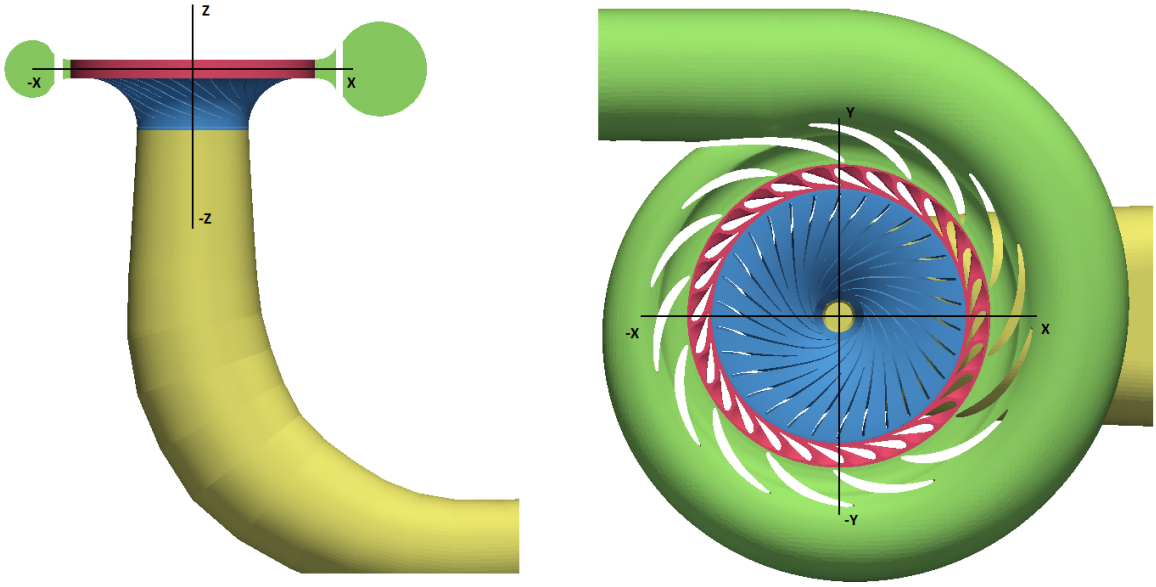

Figure 5.3: Global coordinate system for the measurement locations.

Coordinates of the pressure probes in the global coordinate system are listed in Table 5.2 with the pressure data acquired at the sampling rate of 5kHz.

Table 5.2: Coordinates of the pressure probes.

Sensor	VL2	DT5	DT6
x[mm]	-320.0	-149.1	149.1
y[mm]	62.2	-100.6	100.6
z[mm]	-29.4	-305.8	305.8
Uncertainty[%]	±0.01%	±0.01%	±0.01%

In Table 5.3, coordinates of the lines along which velocity measurements were performed, are shown. Coordinates and measured data are provided in 28 points distributed over each line. Unlike pressure data, velocity data was acquired at the sampling rate of 40 Hz which resulted

in poor accuracy of the acquired data. That will be discussed in more details in the following section.

Table 5.3: Coordinates of the velocity lines.

Velocity lines	L1 start	L1 end	L2 start	L2 end	L3 start	L3 end
x[mm]	25.96	-25.56	25.96	-25.56	0	0
y[mm]	133.55	-131.49	133.55	-131.49	0	0
z[mm]	-338.60	-338.60	-458.60	-458.60	-488.6	-308.6
Total points	28		28		28	

In Fig. 5.4 and Fig. 5.5 we can see positions of the pressure sensors and velocity lines on the model.

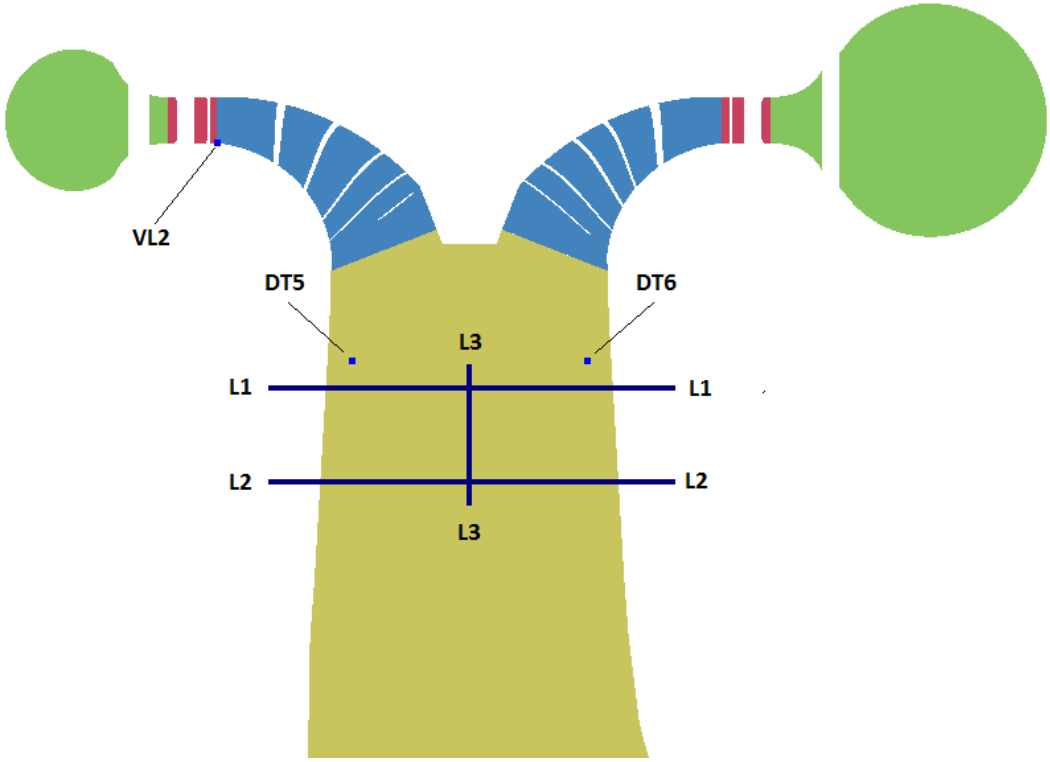

Figure 5.4: Positions of the pressure sensors and velocity lines projected on the y-plane.

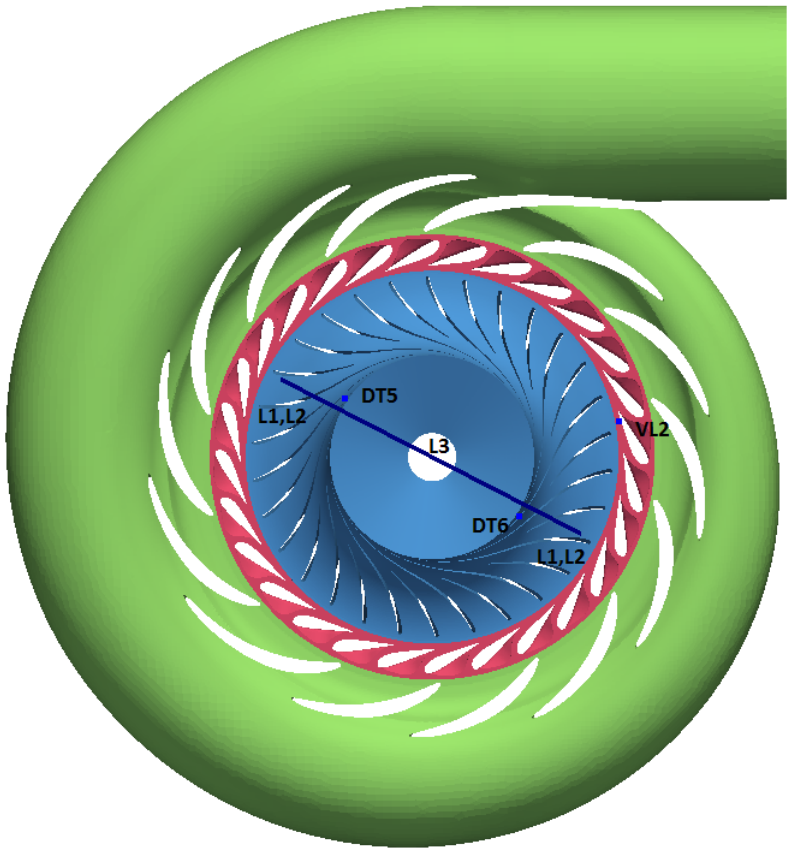

Figure 5.5: Positions of the pressure sensors and velocity lines projected on the z-plane.

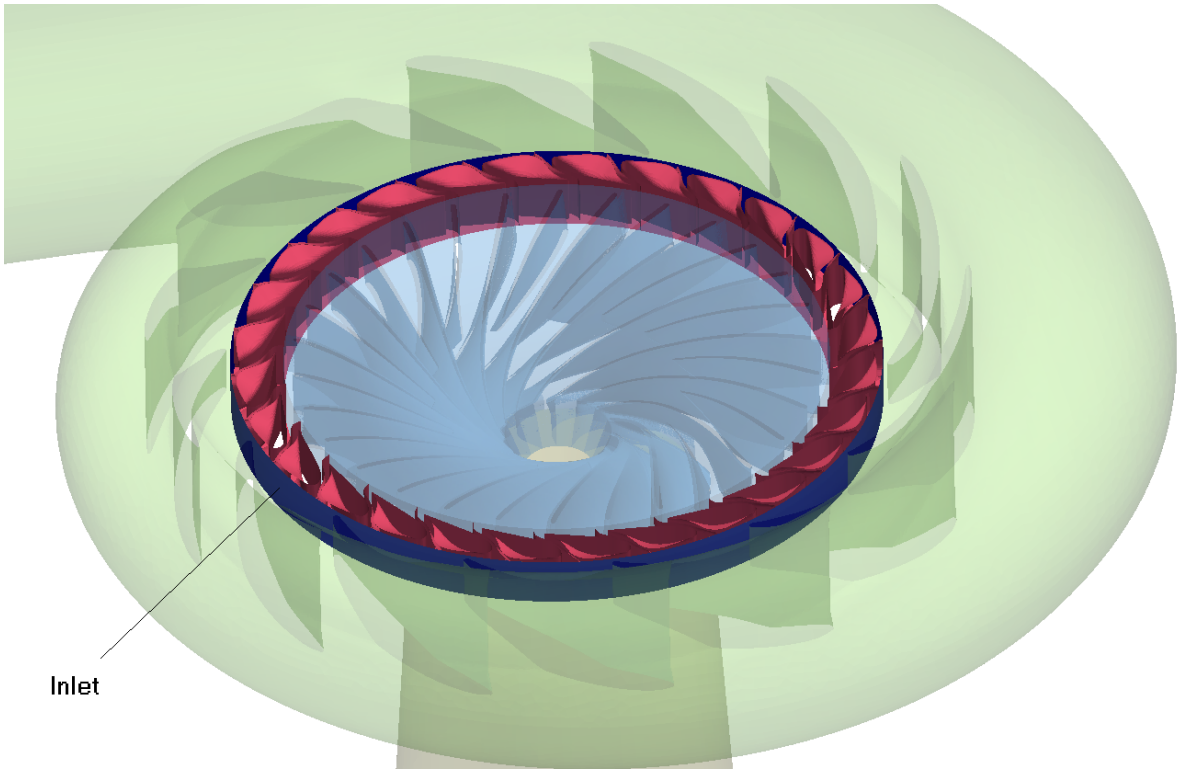

Figure 5.6: Position of the inlet.

5.4 Geometry Generation

In the publications provided by the Francis 99 workshop [1], numerous approaches have been used for the modeling of the turbine. Two most important factors considered while choosing the computational domain, are level of details taken into account and available computational resources. In this study, the model without the spiral casing has been chosen. In the model like that the inlet boundary has shifted from the entrance to the spiral casing to the boundary between the spiral casing and guide vanes. New inlet location is highlighted in Fig. 5.6. Such a reduced model is shown in Fig. 5.7. Guide vanes adn runner are presented in Fig. 5.8, where it is shown that stator domain has 28 blades while rotor domain has 30 blades.

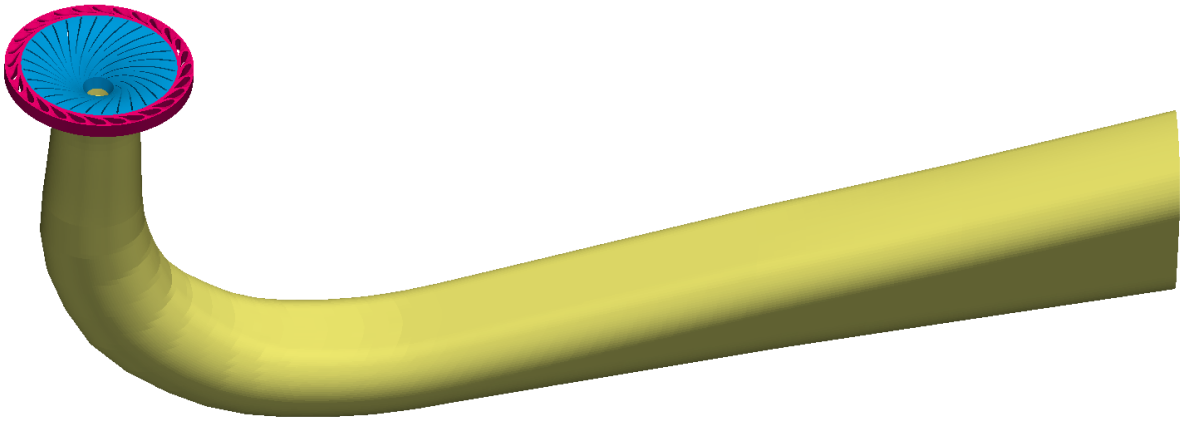

Figure 5.7: Full domain.

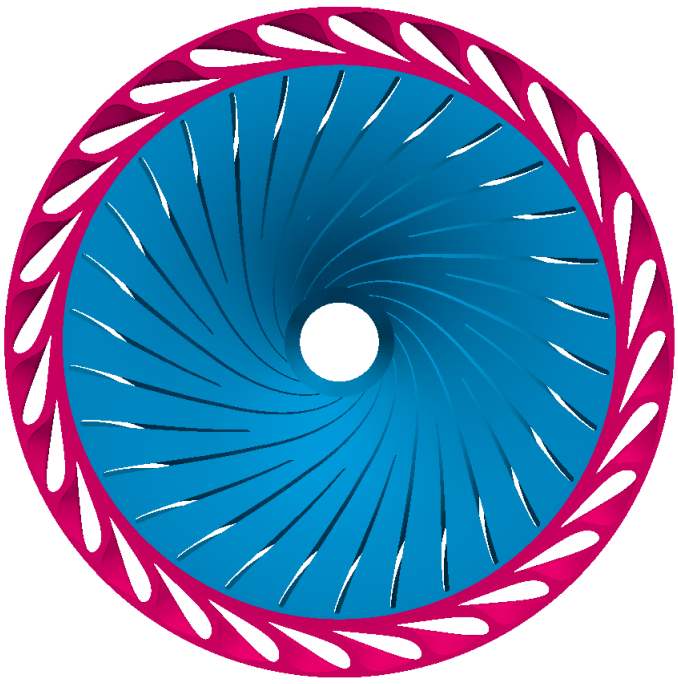

Figure 5.8: Guide vanes and runner domain.

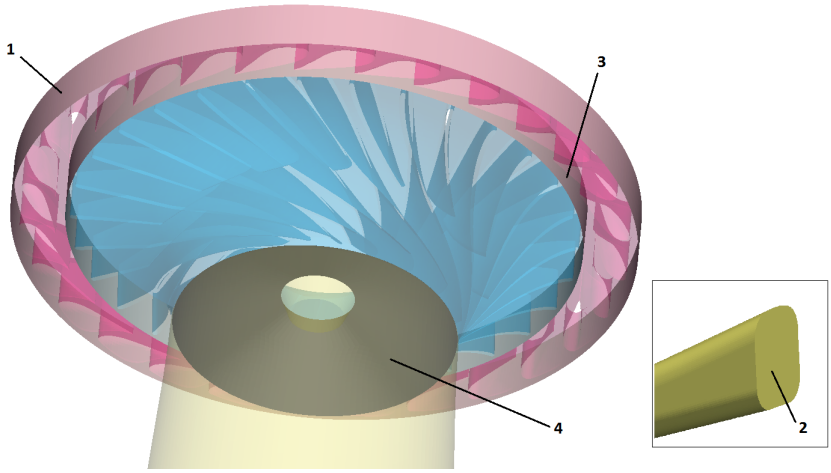

Figure 5.9: Marks of Boundary conditions.

In Fig. 5.9, domain with the assigned boundary conditions is presented. All boundaries that are marked in Fig. 5.9 are listed in Table 5.4. All other patches that are not marked in Fig. 5.9, which includes the hub, shroud and blades are assigned with the wall boundary condition.

Table 5.4: Definition of patch topology.

Boundary No.	Boundary
1	inlet
2	outlet
3	ggi
4	ggi

The test rig measures the outlet static pressure using a ring manifold as specified in the IEC 60193 standard [31]. However, this pressure is measured at a section upstream of the domain, not at the location where boundary conditions will be specified. Consequently, the measured pressure must be adjusted before it is applied as a boundary condition. The outlet cross sectional area corresponds to the experimental pressure measurement section which is located at 1.58 m before the actual draft tube outlet in the numerical model. The static pressure applied at the downstream boundary is approximated using Bernoulli's principle as given in Eqn. 5.1.

$$p_1 + \frac{1}{2}\rho \mathbf{v_1}^2 + \rho g z_1 = p_2 + \frac{1}{2}\rho \mathbf{v_2}^2 + \rho g z_2. \tag{5.1}$$

Let 1 be the measurement plane and 2 be the domain outlet. The absolute static pressure at the outlet can be calculated by combining Eqn. 5.1 and equation for discharge $Q = vA$, which is known from the experiments:

$$p_2 = p_1 + \rho \left[\frac{Q^2}{2} \left(\frac{1}{A_1^2} - \frac{1}{A_2^2} \right) + g(z_1 - z_2) \right]. \tag{5.2}$$

where $\rho = 999.8\,\mathrm{kg/m^3}$, $g = 9.82\,\mathrm{m/s^2}$ and the difference in the vertical positions $z_1 - z_2 = 0.4031\,\mathrm{m}$. The cross sectional areas A_1 and A_2 are measured from the provided geometry to be $0.2292\,\mathrm{m^2}$ and $0.3468\,\mathrm{m^2}$.

5.5 Mesh Generation

Based on the geometry provided by Francis 99 workshop, meshing is performed in the commercial meshing software Pointwise [4]. Pointwise is a meshing software for manual grid generation with various types of finite volume elements available (tetrahedra, hexahedra, prisms, pyramids). Depending on the used elements, mesh can be structured, unstructured or hybrid. Meshes used in this thesis are fully hexahedral and structured. The mesh around guide vanes and runner blades, which are extremely twisted, had to be designed carefully. Another focus in mesh generation is related to near wall spacing, in order to allow proper wall function modeling.

In Table 5.5, number of cells in each zone is presented. As mentioned earlier, all cells are hexahedral.

Table 5.5: Mesh size data.

Zone	Number of cells
Guide vanes	1 764 980
Runner	4 047 225
Draft tube	430 474
Total	6 242 679

Table 5.6: Mesh quality data.

	Average	Maximum	Threshold
Non-orthogonality	25.58	67.95	70.0
Skewness		3.45	4.0
Aspect ratio		27.57	

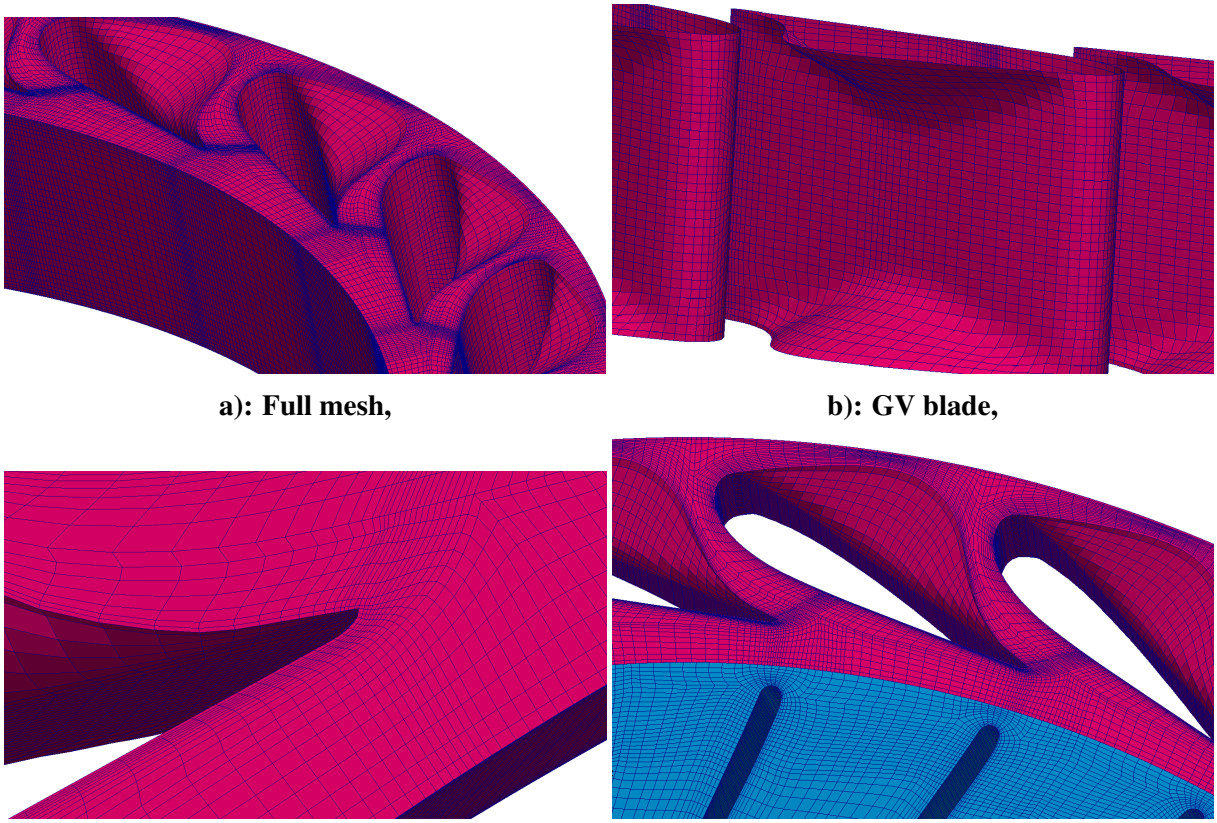

a): Full mesh, **b): GV blade,**

c): Trailing edge, **d): Boundary between guide vanes and runner,**

Figure 5.10: Mesh of guide vane zone.

Quality of the mesh was assessed with `foam-extend` utility `checkMesh`. Results can be seen in Table 5.6, which shows that the quality of the mesh is good with no non-orthogonally or critically skewed cells.

In Fig. 5.10, Fig. 5.11 and Fig. 5.12 meshes of three zones described in Table 5.5 are shown.

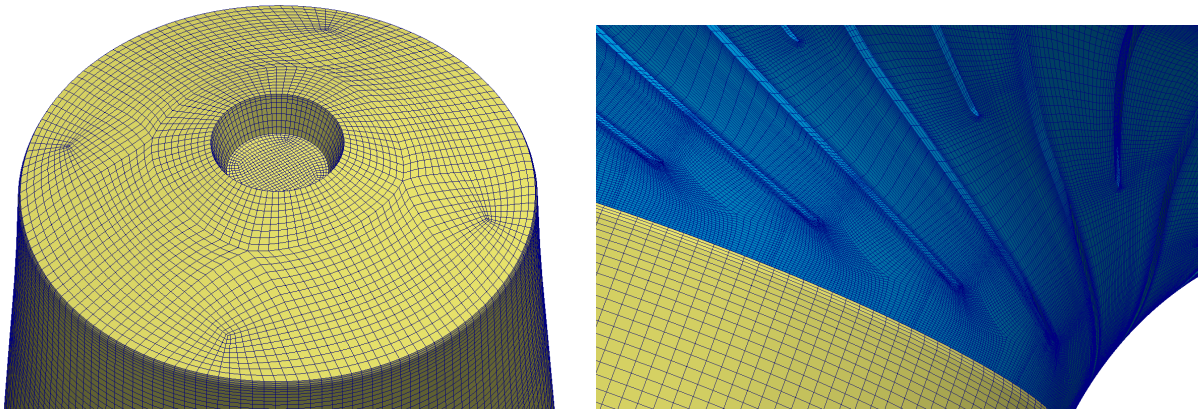

a): Patch surface between the runner and the draft tube, **b): Boundary between the runner and the draft tube,**

Figure 5.11: Mesh of draft tube zone.

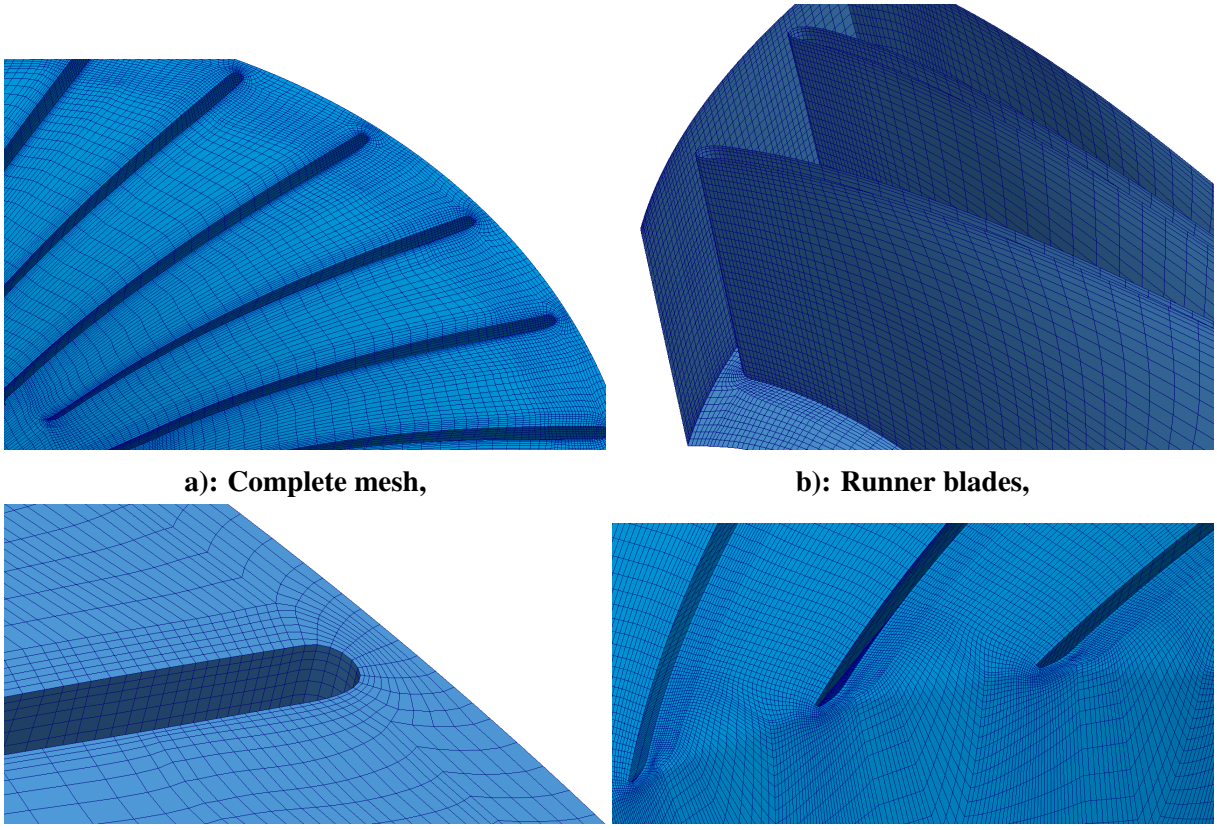

a): Complete mesh, **b): Runner blades,**

c): Leading edge, **d): Trailing edge,**

Figure 5.12: Mesh of runner zone.

5.6 Closure

Within this section, the overview of required preprocessing steps for numerical simulation is presented. First, the Francis-99 workshop is introduced, with prototype and model of the Francis turbine described. Next, operating points in which the experiments were run are listed. Locations of the pressure and velocity sensors are shown in detail in order to be able to replicate it during the following simulations. Moreover, geometry of the full model is shown, which is then reduced to the final form in order to achieve additional CPU time savings. The subsequent section deals with the generated results and comparison with the experimental results.

6 Numerical Results

In this chapter, a comparison is made between the CFD simulations and experimental values obtained on the Francis-99 Workshop. First, numerical and experimental results obtained for the BEP operating point are presented and compared, due to the fact that the largest number of experimental data is provided in BEP operating point. Afterwards, the comparison will be made regarding the shut-down and start-up processes.

This chapter is divided into five sections. In the first section, the boundary conditions used in simulations are presented. Next, the setup that is used for simulations is shown. In the third section, results of the BEP simulation are shown and compared with experimental results. The final section discusses the results obtained for the shut-down and start-up simulations.

6.1 Boundary Conditions

The role of boundary conditions is described in Section 2. In this section, the types of boundary conditions for each physical variable and each patch are described. The main difference in boundary conditions for different operating points is at the domain inlet for the velocity value.

Patches, on which boundary conditions are prescribed, are marked in Fig. 5.9 and listed in Table 5.4. Patches that are not listed in Table 5.4 are prescribed with wall boundary conditions. In all simulations the $k-\varepsilon$ turbulent model is used [32] and corresponding boundary conditions are assigned. On the patches 3 and 4, which are separating different regions, ggi boundary condition is imposed for all variables (k, ε, p and U). At the outlet Dirichlet boundary condition is assigned for all variables expect the pressure, which has von Neumann boundary condition. For the walls, it is the opposite. For the pressure, Dirichlet boundary condition is selected while velocity had von Neumann boundary condition and for turbulence variables wall functions are used. In Table 6.1, type of the boundary conditions used in `foam-extend` and values used for all patches are presented.

Table 6.1: Boundary conditions for the BEP operating point.

Quantity	Boundary	Type	Value
U	inlet	`rotatingWallTangentialVelocity`	(1.413, 2.1185, 0) [m/s]
	outlet	`zeroGradient`	-
	walls	`fixedValue`	(0, 0, 0) [m/s]
p	inlet	`zeroGradient`	-
	outlet	`fixedValue`	0 [Pa]
	walls	`zeroGradient`	-
k	inlet	`fixedValue`	0.0521 [m^2/s^2]
	outlet	`zeroGradient`	-
	walls	`hbKqRWallFunction`	0.0521 [m^2/s^2]
ε	inlet	`fixedValue`	25.5356 [m^2/s^3]
	outlet	`zeroGradient`	-
	walls	`hbEpsilonWallFunction`	25.5356 [m^2/s^3]

`rotatingWallTangentialVelocity` boundary condition is used to impose the velocity on the patch given in the cylindrical coordinates. Therefore, first value represents the radial component, second tangential and third axial component. Result of this boundary condition is shown in Fig. 6.1 .

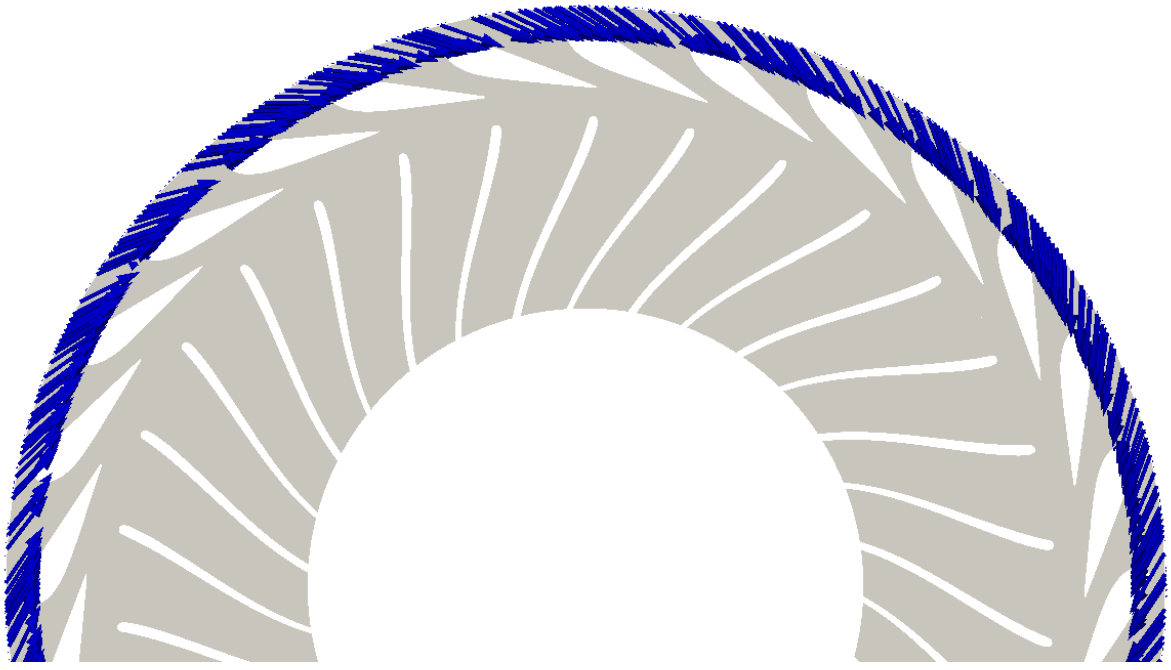

Figure 6.1: Direction of the inlet velocity.

Values presented in Table 6.1 are values for the BEP operating point. For all other operating points, boundary conditions remain the same just the values are changed. In the experiments, the flow rate is regulated by changing the position of the guide vanes, which is linearly increasing or decreasing during the process of start-up or shut-down and consequently

increasing or decreasing the flow rate. In Fig. 6.2 a change of the flow rate during the shut down can be seen. The red line represents measured flow rate while black line represents the flow rate that has been recommended by experimentalists. According to them there is some delay in the flowmeter and therefore the measured flow rate is not accurate. Instead, a linear approximation should be used. That is confirmed in [33], where both experimental and approximated flow rate were investigated, and it is shown that simulations with the approximated flow rate at the inlet provide better results. The same approach is used for the evaluation of the flow rate during the start-up.

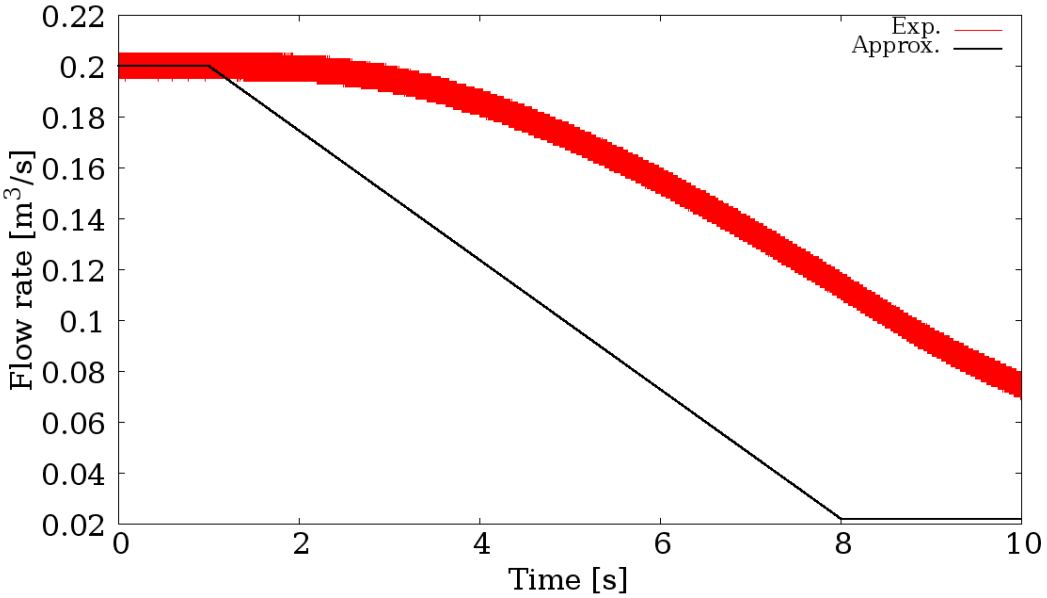

Figure 6.2: Flow rate during the shut-down process.

In this thesis, the approximated flow rate is used and according to it radial and tangential components of inlet velocity are calculated. Radial velocity is obtained using the following relation:

$$v_r = Q/A_I \tag{6.1}$$

$A_I = 0.141276\,\mathrm{m}^2$ is inlet area measured on the provided geometry. Q is the approximated flow rate. In Fig. 6.3, radial velocity is presented for the whole process of shut-down and start-up. Black line represents the change of the radial velocity in accordance with the linear change of the flow rate during both shut-down and start-up. First 2.1 seconds turbine is working in the BEP regime, followed by the shut-down. During 7 seconds of shut-down, operating point is changed from BEP to minimum load. At minimum load, load coupling/decoupling occurs during the start-stop conditions. Also, this is the operating point with the lowest flow rate for which experimental data is provided. In the period between 9.1 seconds and 10.5 seconds, the turbine is working at minimum load. After that, start-up follows, during which the rotor is

accelerated to the BEP operating point, which takes 7 seconds.

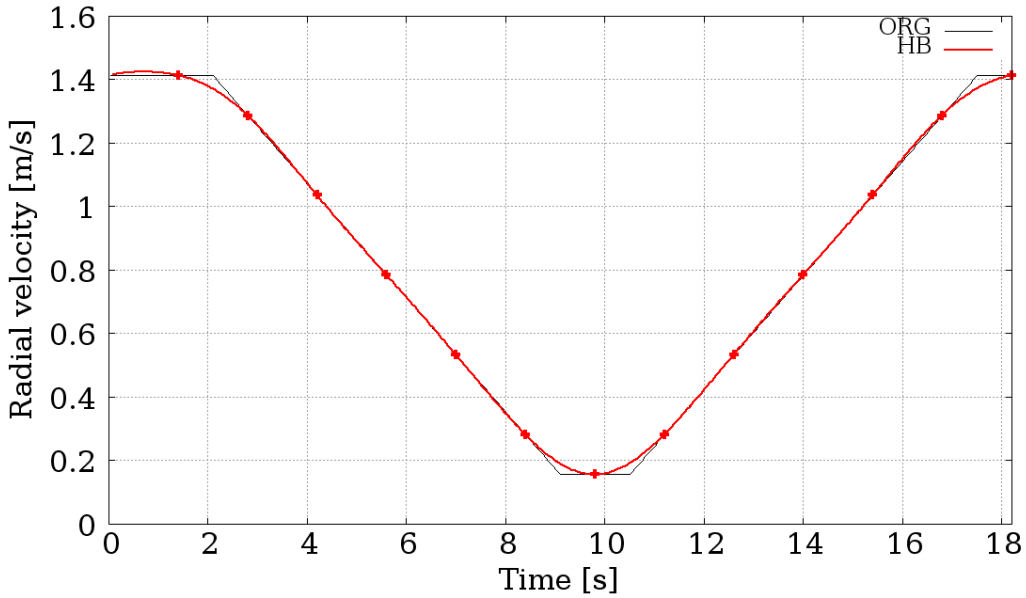

Figure 6.3: Radial inlet velocity during shut-down(2.1-9.1s) and start-up.(10.5-17.5s)

Change of the flow rate during the experiment is achieved by changing the opening of the guide vanes. In this thesis, the flow rate change is achieved by changing the inlet velocity. Consequently, angle of the guide vanes remains the same for all operating points, meaning that the angle of the tangential velocity. Considering that, the direction of the tangential velocity stays the same, but the value is changed during the shut-down and start-up.

In Table 6.2, change of the values prescribed as boundary conditions is presented. k and ε are calculated according to Eqn. 6.2 and Eqn. 6.3.

The turbulent kinetic energy is calculated as:

$$k = \frac{3}{2}(UI)^2, \tag{6.2}$$

where U is inlet velocity magnitude and $I = 0.0724$ is the turbulence intensity. Turbulence dissipation rate ε is calculated as:

$$\varepsilon = C_\mu \frac{k^2}{\beta \nu}. \tag{6.3}$$

where $C_\mu = 0.09$, $\beta = 10$ and $\nu = 9.57 \cdot 10^{-7}$.

The red line in Fig. 6.3 represents reconstruction of the function of the radial velocity (black line). Reconstruction is done with 6 harmonics, which is same as the number of harmonics that is used in outer simulation later on. Also it can be seen that function is made symmetric concerning the time instants of the outer simulation in order to reduce the number of

simulations needed, as it is described in subsection 3.6. Taking that into the account, velocity and turbulent variables for the seven time instants are presented in Table 6.2. These seven values are boundary conditions for the seven inner simulations that need to be calculated.

Considering all of this, following procedure is done in order to simulate start-up and shut-down. First, seven inner simulations are done using the HB solver with one harmonic. Boundary conditions are same as for BEP simulation and the values are changed according to Table 6.2. Next, results from these seven simulations are taken and imposed as starting points for the outer simulation. After running the big simulation, results for the whole process of shut-down and start-up are obtained.

Table 6.2: Boundary conditions for the start-up and shut-down process.

Quantity	Point 1	Point 2	Point 4	Point 3	Point 5	Point 6	Point 7
U_r $[\mathrm{m/s}]$	1.413	1.287	1.036	0.784	0.533	0.281	0.156
U_t $[\mathrm{m/s}]$	2.118	1.930	1.553	1.176	0.799	0.422	0.233
k $[\mathrm{m^2/s^2}]$	0.052	0.042	0.027	0.016	0.007	0.002	0.0006
ε $[\mathrm{m^2/s^3}]$	25.535	16.938	7.101	2.321	0.495	0.038	0.004

6.2 Simulation Setup

For the inner simulations steady state HB solver from `foam-extend` is used. It uses the same set of equations described in Section 3. For all the variables a stabilized bi-conjugate gradient (BiCGStab) solver is used with the diagonal incomplete LU decomposition preconditioner [34], shown in Table 6.3. Values of the relaxation factors for each variable are given in Table 6.4

Table 6.3: Solver settings.

Variable	Solver	Preconditioner	Tolerance	Relative Tolerance
p	`BiCGStab`	DILU	$1e-06$	0.01
U	`BiCGStab`	DILU	$1e-06$	0.10
k	`BiCGStab`	DILU	$1e-06$	0.10
ε	`BiCGStab`	DILU	$1e-06$	0.10

Table 6.4: Relaxation factors.

Variable	Relaxation Factor
p	1.0
U	0.2
k	0.2
ε	0.2

The `Gauss linear method` is used for terms in turbulence model equations while the terms in the rest of the equations use the `Gauss upwind method`. The diffusion terms are

calculated with the `Gauss linear limited` method which compesates for mesh non-orthogonality.

6.3 Simulation of the Best Efficiency Point

Since the BEP has been very well investigated in numerous scientific papers provided at the first Francis-99 Workshop and there are a lot of experimental results, HB simulation of the BEP is presented in this subsection. First, comparison between integral quantities is made. Three quantities that are compared are: effective turbine power, turbine head and turbine efficiency. Following equations present relations used for calculating these quantities.

The turbine head is determined by total pressure difference between the inlet and outlet surfaces of the runner:

$$H = \frac{\Delta p_0}{\rho g} = \frac{\Delta p}{\rho g} + \frac{\mathbf{v_i}^2 - \mathbf{v_o}^2}{2g} + \Delta z \tag{6.4}$$

where Δp is is the static pressure difference between the inlet and outlet surfaces, $\mathbf{v_i}$ is the velocity at the inlet surface, $\mathbf{v_o}$ is the velocity at the outlet surface and $\Delta z = z_i - z_o$ is the distance between runner inlet and outlet surfaces in z axis direction.

Effective turbine power output is defined as:

$$P = \omega \tau \tag{6.5}$$

where ω is the angular velocity of turbine runner and τ is the torque exerted on the turbine shaft.

Turbine efficiency is defined as:

$$\eta = \frac{\omega \tau}{\Delta p_0 Q} \tag{6.6}$$

In Table 6.5 these three quantities are compared for the experiment and simulation. As it can be seen, fluid flow is predicted well by the simulation.

Table 6.5: Comparison of integral quantities.

	P [W]	H [m]	η [%]
Experiment	21 617	11.94	92.39
Simulation	22 457	11.53	94.40
Error	3.74%	3.43%	2.13%

Experimental pressure measurements are described in subsection 5.3, with Table 5.2, Fig. 5.4 and Fig. 5.5 displaying pressure probe locations. Simulation results adjusted for atmospheric

conditions are shown in comparison with experiments in Table 6.6. The gauge pressure distribution in distributor and runner flow sections is pictured in Fig. 6.4. Fig. 6.5 shows gauge pressure isobars, where the guide vane trailing edge suction area is clearly visible, as well as the action of the pressure on runner blade sides, contributing to energy transformation which occurs in reaction turbines of Francis type.

Table 6.6: Comparison of pressure values in three different points.

Measurement locations	VL2	DT5	DT6
Experimental pressure, [kPa]	173.60	105.01	104.80
Simulation pressure, [kPa]	170.43	109.53	109.15
Error	1.80%	4.12%	3.98%

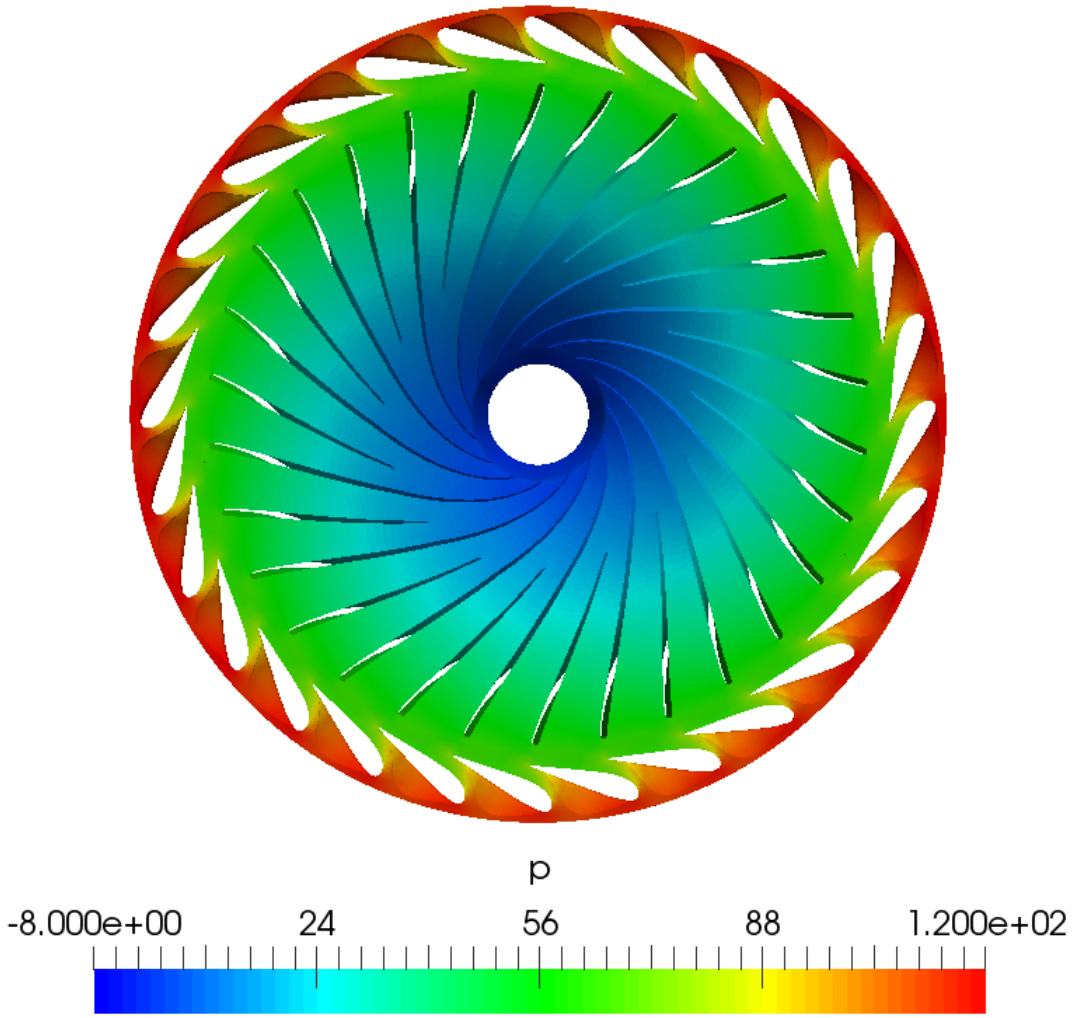

Figure 6.4: Gauge pressure p in the guide vane and runner flow domains.

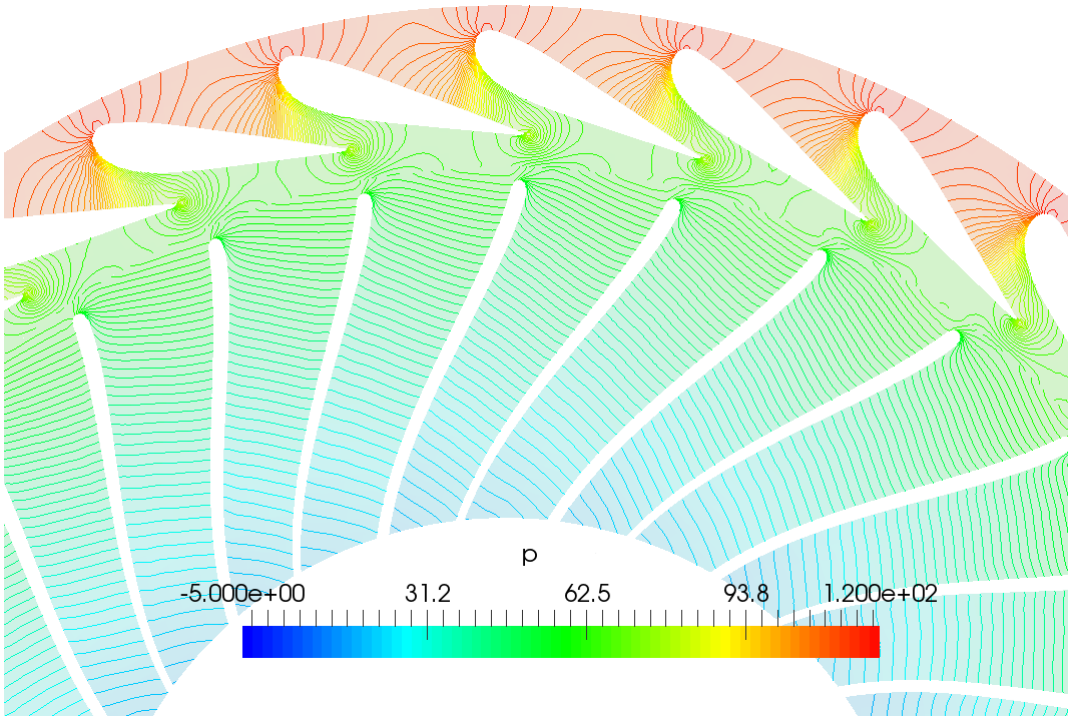

Figure 6.5: A detail of gauge pressure p contours around guide vanes and runner edges.

Rotor-stator interaction is of key interest in turbomachinery flow analysis. Velocity magnitude distribution in Fig. 6.6 shows guide vane trailing edge wakes interacting with runner blades in this area.

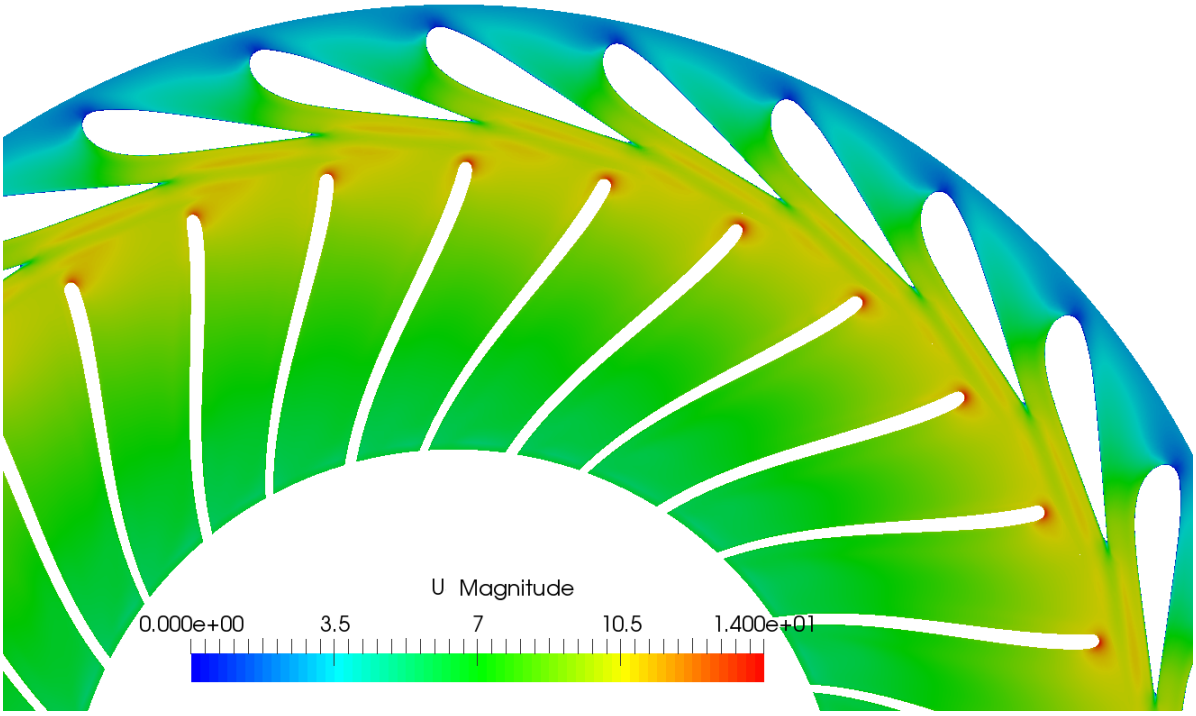

Figure 6.6: Velocity magnitude distribution.

Illustrated by streamlines initiated at the runner/draft tube interface, Fig. 6.9 and Fig. 6.10 show that there are no flow circulations of significance in the draft tube at BEP, as expected.

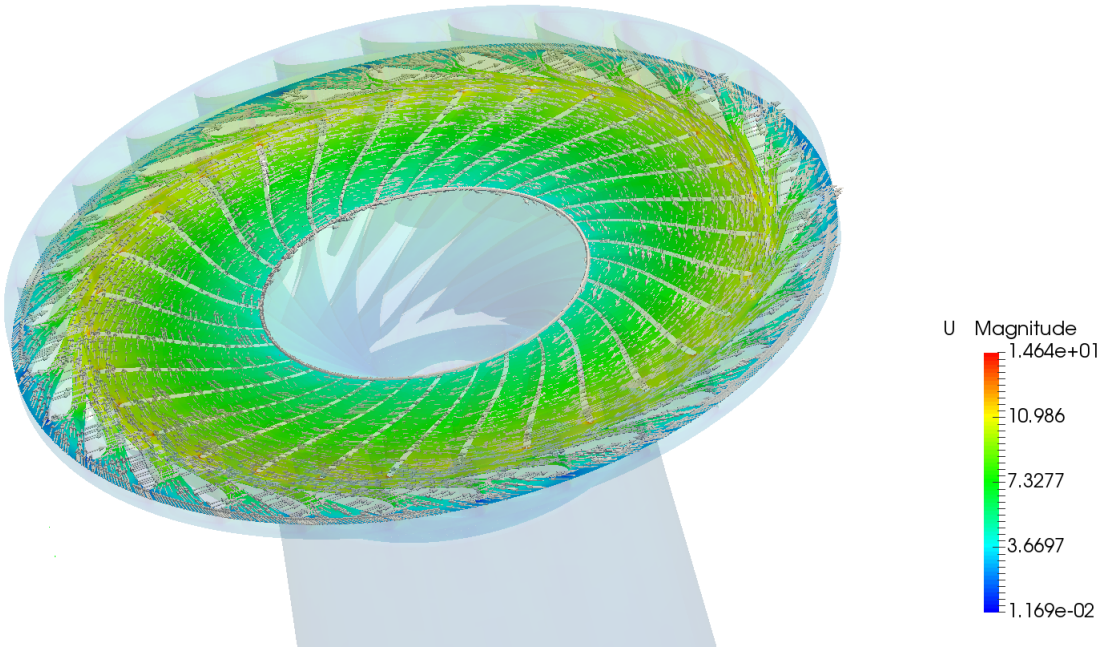

Figure 6.7: Velocity field at the beginning of the runner.

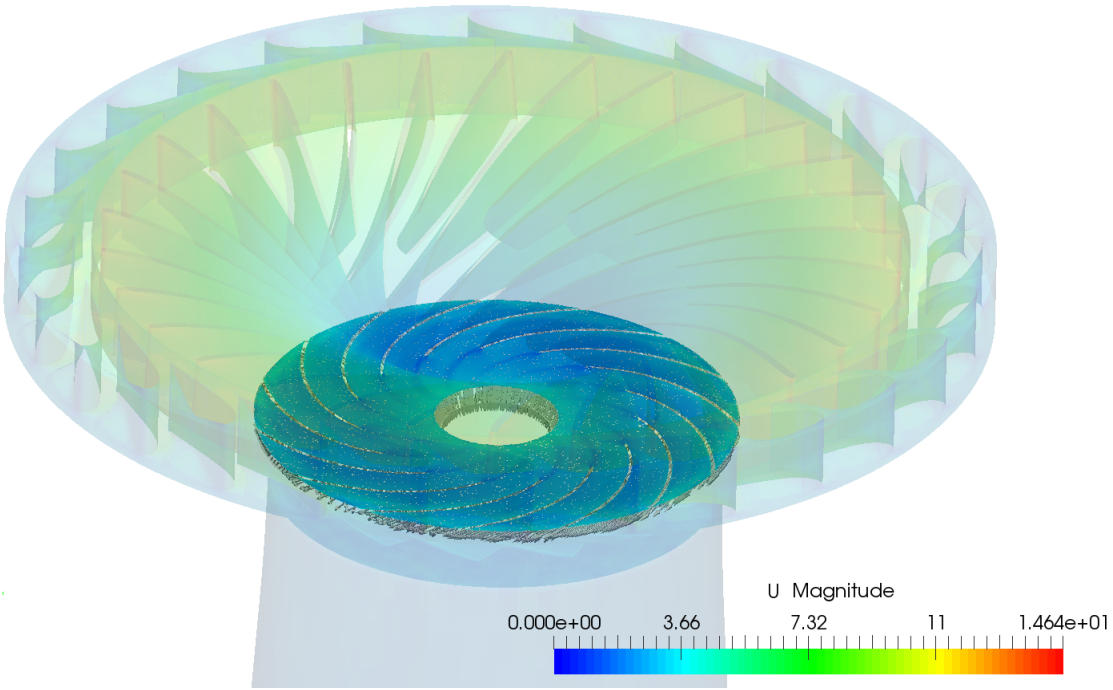

Figure 6.8: Velocity field at the end of the runner.

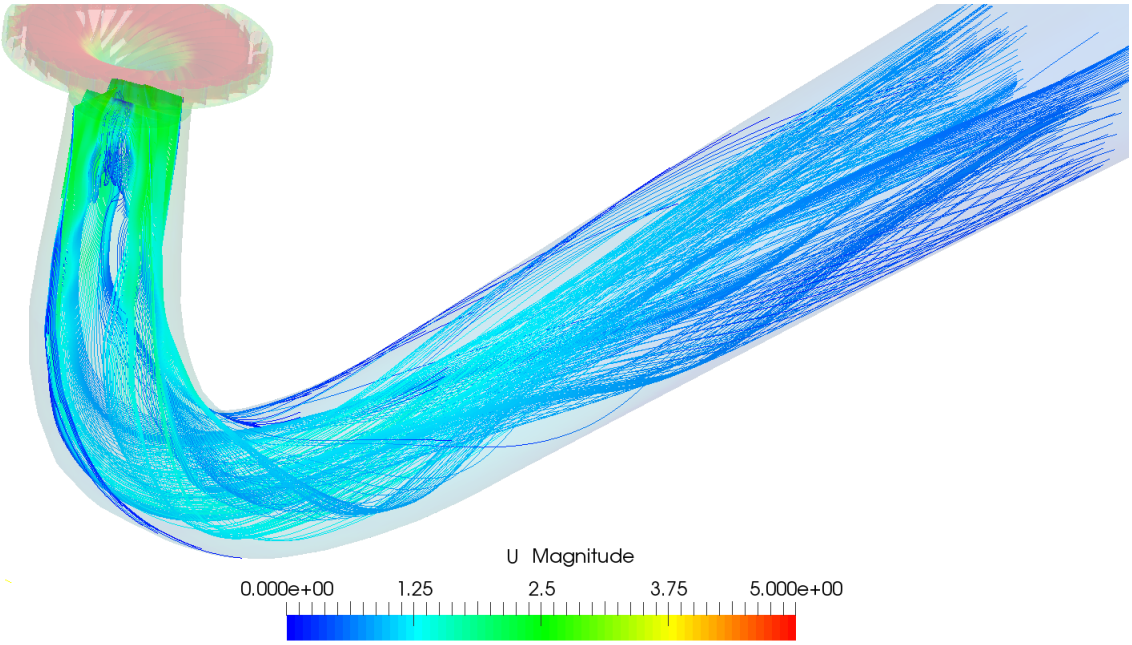

Figure 6.9: Streamlines initiated at the runner/draft tube interface.

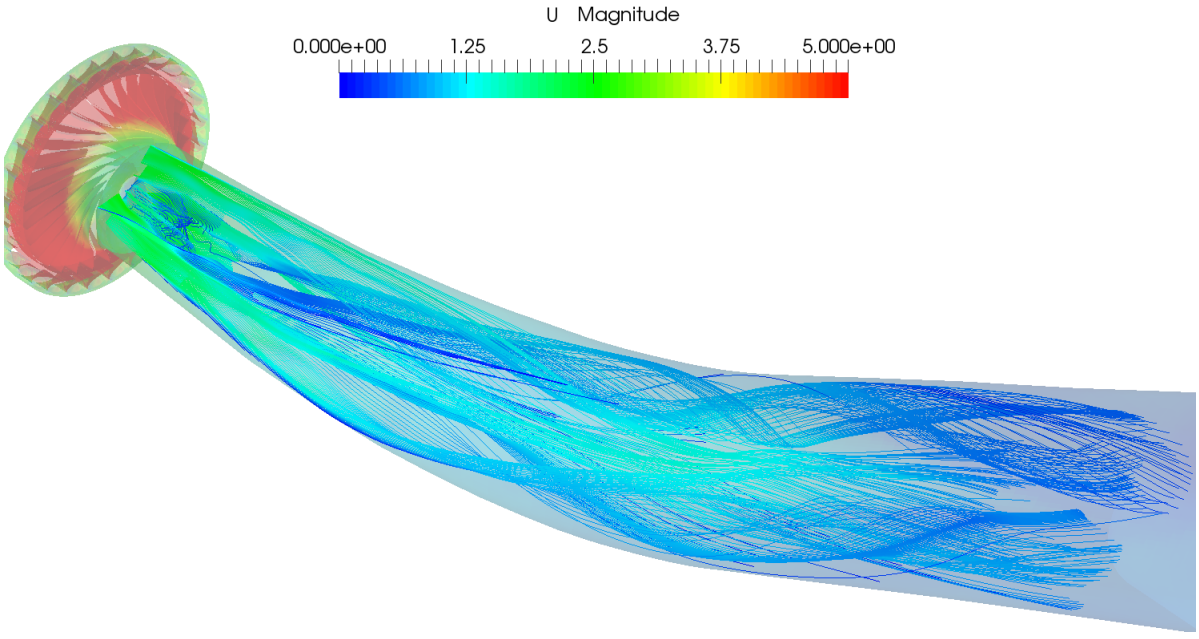

Figure 6.10: Streamlines initiated at the runner/draft tube interface, bottom view.

6.4 Shut-Down and Start-Up Simulation

After the comparison of the results for the BEP, results for shut-down and start-up are presented in this section. Boundary conditions for the shut-down and start-up simulation are presented in subsection 6.1. Outer simulation has 6 harmonics which is considered optimum between

accuracy and CPU time. In Fig. 6.3 inlet radial velocity is presented, from which it can be seen that reconstruction with 6 harmonics approximates well the original function for the change of radial velocity.

After all seven inner and one outer simulation are performed, pressure in the point VL2 is corrected. Pressure calculated in simulations is the static pressure, while the experimental results provide total pressure. In Fig. 6.11 we can see corrected pressure, and it can be concluded that pressure from simulations shows good agreement with the experimental data as the trend in pressure drop matches between the two, suggesting the qualitative agreement between the simulated and real physical processes. At the vane-less space (VL2) pressure probe, results show the relative difference of around 4%, matching those in BEP simulation.

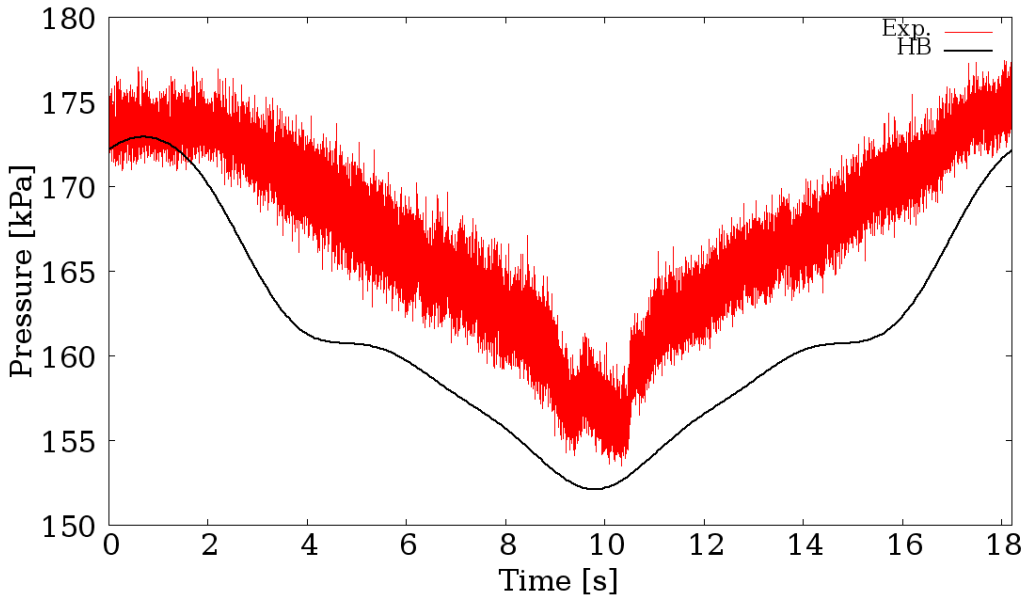

Figure 6.11: Pressure over time in point VL2.

Next, in Fig. 6.12 and Fig. 6.13 the change of pressure and velocity fields in the runner are shown. The first time instants correspond to BEP while last time instant correspond to minimum load point. For each time instant, inlet velocity is also listed. As it can be seen in Fig. 6.13, that the velocity magnitude in the runner stays practically the same through all time instants because rotation speed is held constant during the whole process and its value is much higher than the imposed inlet velocity. In both figures only the shut-down part is presented, as start-up is identical.

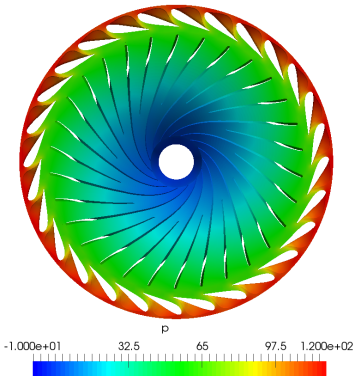

a): $U_{inl} = 2.546\text{m/s}$, $t = 1.4\text{s}$

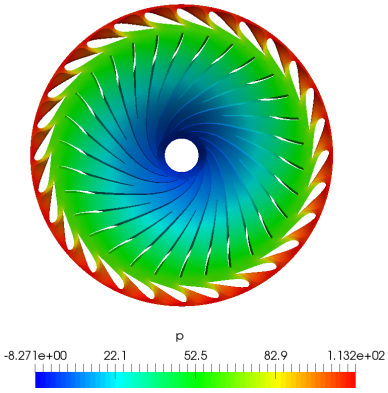

b): $U_{inl} = 2.320\text{m/s}$, $t = 2.8\text{s}$

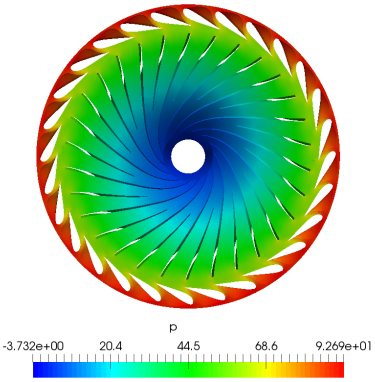

c): $U_{inl} = 1.866\text{m/s}$, $t = 4.2\text{s}$

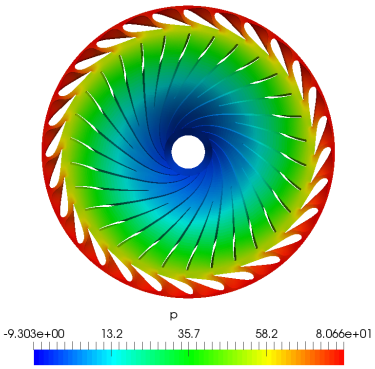

d): $U_{inl} = 1.413\text{m/s}$, $t = 5.6\text{s}$

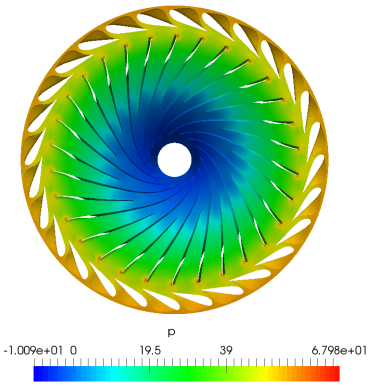

e): $U_{inl} = 0.960\text{m/s}$, $t = 7.0\text{s}$

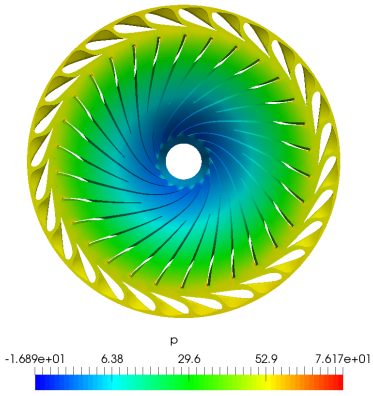

f): $U_{inl} = 0.507\text{m/s}$, $t = 8.4\text{s}$

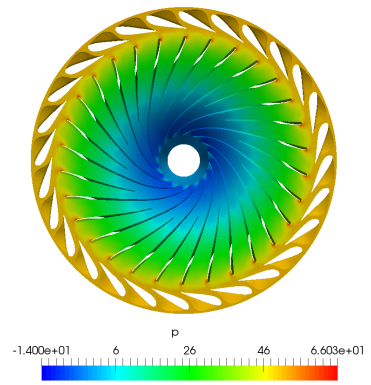

g): $U_{inl} = 0.281\text{m/s}$, $t = 9.8\text{s}$

Figure 6.12: Pressure fields in runner over time.

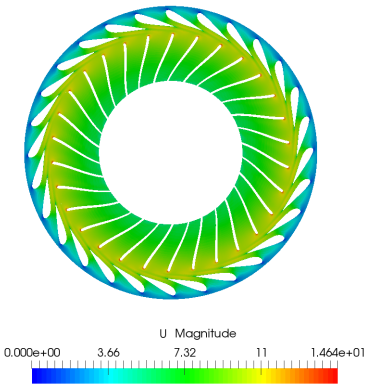

a): $U_{inl} = 2.546\text{m/s}$, $t = 1.4\text{s}$

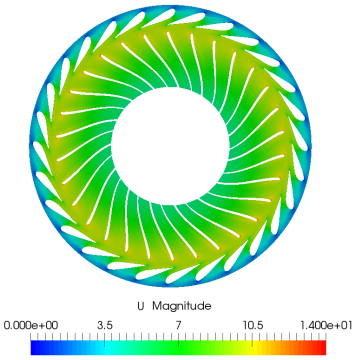

b): $U_{inl} = 2.320\text{m/s}$, $t = 2.8\text{s}$

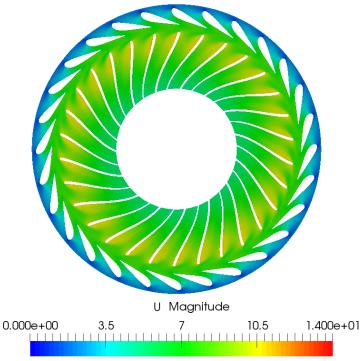

c): $U_{inl} = 1.866\text{m/s}$, $t = 4.2\text{s}$

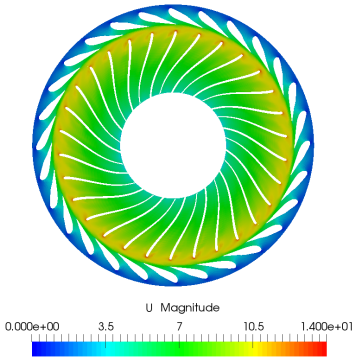

d): $U_{inl} = 1.413\text{m/s}$, $t = 5.6\text{s}$

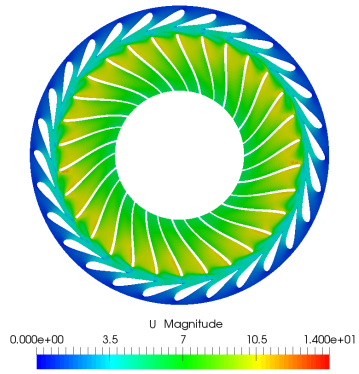

e): $U_{inl} = 0.960\text{m/s}$, $t = 7.0\text{s}$

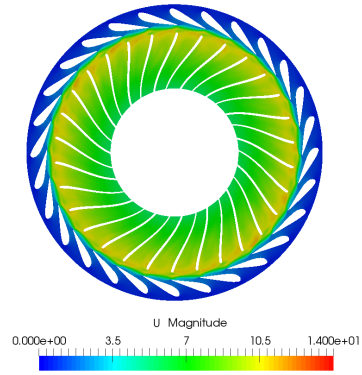

f): $U_{inl} = 0.507\text{m/s}$, $t = 8.4\text{s}$

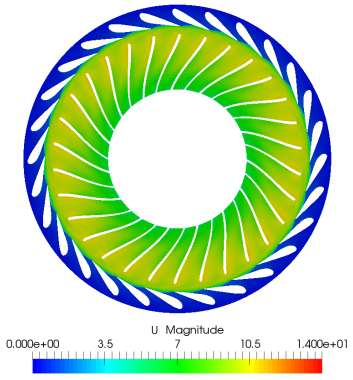

g): $U_{inl} = 0.281\text{m/s}$, $t = 9.8\text{s}$

Figure 6.13: Velocity fields in runner over time.

In all papers provided at Francis99 Workshop, during the investigation of Part Load creation of vortex rope is reported, which is not observed in BEP. Consequently, in Fig. 6.14 formation of the vortex rope in draft tube over time is presented. In four different moments iso-countours of pressure are calculated and presented. In the beginning vortex rope is smaller, but is has higher radial velocity and it shows much more unsteadiness. At the end, when the flow rate is at minimum, vortex rope is much bigger but also the radial velocity is smaller, resulting in a more stable form.

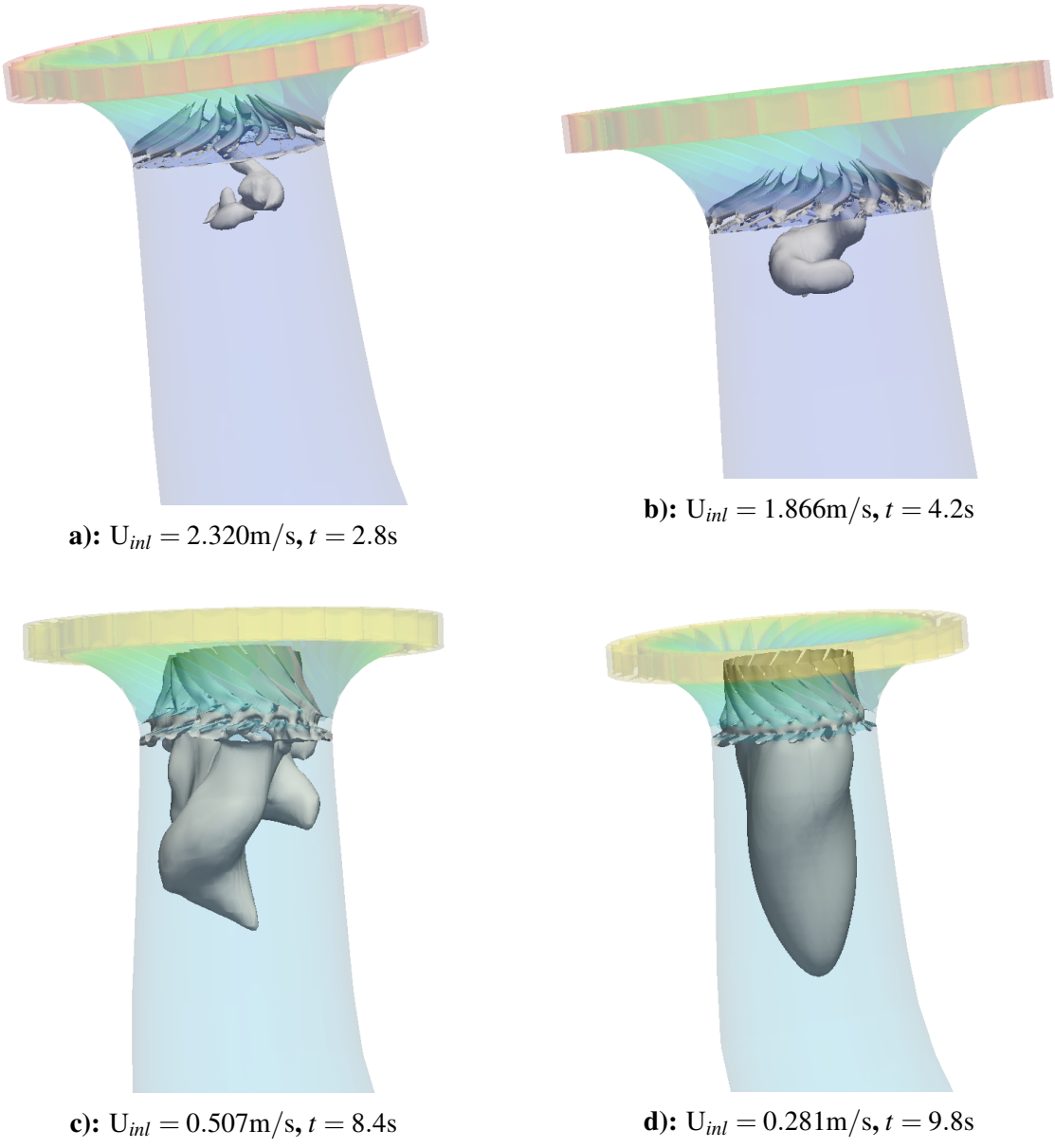

a): $U_{inl} = 2.320\text{m/s}$, $t = 2.8\text{s}$

b): $U_{inl} = 1.866\text{m/s}$, $t = 4.2\text{s}$

c): $U_{inl} = 0.507\text{m/s}$, $t = 8.4\text{s}$

d): $U_{inl} = 0.281\text{m/s}$, $t = 9.8\text{s}$

Figure 6.14: Formation of the vortex rope in draft tube over time.

6.5 Closure

The objective of this chapter was to present numerical results for the simulations of Francis turbine. First, boundary conditions and the solver setup are presented. After which inlet velocity profiles and procedure for the HB method are shown. Both steady state and transient operation of turbine are investigated, with shut-down and start-up processes in focus of transient regime simulations. First the results for the BEP are shown. Pressure values in different locations and three integral quantities are compared to experimental results and it can be seen that results obtained with the HB method correspond well with the experimental results.

After that, shut-down and start-up simulation is presented. Pressure values at the VL2 point are compared with the experimental results and it is shown that both follow the same trend while values have a relative difference of 4%, which is similar to the error computed for the BEP. Next, formation of the vortex rope in the draft tube caused by flow field in the runner is shown.

7 Conclusion and Future Work

This thesis presents a novel approach for start-up and shut-down simulations which is based on the HB method. The approach is tested on two cases. First, a preliminary test case consists of a 2D geometry used for validation and the results of the HB method are compared to transient method. In the second case, results are compared with the experimental results provided at the Francis-99 workshop.

In order to fully understand a new method for the start-up and shut-down governing equations of fluid flow are shown. Next, fundamentals of the HB method are presented and implementation for the governing equations is explained. After that,a method for the start-up and shut-down is described.

Validation is performed on the preliminary test case with a simple geometry. The goal of this test case is to compare the results of the HB method with the transient simulation and also to compare the CPU time required. Results show that the HB method can capture transient flow and local instabilities and results are almost the same as the results of transient simulation. One of the most important findings is the time reduction achieved with the HB method. Time needed for the HB simulations, compared to transient simulations, is 96.48% shorter, which is the main purpose why this new approach was developed.

In the second case, simulation of the flow in the Francis 99 high head turbine has been presented. Both steady state and transient operation of turbine are investigated, with shut-down and start-up processes in focus of transient regime simulations. An original computational grid was created completely from scratch for this purpose. This was done to avoid some of the quality issues regarding the official Francis 99 meshes, reported in the first workshop papers [35, 36] to tightly control the requirements for computational resources for present work which are relatively modest. First, results for the BEP are shown. Pressure values in different locations and three integral quantities are compared to experimental results and it can be seen that results obtained with HB method correspond well with the experimental results. After that, shut-down and start-up simulation is presented. Detailed description of case setup and boundary conditions used for simulating shut-down and start-up is provided. In this case, outer simulation was simulated with 6 harmonics, meaning 7 inner simulations need to be calculated, considering time instants symmetry. Comparison of the pressure values in the vaneless space(VL2 location) is made. It is concluded that the pressure from simulations shows good agreement with the experimental data as the trend in pressure drop matches between the two, suggesting the qualitative agreement between the simulated and real physical processes. Next, pressure and velocity fields in the runner are shown for the shut-down part.

In this thesis guide vane motion is not considered. Effect of the guide vane motion is accomplished by reducing the inlet velocity, and consequently reducing the flow rate on the inlet. Furthermore, some geometry simplifications are made, such as removal of the spiral

casing. Although good results are accomplished even with this simplification, the next step would be to test the HB method on a case with the full mesh and guide vane motion in order to fully replicate the experimental model and capture local instabilities even better.

References

[1] "https://www.ntnu.edu/nvks/francis-99," Norwegian Hydropower Center Research Francis-99, last access: 2018-02-14.

[2] "foam-extend project," https://sourceforge.net/projects/foam-extend/, last access: 2018-01-08.

[3] Jasak, H., "Numeričke metode u mehanici kontinuuma (Numerical Methods in Continuum Mechanics)," Material for lectures, 2016.

[4] "Pointwise V18.0R4 Release Notes," http://www.pointwise.com/support/release-notes.shtml, last access: 2018-02-14.

[5] A. Zervos, "Renewables 2014 global status report," Paris, 2014.

[6] N. Kroner, R. Berube, B.N. Kroner, Company AG, "Maintaining power grid reliability through individual unit stability," HydroVision 2008, HCI Publications, 2008, pp. 1e10.

[7] Trivedi, C., Cervantes, M. J., Gandhi, B. K., and Ole, D. G., "Pressure Measurements on a High Head Francis Turbine During Load Acceptance and Rejection," J. Hydraulic Res., 52(2), pp. 1–15., 2013.

[8] Nilsson, O., and Sjelvgren, D., "Hydro Unit Start-Up Costs and Their Impact on the Short Term Scheduling Strategies of Swedish Power Producers," IEEE Trans. Power Syst., 12(1), pp. 38–44., 1997.

[9] Nilsson, O., and Sjelvgren, D., "Hydro Unit Start-Up Costs and Their Impact on the Short Term Scheduling Strategies of Swedish Power Producers," IEEE Trans. Power Syst., 12(1), pp. 38–44., 1997.

[10] Harlow, F. H., "Fluid dynamics in Group T-3 Los Alamos National Laboratory:(LA-UR-03-3852)," Journal of Computational Physics. Elsevier. 195 (2): 414–433. Bibcode:2004JCoPh.195..414H. doi:10.1016/j.jcp.2003.09.031., 2004.

[11] "OpenFOAM," https://www.openfoam.com/, last access: 2018-03-19.

[12] Jasak, H., "Numerical Solution algoritams for Compressible Flows," Lecture notes, 2007.

[13] Beaudoin M., Jasak H., "Development of a Generalized Grid Interface for Turbomachinery simulations with OpenFOAM," Open Source CFD International Conference, Berlin, Germany, 2008.

[14] He, L., "Method of simulating unsteady turbomacinery flows with multiple perturbations," Vol. 30, 11 1992,pp. 2730-2735.

[15] Cvijetić G., Gatin I., Vukčević V., Jasak H., "Harmonic Balance Developments in OpenFOAM," Computers and Fluids (2018), doi: 10.1016/j.compfluid.2018.02.023.

[16] Hall, K., Thomas, J., Ekici, K., and Voytovych, D., "Frequency domain techniques for complex and nonlinear flows in turbomachinery," Vol. 3998, 2003, p. 2003.

[17] Journee, J. M. and Massie, W., "Offshore hydrodynamics," Delft University of Technology, Vol. 4, 2001, pp. 38.

[18] Jain, P. C. and Goel, B. S., "Shedding of vortices behind a circular cylinder," Comput. Fluids, Vol. 4, 1976, pp. 137–142.

[19] Campobasso, M. S., Piskopakis, A., Drofelnik, J., and Jackson, A., "Turbulent Navier–Stokes analysis of an oscillating wing in a powerextraction regime using the shear stress transport turbulence model," Computers and Fluids, Vol. 88, 2013, pp. 136–155.

[20] "WolframMathWorld," http://mathworld.wolfram.com/FourierSeries.html, last access 14.01.2018.

[21] "Fourier Series Examples," http://lpsa.swarthmore.edu/Fourier/Series/ExFS.html, last access 14.01.2018.

[22] Hall, K. C., Thomas, J. P., and Clark, W. S., "Computation of Unsteady Nonlinear Flows in Cascades Using a Harmonic Balance Technique," Ph.D. thesis, Imperial College of Science, Technology and Medicine, London, 2002.

[23] Jasak, H., "Error analysis and estimation for the Finite Volume Method with applications to fluid flows," PhD Thesis, 1996.

[24] Rusche, H., "Computational Fluid Dynamics of Dispersed Two - Phase Flows at High Phase Fractions," AIAA Journal, Vol. 50, No. 5, 2002, pp. 879–886.

[25] "https://openfoamwiki.net/index.php/OpenFOAM guide/The SIMPLE algorithm in OpenFOAM," The SIMPLE algorithm in OpenFOAM, last access: 2018-03-14.

[26] Zivkovic D., "Simulations of Francis hydraulic turbine load variation," Master's Thesis, 2016.

[27] Mariusz Banaszkiewicz, "Steam turbines start-ups," The Szewalski Institute of Fluid Flow Machinery, Polish Academy of Sciences, Energy Conversion Department, Fiszera 14, 80-231 Gdańsk, Poland.

[28] Guédeney, T., Gomar, A., Gallard, F., Sicot, F., Dufour, G., and Puigt, G., "Non-uniform time sampling for multiple-frequency harmonic balance computations," Journal of Computational Physics, Vol. 236, 2013, pp. 317–345.

[29] Chirag Trivedi, "Experimental and numerical investigations on steady state and transient characteristics of a high head model Francis turbine," Ph. D. thesis, Indian Institute of Technology Roorkee., 2014.

[30] Trivedi, C., Cervantes, M.J., Gandhi, B., Dahlhaug, O.G., "Experimental and numerical studies for a high head francis turbine at several operating points," Journal of Fluids Engineering 135 (11) (2013) 111102.

[31] "Technical Report IEC 60193, 3, rue de Varemb, PO Box 131, CH-1211 Geneva 20, Switzerland, 1999. Second Edition." International Electrotechnical Commission. Hydraulic turbines, storage pumps and pump-turbines: Model acceptance tests.

[32] "https://www.openfoam.com/documentation/cpp-guide/html/guide-turbulence-ras-k-epsilon.html," The k-ε turbulence model, last access: 2018-03-14.

[33] Minakov, A., Sentyabov, A. and Platonov, D., "Numerical investigation of flow structure and pressure pulsation in the Francis-99 turbine during startup," IOP Conf. Series: Journal of Physics: Conf. Series 782 (2017) 012004.

[34] "https://cfd.direct/openfoam/user-guide/fvsolution/," OpenFOAM v5 User Guide: Solution and algorithm control, last access: 2018-03-14.

[35] Trivedi, C., Cervantes, M. J., Dahlhaug, O. G., "Experimental and numerical studies of a high-head francis turbine: A review of the francis-99 test case," Energies 9 (2) (2016) 74.

[36] Stoessel, L., Nilsson, H., "Steady and unsteady numerical simulations of the flow in the tokke francis turbine model, at three operating conditions," Journal of Physics: Conference Series 579 (1) (2015) 012011.